

***Poly(vinyl methyl ether-alt-maleic anhydride)  
based nanoparticles and nanocapsules:  
formulation and characterization***

Dissertation

zur Erlangung des  
Doktorgrades der Naturwissenschaften (Dr. rer. nat.)

der

Naturwissenschaftlichen Fakultät I - Biowissenschaften

der Martin-Luther-Universität  
Halle-Wittenberg,

vorgelegt

von Ligia Elena de Souza

geboren am 27.09.1976 in Belo Horizonte, Brasilien

Gutachter:

1. Prof. Dr. Karsten Mäder
2. Prof. Dr. Lea Ann Dailey
3. PD Dr. Michael C. Hacker

Datum der Verteidigung: 19.12.2017

## Contents

1. Introduction .....	1
1.1. Nanotechnology – Theoretical Background.....	1
1.2. PVM/MA – General characteristics and its applications until the present moment .....	8
1.3. Research objectives.....	9
2. Materials .....	13
3. Methods .....	13
3.1. Nanoparticle preparation.....	13
3.2. Preparation of Medium Chain Triglycerides (MCT) nanocapsules.....	13
3.3. Particle size measurements .....	14
3.3.1. Dynamic light scattering.....	14
3.3.2. Nanoparticle tracking analysis.....	14
3.3.3. Static light scattering.....	15
3.4. Zeta potential measurements.....	15
3.5. pH measurements.....	15
3.6. Transmission electron microscopy – Freeze-Fracture and Cryo.....	15
3.7. Impact of pH of the medium on the nanoparticles .....	16
3.8. Impact of polymer concentration on the DLS results of nanoparticles .....	17
3.9. Impact of pH of the medium on the nanocapsules.....	17
3.10. ATR-FTIR – Attenuated total reflectance - Fourier transform infrared spectroscopy .....	17
3.11. Benchtop <sup>1</sup> H NMR Imaging experiment .....	18

3.12.	Nanoparticle Titration .....	18
3.13.	EPR spectroscopy .....	18
3.13.1.	Nanoparticle loaded with TEMPO-benzoate .....	18
3.13.2.	Nanocapsules loaded with TEMPO-benzoate .....	19
4.	Results and discussion.....	20
4.1.	PVM/MA investigation .....	20
4.1.1.	ATR-FTIR spectroscopy.....	20
4.1.2.	Benchtop <sup>1</sup> H NMR Imaging experiment.....	21
4.1.3.	Conclusion.....	22
4.2.	PVM/MA Nanoparticles – study of polymer hydrolysis.....	23
4.2.1.	Particle size, zeta potential, and pH measurements.....	23
4.2.2.	Impact of pH of the medium on the plain and cross-linked nanoparticles 31	
4.2.3.	Impact of polymer concentration on the DLS results of nanoparticles .	35
4.2.4.	Transmission electronic microscopy – Freeze-Fracture and Cryo .....	38
4.2.5.	ATR-FTIR spectroscopy.....	39
4.2.6.	Nanoparticle Titration.....	42
4.2.7.	EPR spectroscopy – Nanoparticles loaded with TEMPO-benzoate ....	44
4.2.8.	Conclusion.....	48
4.3.	PVM/MA-MCT Nanocapsules: development and characterization .....	50
4.3.1.	Particle size, zeta potential, and pH measurements.....	50
4.3.2.	Transmission electronic microscopy – Freeze-Fracture and Cryo .....	60
4.3.3.	Impact of pH of the medium on the on the nanocapsules size.....	61

---

4.3.4.	EPR Spectroscopy - Nanocapsules loaded with TEMPO-benzoate ....	64
4.3.5.	Conclusion.....	73
5.	Summary and Perspectives.....	77
5.1.	PVM/MA nanoparticles – study of polymer hydrolysis .....	77
5.2.	PVM/MA Nanocapsules: development and characterization .....	80
6.	Appendix.....	I
7.	List of abbreviations .....	IX
8.	Bibliography .....	XIII
9.	Acknowledgements .....	XX
10.	Curriculum Vitae.....	XXI
11.	Erklärung.....	XXIV

# 1. Introduction

## 1.1. Nanotechnology – Theoretical Background

Besides the search for new therapeutic and diagnostic agents and the effort to create new powerful drugs more effective and less toxic, there is also a constant search for improvements in the pharmacokinetic profile and bioavailability of drugs that already exist. Indeed, delivering the drug directly to the target site altering the biodistribution of the drug molecule may increase its effectiveness and decrease its side effects. The concept of controlled drug delivery, where the conjugation of a drug molecule with a carrier system, which has a better pharmacokinetic profile, to improve the effectiveness of the drug has been studied for at least 60 years. The evaluation of the controlled drug delivery systems have begun with the understanding of the mechanisms of controlled release systems and evolved to development of technologies such as polymer carriers and hydrogels triggered by environmental factors, solid implants, *in situ* gel-forming implants and finally into nanotechnology-based drug delivery systems [1]–[3].

Pharmaceutical nanotechnology is the term applied to the activities related to design, characterization and production of pharmaceutical products with nanometric dimensions - the nanotechnology-based drug delivery systems. There are still ambiguities in size range definition of nano, while the United States Food and Drug Administration (FDA) considers 1000 nm as an upper limit for the nanostructures, for the National Institute of Health (NIH) the nanostructures must be smaller than 100 nm. Moreover, according to a study developed a few years ago by Etheridge and co-workers, the mean size of nanostructures in the field of nanomedicine was mostly below 300 nm. These nano-based drug delivery systems include polymeric and metallic nanoparticles, liposomes, micelles, dendrimers, micro and nanocapsules, lipoproteins, cyclodextrins, solid-lipid nanoparticles, among others. The most studied structures are liposomes, micelles, emulsions and polymeric nanospheres, mainly focusing on cancer treatment, *in vitro* testing or *in vivo* imaging. Due to their small size and consequent large surface area, the nano-based systems exhibit different physical, chemical and biological properties, presenting the ability to achieve singular biodistribution profiles that are not possible with molecular or microscopic scaled systems [2], [4]–[6].

Drug carriers, including nano-based drug delivery systems, are tools to:

- i. Improve drug stability and solubility and minimize its degradation.
- ii. Increase drug bioavailability and prevent undesirable side effects.
- iii. Recognize and bind to specific target cells and accumulate in the desired area of action.
- iv. Respond to endogenous stimuli characteristic of a pathological site, such as pH, temperature, enzymatic activity or presence of reactive oxygen species.
- v. Respond to external stimuli, such as local application of magnetic, electrical, ultrasound or thermal source of energy to release the drug.

Beyond that, they should have a small particle size with narrow size distribution, possess high loading capacity and prolonged time circulation in blood, be biodegradable and be economically viable for large-scale production [3], [4], [7].

Nano-based drug delivery systems have been successfully translated into clinical applications. Liposomes, drug-polymer conjugates, antibodies, antibody fragments and antibody conjugates, drug nanoparticles, and nanoparticle based on the natural protein albumin are already marketed worldwide. Nowadays, neither the nanoparticle formulations, which is the most popular topic in drug delivery field nor nanocapsules have been successfully translated into clinical applications, although a number of them are currently in different phases of clinical trials. Development of effective nanoparticulate drug delivery system still requires a better understanding of the interactions of the particles and the body and the variables that have a relevant impact on this interaction [2], [3], [5].

Considering the aim of this work, two of the nanostructures mentioned above will be deeply detailed: polymeric nanoparticles and nanocapsules. The term nanoparticle is employed to describe colloidal drug carriers ranging in size from about 10 to 1000 nm, including polymeric nanospheres and nanocapsules. Nanospheres are dense polymeric matrix and nanocapsules are vesicular structures that exhibit an oil core enclosed by a polymeric shell, as depicted in Fig. 1 below. In this work, the term nanoparticle is used as a synonym of nanospheres, as vastly employed in the literature.

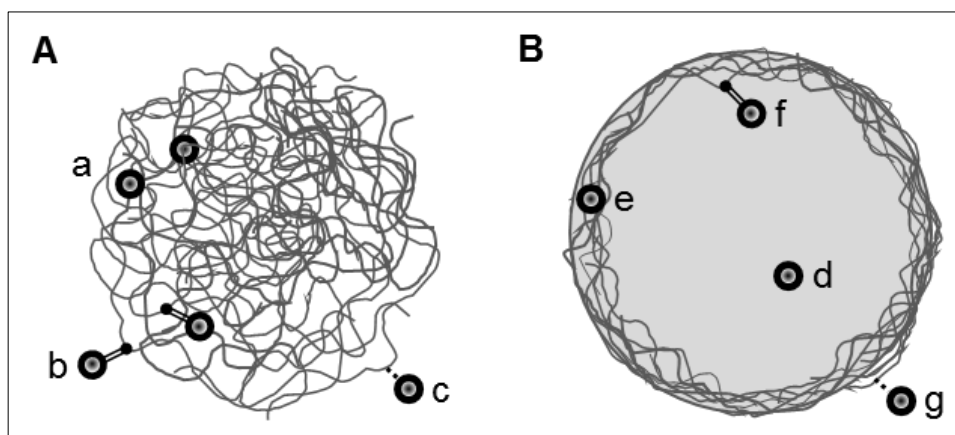


**Fig. 1.** Schematic representation of nanoparticles (A) and nanocapsules (B). The loaded active substance may be physically entrapped into the polymeric matrix (a), covalently attached to the polymer backbone (b and f), adsorbed on the particle surface (c and g), encapsulated inside the core (d) and incorporated into the polymeric shell.

### ***Polymeric nanoparticles***

Polymeric nanoparticles are solid colloidal particles made of biodegradable or non-biodegradable polymers from natural or synthetic sources, ranging in size typically from 100 to 500 nm. They are an option for controlled drug delivery by parenteral, oral, pulmonary, nasal or topical routes. Nanoparticles, as other controlled drug delivery systems, can overcome drug solubility and stability issues, target specific tissues and minimize side effects. These nanostructures may be prepared directly from natural or synthetic preformed polymers or by *in situ* polymerization of monomers. The most commonly applied polymers are poly(D, L-lactide-co-glycolide), poly(anhydrides), poly(amides), poly (L-lactide), poly- $\epsilon$ -caprolactone, poly (alkyl cyanoacrylates), albumin and chitosan. While naturally occurring polymers are biocompatible, biodegradable, and are found in abundance in nature, synthetic polymers present more reproducible characteristics from batch-to-batch and, therefore, more reproducible results when employed to prepare drug-delivery systems. [3], [8].

The nature of the polymer, the characteristics of the drug and the method employed to prepare the nanoparticles will directly influence the *in vitro* release profile of the loaded drug. The active substance can be encapsulated into the carrier, covalently attached to the polymer or adsorbed onto its surface, Fig. 1 (A). When the drug is uniformly incorporated into the matrix, the release occurs by drug diffusion or by erosion of the matrix with consequent exposure of the drug to the medium. Covalently attached drugs present slow a release profile, attributed to chemical degradation of the polymer matrix followed by its solubilization in the medium and, eventually, the release of the drug. Adsorbed drugs show, generally, a rapid release, due to the weak bound to the surface

of the carrier [9]. A variety of different methods may be employed to prepare nanoparticles, which include: *in situ* polymerization, emulsification/evaporation, solvent displacement, electrospraying, and microfluidics.

*In situ* polymerization yields nanoparticles from a solution containing the active substance and the monomers, which are polymerized by the addition of catalysts or by irradiation. This method presents important drawbacks such as residues of monomers, oligomers, and catalysts, undesirable reactions between the monomers and the active substance, and degradation of the active substance.

Emulsification-evaporation methods encompass two different techniques, single and double-emulsion, and are characterized by the formation of an emulsion followed by the evaporation of the organic solvent. Single-emulsion technique is suitable to entrapping hydrophobic drugs based on the formation of oil-in-water (o/w) emulsion. In this method, the preformed polymer and the drug are dissolved in a water-immiscible volatile organic solvent, and the organic phase is emulsified in an aqueous solution containing the required amount of a surfactant. The organic solvent is removed forming a colloidal dispersion of nanoparticles [10]. Double emulsion method may be used to encapsulation of hydrophilic drugs and proteins. Here, the drug and a surfactant are dissolved in a small volume of an aqueous phase, and this is emulsified in an organic phase containing the polymer. The final water-in-oil (w/o) emulsion formed is dispersed in external aqueous phase, with or without surfactant, to form the water-in-oil-in-water (w/o/w) emulsion. The organic solvent is evaporated yielding the nanoparticles [11].

Solvent displacement method was firstly described by H. Fessi and co-workers in 1989 [12]. In this method the polymer and drug are dissolved in a semipolar water-miscible solvent, this solution is then poured or injected into an aqueous solution under stirring. The hydrophobic polymer precipitates instantaneously leading to the formation of nanoparticles. Finally, the organic solvent is evaporated. The mechanism of formation of nanoparticles in this technique has been explained by 'interfacial turbulence and thermal inequalities' caused by the difference in the surface tension of organic and aqueous phases, which lead to the formation of eddies of solvent at the interface of both liquids. As a consequence, the spreading of organic solvent occurs due to mutual miscibility between the solvents, forming droplets. If the solvent droplets formed have polymer inside, the polymer would tend to aggregate and form nanoparticles due to the continuous diffusion of solvent and because of the presence of a non-solvent medium [13].



In the electrospraying or electrohydrodynamic atomization (EHDA) method, a solution containing polymer and drug dissolved in a conductive solvent is used. A strong electrical potential is applied to this polymer/drug solution and a charged jet is ejected from the equipment tip. This continuous jet is then broken into small droplets resulting in particles with defined size and shape. The method yields particles with high loading efficiencies and narrow particle size distributions [14], [15].

Microfluidics technique employs reactors having micrometer length scale, composed of pneumatically activated valves and rapid mixers. These microreactors can mix rapidly very small amounts of reagents and provide homogeneous reaction environments. Microfluidic reactors can produce nanoparticles with narrow size distributions compared to bulk synthesis methods and higher encapsulation without an increase in nanoparticle size [16], [17].

Emulsification-evaporation methods yield nanoparticles with moderate drug loading and encapsulation efficiency usually higher than those observed for solvent displacement method. It is important to note that the emulsification step is determinant to the final particle size since each oil droplet will form one particle when the organic solvent is removed. Therefore these methods employ high energy input in the formation of the nanoemulsion. Solvent displacement method, however, requires only mild stirring under minimal shear stress. The poor entrapment of hydrophilic drugs and residual organic solvent at the final formulation are limitations of this technique. Among the methods described above, solvent displacement provides a versatile and simple way to prepare nanoparticles, being one of the most applied methods to prepare these nano-carriers, while electrospraying and microfluidics are emerging techniques to prepare nanoparticles from preformed polymers [3], [8], [13], [18].

### ***Nanocapsules***

Nanocapsules are core-shell nanostructures in which the drug is preferably confined to a liquid core surrounded by a polymeric shell. The core can be lipophilic or hydrophilic according to the preparation method and to the materials used. The active substance can be entrapped inside the core, incorporated or attached to the polymeric shell, Fig. 1 (B). Nanocapsules have lower polymer content when compared to other polymeric nanoparticulate systems, and higher loading capacity due to the drug solubility in the core medium. Furthermore, the drug contact with the external medium is minimized, which may avoid the burst effect, protect the drug against degradation and prevent irritation on the site of administration. The characteristic size of

nanocapsules is between 250 and 500 nm and depends on the chemical nature and the concentration of the polymer and drug, the concentration of surfactants, the ratio of organic solvent and water, oil viscosity and its concentration in the organic solution. Poly-ε-caprolactone, poly(lactide), poly(lactide-co-glycolide) and poly(alkyl cyanoacrylate) are the most commonly used polymers to prepare nanocapsules. The choice of the oil should consider a high capacity to solubilize the active substance, absence of toxicity and absence of risk of polymer degradation [8], [18], [19].

As the nanoparticles, nanocapsules can be obtained from different methods of preparation, including interfacial polymerization, solvent displacement method, emulsion-diffusion, double emulsification, emulsion coacervation, polymer coating, and layer-by-layer deposition.

In interfacial polymerization method, the polymer is synthesized at the interface of a nanoemulsion template. Alkyl-cyanoacrylates are the most common monomers employed in this technique, and hydroxyl groups from water or other nucleophilic group, are used as initiators. The technique is suitable to encapsulate both hydrophilic and lipophilic active substances. However, unwanted chemical reactions, toxic residues of solvents, monomers and oligomers and drug degradation are drawbacks of this technique, similarly to nanoparticles [8], [19].

In the emulsion-diffusion technique, the organic and aqueous phase are mutually saturated before use to ensure initial thermodynamic equilibrium of both liquids. The polymer, oil and active substance are solubilized on the organic water-saturated phase, and this solution emulsified with the saturated aqueous solution containing a stabilizer, under vigorous agitation. The subsequent addition of water to the system induce the diffusion of the organic solvent to the external phase leading to the formation of nanocapsules. The organic solvent can be eliminated by distillation or cross-flow filtration. The technique relies on the rapid diffusion of the solvent from the internal to the external phase and polymer aggregation around the oil droplets forming capsules [13], [18].

Double emulsification is w/o/w emulsions usually prepared by a two-step emulsification process. In the primary w/o emulsion, the oil is changed by an organic solvent in which a polymer and a hydrophobic surfactant are solubilized. This organic phase is emulsified with the aqueous phase containing the hydrophilic active ingredient. The w/o emulsion is added to the bulk water phase containing a stabilizing agent. The

organic phase diffuses through the external medium precipitating the polymer at the interface forming the nanocapsules [20], [21].

The emulsion-coacervation method uses an o/w emulsion as a template for the nanocapsule formation. The oil phase containing the active substance, and a solvent if necessary, is emulsified with a water phase containing the polymer and a stabilizing agent. The addition of the aqueous external phase containing a dehydration agent or a water miscible solvent causes the polymer precipitation around the oily phase. This method is mainly applied to produce nanocapsules from natural polymers, like gelatin or sodium alginate [22].

Nanoprecipitation or interfacial deposition or solvent displacement method is widely applied to nanocapsules preparation. It needs solvent and non-solvent phases. The solvent phase, or organic phase, contains the polymer, the active substance, the oil and a lipophilic surfactant. The non-solvent phase, generally the aqueous phase, contains one or more surfactants. The organic phase is added slowly and with moderate stirring to the aqueous phase and finally removed under reduced pressure. The organic water-miscible phase containing the oil, polymer, and drug is spontaneously emulsified when added to the aqueous phase forming nano-droplets. The polymer migrates towards the organic/inorganic interface where it is deposited, since it is insoluble in the aqueous phase, forming the nanocapsule shell. The driving force to nanocapsules formation is the interfacial turbulence and thermal inequalities caused by the difference between the surface tension of the liquids forming the organic and the aqueous phase, as described above for nanoparticles prepared by solvent displacement method [8], [12].

Polymer coating method is based on the deposit of a thin layer of charged polymer onto the surface of a preformed nanocapsule or nanoemulsion that works as templates [23]. The layer-by-layer method requires a colloidal template onto which layers of polycations and polyanions are intercalated forming the nanocapsule [24].

*In vitro* release of the active substance from nanocapsules are influenced by several factors, among them the concentration and physicochemical characteristics of the drug, chemical properties, concentration and molecular weight of the polymer and the preparation method. There is a fast-initial release phase attributed to desorption of the drug located at the nanocapsules surface, followed by a release determined by the partition coefficient of the drug between the oily core and the aqueous external medium

and the relative volume of both phases. Although the polymeric shell cannot be considered an effective barrier to the encapsulated active substance, the polymer concentration and its molecular weight have an impact on this process, the higher the polymer concentration and molecular weight, the lower the drug release. The inability of the polymer shell to change the diffusion properties of the encapsulated drugs may be considered a challenge to develop nanocapsules with release profiles, which may be controlled not only by the partition coefficient but also by the nature or morphology of the surrounding membrane [7], [18].

## 1.2. PVM/MA – General characteristics and its applications until the present moment

Poly(methyl vinyl ether-alt-maleic anhydride) – PVM/MA is a commercially available copolymer obtained by radical polymerization using a free radical-generation agent, such as peroxides [25] and it is available in a range of molecular weight, from 216000 to 1980000. PVM/MA and its free acids derivatives have many applications in cosmetics and health care (as a binder, a hair fixative, denture adhesive, film forming agent, emulsion stabilizer, viscosity-increasing agent or as an enhancer for bio-adhesiveness). It has a good safety profile [26], despite the observation of genotoxicity in mice after oral administration of very high doses [27].

The polymer is water-insoluble. However, when dispersed in aqueous solutions, the maleic anhydride group is hydrolyzed in a diacid giving a water-soluble free acid polymer, Fig. 2. PVM/MA is considered a pre-activated polymer due to the presence of maleic anhydride moieties, which is very reactive to primary amines and slightly less reactive to alcohols, forming a half-amide or a half-ester, respectively [28].

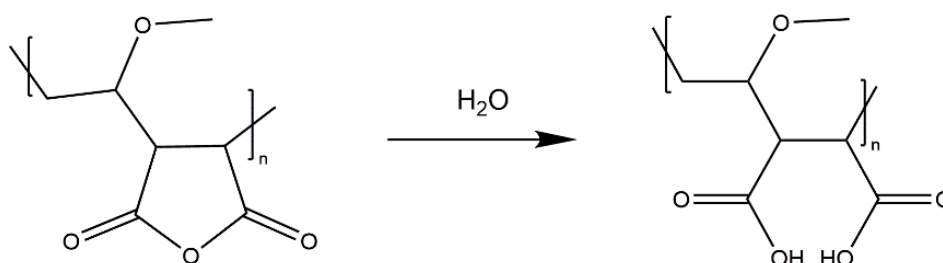


Fig. 2. Chemical structure of PVM/MA copolymer and its hydrolyzed form.

The first work that described the use of PVA/MA ( $M_w$  216000) to prepare nanoparticles for oral delivery was published on 2002 by Arbós and co-workers. In that work, cross-linked nanoparticles were coated with bovine serum albumin (BSA) that develops non-

specific interactions with the mucosa of the gastrointestinal tract, and with *Sambucus nigra* lectin, which has the capacity to interact specifically with sugar residues located at the surface of epithelial cells. The tropism of the different yielded nanoparticles and their capacity to increase the absorption of poorly water soluble drugs were evaluated in a number of publications [29]–[32]. Plain PVM/MA nanoparticles were modified by the incorporation of PEG, dextran, cyclodextrins or lipids, loaded or not with active substances [33]–[38]. Different proteins and carbohydrates were bound to the polymer backbone as a strategy to vaccination and immunotherapy [39]–[45]. The polymer was used to produce hydrogels in association with poloxamer [46] or PEG [47]. PVM/MA was also applied to encapsulate selenite-triacylglycerides, a cytostatic agent tested against pulmonary adenocarcinoma cells [48].

### **1.3. Research objectives**

PVM/MA is not a biodegradable polymer, and its elimination by the kidney is not possible considering its high molecular weight. This characteristic makes the polymer suitable for the development of drug carrier for topical and oral drug delivery, but not for intravenous administration. The development of drug carriers for oral delivery systems is an important field of pharmaceutical nanotechnology regarding the number of drugs that are poorly-soluble in water, which hinders its administration for parenteral routes. Besides, the oral route is associated with higher patient compliance being the simplest, most convenient and safest means of drug administration [49].

PVM/MA was proposed to be the polymeric matrix of nanoparticles considering its ability to develop adherence with mucosa, lowering the elimination rate from the gastrointestinal tract (GIT). When the nanoparticle adheres to the GIT mucosa the drug absorption is enhanced since it is maintained for more time close to the absorption site. Although PVM/MA shows unspecific adherence, it is possible to insert targeting groups on the developed drug carrier, which will be adhered to specific sites according to the profile of the administered drug [30], [32], [45]. The polymer is sensitive to water, and it is completely hydrolyzed in a few hours. For this reason, the use of a cross-linker agent to stabilize the nanoparticle structure was proposed. Nevertheless, the encapsulation efficiency of the PVM/MA nanoparticles is quite low - below 5% in the most cases. Hence its association with cyclodextrins, dextran or PEG was proposed as an alternative to improve the nanoparticles loading efficiency [35], [37], [50]. Although it is possible to find few studies about the PVM/MA hydrolysis as a bulk polymer, film or discs, up-to-now no study was developed to analyze the polymer

hydrolysis and its consequences over the plain or cross-linked nanoparticles structures. Moreover, the influence of the pH of the medium on the polymer hydrolysis over the polymeric colloidal structures remains unknown.

Understanding the polymeric matrix behavior under relevant physiological conditions is crucial to the development of more efficient drug delivery systems. For this reason, the first aim of this work was to investigate the velocity of the hydrolysis of the polymer, and the effect of polymer hydrolysis on the nanoparticles structure, considering the environmental pH conditions the nanoparticle will face after oral administration along gastro intestinal tract, altering their capacity to keep the loaded active substance.

The second goal of my work was the development and characterization of a new nanocapsules system employing PVM/MA. The development of nanocapsules can circumvent PVM/MA-nanoparticle drawbacks enhancing the drug loading and encapsulation efficiency and keeping the ability of the PVM/MA to develop adhesiveness with the mucosa along the GIT. Although so many possibilities to apply the PVM/MA nanoparticles as a drug carrier were seen, there is no report about the development of a nanocapsules formulation for oral drug delivery. Indeed, PVM/MA nanocapsules can, theoretically, combine the mucus adherence of the polymer and the higher capacity of the oil core of solubilizing poorly water-soluble drugs, improving the efficiency of the colloidal carrier. The chosen oil was medium-chain triglycerides (MCT), which has been already reported as an enhancer of drug absorption, increasing the bioavailability of orally administered drugs [51], [52].

An appropriate characterization of the yielded nanosystems was needed. For that, dynamic light scattering (DLS), nanoparticle tracking analysis (NTA), static light scattering (SLS), and transmission electron microscopy (TEM) were employed to size measurements and structure elucidation, and laser Doppler anemometry was applied to determine their zeta potential.

The behavior of PVM/MA nanoparticles was analyzed by dynamic light scattering (DLS) and nanoparticle tracking analysis (NTA). The techniques were applied to determine the particle size immediately after the preparation of nanoparticles and to monitor its changes over time as a consequence of the polymer hydrolysis, at its intrinsic pH or under different pH conditions that mimic those observed in the gastrointestinal tract – pH 1.2, 5.0 and 7.4. NTA was especially useful to observe the dissolution of the nanoparticles after polymer hydrolysis, due to the change in the

density of the polymeric matrix. Together with zeta potential determination, the pH measurement was used to detect the progression of polymer hydrolysis over time.

Particle size determination of nanocapsules was performed using DLS and static light scattering (SLS), which is a helpful technique to evaluate the presence of particles at micrometer range and the formation of aggregates. Zeta potential was applied to determine the external charge of the particles, which is related to its stability against aggregation.

Freeze-fracture and cryo-TEM were used to size determination and to elucidate the ultrastructure of both colloidal systems.

Attenuated total reflectance - Fourier transform infrared (ATR-FTIR) spectroscopy was applied initially for the characterization of PVM/MA and also for the qualitative evaluation of polymer hydrolysis in different pH conditions.

Auto-titration of the nanoparticles formulation with NaOH was employed to evaluate the velocity of the hydrolysis of PVM/MA as a function of pH.

Benchtop-NMR imager was employed to resolve the hydration and swelling of PVM/MA discs. The technique was applied to predict the velocity of hydration of bulk PVM/MA under sink conditions. Magnetic resonance imaging (MRI) is a non-invasive technique, which can provide cross-sectional images from inside solid materials and living organisms. The images are formed from the nuclear magnetic resonance signal which is generated by certain nuclei when subjected to a strong magnetic field and irradiated with radio waves. MRI is based on using a magnetic field to encode the NMR signal with spatial information. The NMR signal is intrinsically weak. Therefore MRI is generally only applied to samples containing  $^1\text{H}$  nuclei in high concentrations, is mostly applied to measures the distribution of water inside the samples. Using a permanent magnet technology, the benchtop-NMR (BT-NMR/MRI) instrument is employed to detect the total amount of protons and their spin-lattice ( $T_1$ ) and spin-spin ( $T_2$ ) relaxation times, permitting relaxometry measurements and imaging. BT-MRI machines use low magnetic field (0.5 Tesla), and for this reason, their sensitivity and resolution are limited. However, its resolution is enough to resolve the hydration and swelling of different kinds of tablets, being useful for pharmaceutical research [53]–[55].

EPR spectroscopy is a non-invasive technique widely applied in different research fields like physics, chemistry, and biology. EPR spectroscopy permits the quantitative measurement of micropolarity, microviscosity and, using special probes, it is also possible to quantify microacidity and oxygen content inside a sample. Stable free radicals, such as nitroxides, are widely employed as model drug reporting the microenvironment of pharmaceutical formulations [56]–[58]. Electronic paramagnetic spectroscopy (EPR) was used to evaluate the microenvironment of the nanostructures and their ability to retain the molecule used as a drug model.



## **2. Materials**

Poly(methyl vinyl ether-alt-maleic anhydride) – PVM/MA,  $M_w$  216000,  $M_n$  80000, batch MKBP4375V, and 1,3-diaminopropane (DP) were purchased from Sigma Aldrich, Germany. TEMPO-benzoate (4-hydroxy-2,2,6,6-tetramethylpiperidine 1-oxyl benzoate) was obtained from Aldrich Chem. Co., USA. Medium chain triglycerides (MCT) (Miglyol 812/Neutraloel), were purchased from Sasol, Witten, Germany. Buffer substances (potassium chloride, citric acid, sodium phosphate dibasic, potassium phosphate monobasic and sodium hydroxide) were of pharmaceutical grade. All other substances and solvents were of reagent grade and were used as received from the suppliers.

## **3. Methods**

### **3.1. Nanoparticle preparation**

The polymeric nanoparticles (NP) were prepared by solvent displacement method [12], following a previously established method [29]. Briefly, the polymer was dissolved in acetone (20 mg/mL), and the acetone solution was poured into water/ethanol mixture under magnetic stirring (acetone:ethanol:water 1:1:1, v/v). The organic solvent was evaporated under reduced pressure at 40 °C. Cross-linked nanoparticles (NP-DP) were prepared by the addition of the cross-linker agent 1,3-diaminopropane (DP). For that purpose, DP (0.118 mg DP/mg Polymer) was dropwise added to the nanoparticles immediately after solvent evaporation step under gentle magnetic stirring, and the formulation was kept under gentle magnetic stirring for more five minutes.

### **3.2. Preparation of Medium Chain Triglycerides (MCT) nanocapsules**

The polymeric nanocapsules were prepared by interfacial polymer deposition after solvent displacement following H. Fessi and co-workers, 1989. [12]. The polymer poly(methyl vinyl ether-alt-maleic anhydride) – PVM/MA, was used as the coating shell and the medium chain triglycerides (MCT) was used as the oil core. The polymer-oil ratio was 1 mg PVM/MA to 4 mg MCT. Three different concentrations of polymer-oil mixture were tested and named as NC I, NC II and NC III, Table 1.

**Table 1.** Polymer and oil concentration in the water phase.

Formulation	Polymer Concentration (mg/mL)	Oil Concentration (mg/mL)	Polymer + Oil concentration (mg/mL)	Polymer + Oil concentration (% w/v)
NC I	0.75	2,96	3.71	0.37
NC II	1.50	5,93	7.43	0.74
NC III	2.25	8.90	11.15	1.11

PVM/MA and the MCT were dissolved in 10 mL of acetone. The acetone solution was dropwise injected into 20 ml of bi-distilled water stirred by magnetic stirrer at 1200 rpm or by a rotor-stator mixer at 11500 rpm (ULTRA-TURRAX IKA 10, Germany). The organic solvent was evaporated under reduced pressure at 40 °C, forming the nanocapsules. The formulations were cross-linked with 1,3-diaminopropane (DP), at final Polymer:DP molar ratio 4:1 (0.118mg DP/mg Polymer) or 2:1 (0.237mg DP/mg Polymer). The DP was added to the formulation immediately after the solvent evaporation and incubated for 5 minutes under gentle magnetic stirring, (NC+DP 4:1 and NC+DP 2:1).

### **3.3. Particle size measurements**

#### **3.3.1. Dynamic light scattering**

Dynamic light scattering (DLS, Zetasizer Nano ZS, Malvern Instruments) was applied to determine the hydrodynamic diameter of nanoparticles (NP) and nanocapsules (NC). The samples were diluted ten times (0.2 mg/mL) in filtered (0.2 µm) bi-distilled water and measured three times at 25 °C with a scattering angle of 173° applying automatic settings and general purpose algorithm. The nanoparticle formulations were measured at 30 minutes, 3, 6, 10 and 24 hours after preparation, while the nanocapsule formulations were measured at 1, 24, 48 hours and 7 days after preparation. At least three samples of each formulation were measured.

#### **3.3.2. Nanoparticle tracking analysis**

Nanoparticle tracking analysis (NTA, NS300, Nanosight, Malvern Instruments) was applied to determine the size distribution of nanoparticles formulations (NP). To perform the measurements, the samples were diluted in filtered (0.2 µm) bi-distilled water, at a volume ratio of 1:200000 or 1:10000 (0.1 or 2 µg PVM/MA/mL). Five videos, 60 s long, were recorded for each sample. The NanoSight was equipped with a 642 nm laser, and the measurements were performed at 25 °C. The sCMOS camera was

set automatically and the focus adjusted visually. The software used to collect and analyze the data was NTA 3.1 Build 3.1.54. The nanoparticle formulations were measured, concomitantly with DLS measurements.

### **3.3.3. Static light scattering**

Static light scattering (SLS) (Mastersizer 2000, Malvern Instruments, UK) was employed to determine the particle size distribution of nanocapsules (NC). The nanocapsule formulations were injected into the instrument until an optical obscuration of 5%. Each sample was analyzed in quintuplicate over 10 seconds, and the results were averaged. At least three different samples from each formulation were analyzed. The particle size was determined concomitantly with DLS measurements at 1, 24, 48 hours and 7 days after preparation.

### **3.4. Zeta potential measurements**

The zeta potential of nanoparticles (NP) and nanocapsules (NC) was measured by electrophoretic laser doppler anemometry (Zetasizer Nano ZS, Malvern Instruments). The samples were diluted ten times (1:10) with KCl 0.1 mM, and the zeta potential determined three times for each, at 25 °C. Nanoparticles were analyzed at 30 minutes, 3, 6, 10 and 24 hours after preparation and the nanocapsules at 1, 24, 48 hours and 7 days after preparation, always after the particle size determination.

### **3.5. pH measurements**

The pH of all formulation, nanoparticles (NP) and nanocapsules (NC), was measured (Inlab semi-micro electrode, Mettler-Toledo) just before the determination of zeta potential.

### **3.6. Transmission electron microscopy – Freeze-Fracture and Cryo**

For transmission electron microscopy the samples were freeze-fixed using propane jet-freeze device JFD 030 (BAL-TEC, Balzers, Liechtenstein). Afterwards, the samples were freeze-fractured at -150 °C without etching with a freeze-fracture/freeze etching system BAF 060 (BAL-TEC, Balzers, Liechtenstein). The surfaces were shadowed with platinum (2 nm layer, shadowing angle 45°) and subsequently with carbon (20 nm layer, shadowing angle 90°). The replica was floated into a sodium chloride solution (4% available chlorine) for 30 minutes, rinsed in distilled water for 10 minutes, then

washed in 30% acetone for 30 minutes and finally rinsed in distilled water for 10 minutes. After that, the replica was mounted on copper grids coated with a Formvar film and observed with an EM 900 transmission electron microscope (Carl Zeiss Microscopy, Jena, Germany) operating at 80 kV. Pictures were taken with a Variospeed SSCCD SM-1k-120 camera (TRS, Moorenweis, Germany). The following nanocapsule samples were analyzed by transmission electron microscopy after freeze-fracture: NC I, NC II, NC III, NC I-DP 2:1 and NC I –DP 4:1 all of them were freshly prepared; NC I 24 hours after preparation. Freshly prepared plain and cross-linked nanoparticles samples (NP and NP-DP, respectively) were also analyzed.

Vitrified specimens for cryo-TEM were prepared by a blotting procedure, performed in a chamber with controlled temperature and humidity using a LEICA grid plunger. A drop of the sample (20 mg/mL for NP and 3.7 mg/ml for NC) was placed onto an EM grid coated with a holey carbon film (C-flat<sup>TM</sup>, Protochips Inc., Raleigh, NC). Excess liquid was then removed with a filter paper, leaving a thin film of the sample spanning the holes of the carbon film on the EM grid. Vitrification of the thin film was achieved by rapid plunging of the grid into liquid ethane held just above its freezing point. The vitrified specimen was kept below 108 K during storage, transferred to the microscope and investigated. Specimens were examined with a LIBRA 120 PLUS instrument (Carl Zeiss Microscopy GmbH, Oberkochen, Germany), operating at 120 kV. The microscope is equipped with a Gatan 626 cryo-transfer system. Images were taken with a BM-2k-120 Dual-Speed on axis SSCCD-camera (TRS, Moorenweis, Germany). Cryo-TEM was used to analyze the nanocapsule formulation NC I and the NP formulation after 24 hours of preparation.

### ***3.7. Impact of pH of the medium on the nanoparticles***

The impact of the medium pH over the nanoparticles has been analyzed as follows. Immediately after preparation the nanoparticles formulation was diluted (10 mg/mL) with different buffers solutions at pH 1.2 (NP:pH 1.2), 5.0 (NP:pH 5.0) and 7.4 (NP:pH 7.4). The size of the diluted formulation was measured by DLS and NTA at 30 minutes, 3, 6, 10 and 24 hours after preparation, under the same conditions described above. Zeta potential and pH were also measured at the same time points, following the protocol already described. Hydrochloric acid/potassium chloride (HCl/KCl) buffer solution pH 1.2, citric acid/phosphate buffer solution pH 5.0 and phosphate buffer solution (PBS) at pH 7.4 were prepared in accordance with USP31. For the formulation

diluted in phosphate buffer solution was necessary to adjust the pH to 7.4 by addition of NaOH 1M.

### ***3.8. Impact of polymer concentration on the DLS results of nanoparticles***

Hydrolyzed nanoparticle formulations at low concentration (0.02%) were analyzed by DLS. For that, nanoparticle formulations were prepared and left at room temperature for 24 hours in order to hydrolyze the polymer. Just before the DLS measurements, the hydrolyzed nanoparticles were diluted in filtered (200 $\mu$ m) bi-distilled water, HCl/KCl buffer solution pH 1.2 or in PBS pH 7.4 to achieve a final polymer concentration equal to 0.02% w/v. The final pH of the diluted samples was 1.2 for those diluted in HCl/KCl buffer solution, 3.5 for those diluted in bi-distilled water and 7.4 for those diluted in PBS. The measurements followed the protocol already described, however multiple narrow mode algorithm (MNM) was applied.

### ***3.9. Impact of pH of the medium on the nanocapsules***

In order to evaluate the polymer hydrolysis and the formulation stability at different pH conditions, the particle size of plain and cross-linked nanocapsules was measured in different buffer solutions (HCl/KCl buffer solution pH 1.2, citric acid/phosphate buffer solution pH 5.0, and PBS pH 7.4, prepared according to USP31). For that, after 24 hours of preparation, 100  $\mu$ L of the formulation were added to 900  $\mu$ L of buffer solution and incubated for 5 minutes, then, the particle size and pH were measured using DLS according to the protocol described for nanocapsules size determination.

### ***3.10. ATR-FTIR – Attenuated total reflectance - Fourier transform infrared spectroscopy***

An IFS28 (Bruker) equipped with Thermo Spectra-Tech, ZnSe crystal and incidence angle of 45° was applied at room temperature. An average of 32 scans in the region of 4000-680  $\text{cm}^{-1}$  with a resolution of 2  $\text{cm}^{-1}$  was used. To promote polymer hydrolysis, PVM/MA was dispersed in bi-distilled water (20mg/mL) and kept under gentle stirring at 67 °C for 5 hours [59] after that it was kept at room temperature for more 24 hours. The final solution was then freeze-dried for 24 hours (Christ Alpha 1-2, Martin Christ, Germany). Hydrolyzed-PVM/MA and PVM/MA were mixed at a mass fraction of hydrolyzed-PVM/MA equal to 0, 10, 20, 30, 40, 50, 60, 70, 80, 90, and 100%. For the evaluation of polymer hydrolysis in nanoparticle formulations, 1 mL of the formulations

was taken at the time points 30 minutes, 3, 6, 10 and 24 hours after preparation. The samples were dried under reduced pressure at 40 °C for 20 minutes. The dried samples, including the bulk polymer, were kept under vacuum and solubilized in THF immediately before the analysis.

### **3.11. Benchtop <sup>1</sup>H NMR Imaging experiment**

PVM/MA discs (3.9 mm height x 13 mm diameter) were produced by pressing 600 mg of polymer in manual hydraulic press (Specac 15T, Specac) at 2 tons for 30 seconds under vacuum. Each disc was placed inside a 15-mm glass tube, over a layer of glass beads (~3mm) which in turn was over a perforated support. The tube was immersed in a flow-through cell containing 900 mL of PBS pH 7.4, at 37 °C, and flow rate 50 mL/min, according to the European Pharmacopoeia 8.0 recommendations on dissolution testing. For MRI measurements, the tube was withdrawn from the flow-through cell at the following time points: 10, 30, 60, 120, 150, 180, 210, 240, 300 minutes. A 20 MHz, 0.5 T NMR benchtop system (Maran DRX 2, Oxford Instruments) was used to resolve the hydration and swelling of polymeric discs. A standard spin-echo sequence was applied with an echo time (TE) of 6.8 ms; repetition time (TR) of 300 ms and acquisition time of about 10 minutes for each image; number of scans = 32; image size = 64 x 64 pixel; field of view = 20 mm x 20 mm.

### **3.12. Nanoparticle Titration**

Fifteen milliliters of NP were pre-titrated (DL 21, Mettler, Germany) to pH 2.9 (NaOH 0.01 M), pH 5.0 or 7.4 (NaOH 0.1 M). Afterwards, the auto-titrator maintained the pH at the pre-titrated values throughout the experiment by adding the necessary volume of NaOH. The experiment ran for 420 minutes for pH 5.0 and 7.4 and for 600 minutes for pH 2.9, and the cumulative consumption of NaOH was recorded. The NaOH consumption was investigated in triplicate at room temperature for all three different pH condition.

### **3.13. EPR spectroscopy**

#### **3.13.1. Nanoparticle loaded with TEMPO-benzoate**

PVM/MA nanoparticles loaded with TB (NP-TB) were prepared by solvent displacement [12], following a previously established method [29]. Briefly, the polymer (20 mg/mL) was dissolved in acetone containing TB (1 mM). The PVM/MA-TB acetone

solution was then poured into water/ethanol mixture under magnetic stirring (acetone:ethanol:water 1:1:1, v/v). The organic solvent was evaporated under reduced pressure at 40 °C. EPR spectra were acquired at 5 minutes, 1 and 24 hours after preparation. In order to evaluate the effect of the pH of the medium on the nanoparticles structure, the freshly prepared formulation was diluted (1:1) in PBS pH 7.4 and the EPR spectra acquired immediately after dilution and after 1 hour. The EPR spectra were recorded at 9.5 GHz (X-Band; Miniscope MS 200) from Magnettech (Berlin; Germany). The measurements were performed with the following typical parameters:  $B_0$ -field: 335.4 mT; scan range: 7.64 mT, scan time: 60 s, modulation amplitude: 0.04 mT.

### **3.13.2. Nanocapsules loaded with TEMPO-benzoate**

To prepare nanocapsules loaded with the spin probe TEMPO-Benzoate (TB) the same protocol described above was applied with the following change. Briefly, TB was solubilized in MCT (7.24 mM), and the MCT-TB was added to the PVM/MA/acetone solution. The organic solution was then injected into the aqueous phase. After the organic solvent evaporation, the water volume of the formulation NC I-TB was reduced given the final concentration of TB equal to 0.15 mM. The NC I -TB formulation was dialyzed (SpectraPor MWCO: 6-8000, Spectrum Laboratories, Inc.) against HCl/KCl buffer pH 1.2 or in PBS pH 7.4 over 24 hours at room temperature under gentle magnetic stirring. EPR spectra were acquired immediately after preparation and after 24 hours for non-dialyzed and after 24 hours of dialysis. EPR spectra were recorded at 9.5 GHz (X-Band; Miniscope MS 200) from Magnettech (Berlin; Germany). The measurements were performed with the following typical parameters:  $B_0$ -field: 335.4 mT; scan range: 7.64 mT, scan time: 60 seconds, modulation amplitude: 0.04 mT. The software Nitroxide Spectra Simulation, version 4.99-2005 were applied to analyse the acquired data.

## 4. Results and discussion

### 4.1. PVM/MA investigation

#### 4.1.1. ATR-FTIR spectroscopy

PVM/MA as received and its hydrolyzed form were analyzed by ATR-FTIR spectroscopy. Besides, mixtures of these two forms at different mass ratios, from 10 to 90% of hydrolyzed-PVM/MA, in steps of 10%, were also subjected to ATR-FTIR spectroscopy. The acquired spectra are shown in Fig. 3.

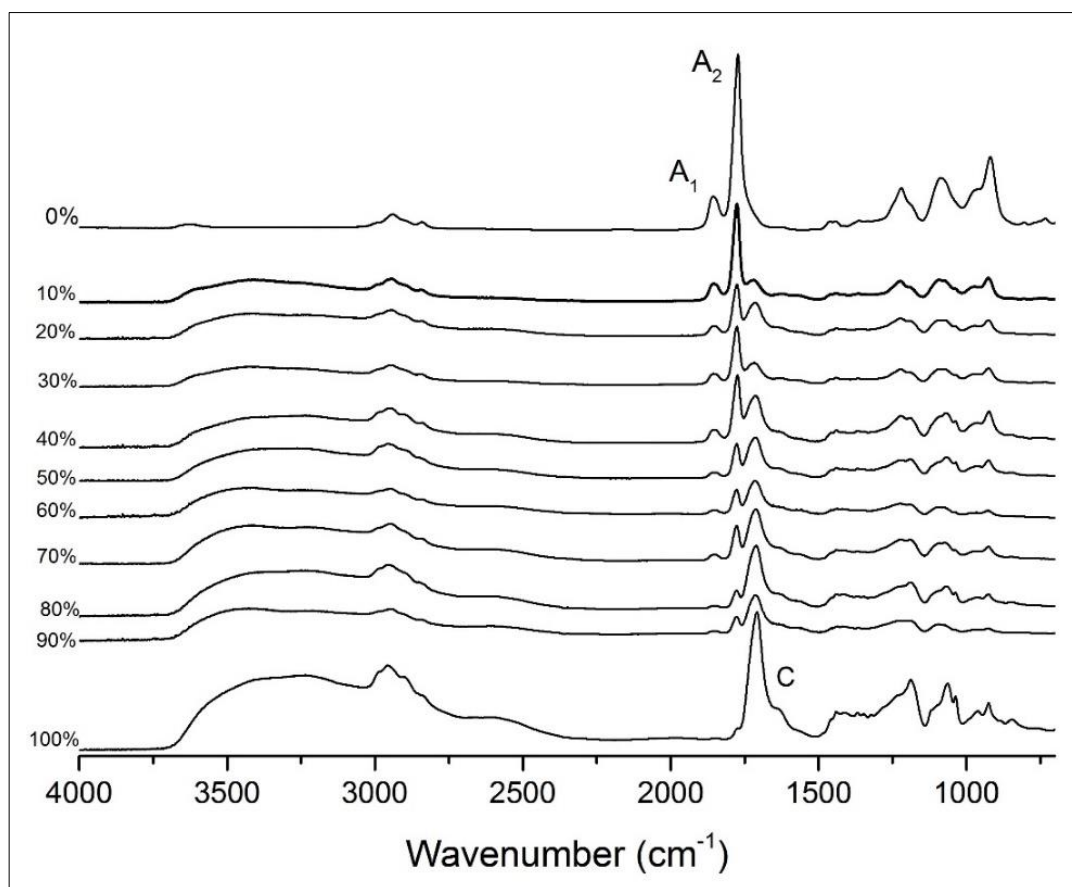


**Fig. 3.** ATR-FTIR spectra of PVM/MA as received from suppliers (0%), hydrolysed-PVM/MA (100%) and of mixtures of both at different mass fractions, from 10 to 90% of hydrolysed-PVM/MA. C=O stretching vibration: maleic anhydride at 1860 and 1780 cm<sup>-1</sup> (A<sub>1</sub> and A<sub>2</sub>) and carboxylic acid at 1710 cm<sup>-1</sup> (C). O-H stretching vibration: carboxylic acid: 2400-3400 cm<sup>-1</sup>.

The most characteristic bands of PVM/M are that related to carbonyl (C=O) stretching vibration of the anhydride group. These bands appear at 1860 cm<sup>-1</sup> and 1780 cm<sup>-1</sup> and are indicated in the figure above as A<sub>1</sub> and A<sub>2</sub>, respectively. When hydrolyzed, each anhydride group form two carboxylic acids that present two typical bands. The first is a sharp band at 1710 cm<sup>-1</sup>, and is related to stretching vibration of carbonyl groups, this band is identified as C in the figure above. The second one is a strong signal



between  $2400\text{ cm}^{-1}$  and  $3400\text{ cm}^{-1}$ , which is related to stretching vibration of hydroxyl groups (OH).

A reduction of the intensity of the anhydride carbonyl bands was observed when the amount of hydrolyzed-PVM/MA was increased from 10 to 90% on the mixture. Since the formation of carboxylic acid is the product of the anhydride hydrolysis the carbonyl band, C, increased at the same time, as well as the hydroxyl band.

#### 4.1.2. Benchtop $^1\text{H}$ NMR Imaging experiment

Benchtop  $^1\text{H}$  NMR Imaging was used to monitor the hydration of PVM/MA discs over time and under sink conditions. Fig. 4 shows axial side images of PVM/MA disc measuring 13 mm diameter and 3.9 mm height. After excitation by a radio-frequency pulse, the nuclear magnetization returns to equilibrium via relaxation, which is characterized by two relaxation times: spin-lattice relaxation time ( $T_1$ ), which describes the exponential recovery of the equilibrium; spin-spin relaxation time ( $T_2$ ), which describes the exponential decay of the precessing component of the magnetization. Relaxation times strongly depend upon the local environment and, in general,  $^1\text{H}$  nuclei associated with solids decay rapidly and therefore may be undetectable, while  $^1\text{H}$  nuclei associated with liquids decay according to their molecular mobility. So, the resultant NMR signal is the free induction decay [53], [55]. The dark areas observed are related to low spin densities or to short  $T_1$  relaxation times, characteristic of solids, and represents the dry parts of the disc. The brighter areas are related to water immobilization into the polymer matrix, in that area, the spin density is higher, and the relaxation time  $T_1$  is longer than in the solid dry material. The repetition time applied to the samples was shorter than the  $T_1$  of free water in the medium, as a consequence, its magnetization does not return to the equilibrium and is not acquired. Thus, monitoring the bright outside area and dark area inside the disc, it was possible to monitor the water penetration inside the disc.

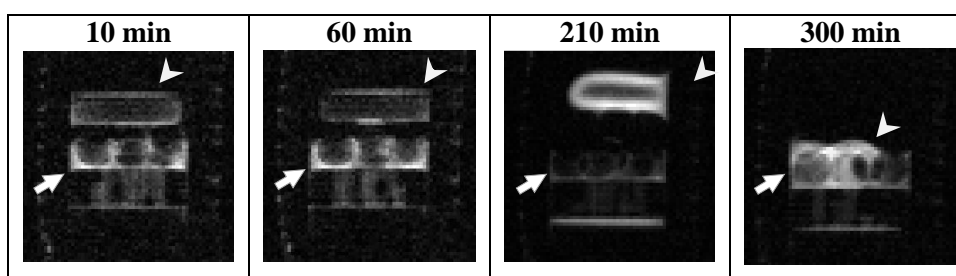


**Fig. 4.** BT-MRI image of a 3.9 mm height PVM/MA disc (arrowhead) placed on a layer of glass beads on a perforated support (arrows), inside a flow-through cell with 900 mL of PBS pH 7.4, flow rate 50 mL/min at 37 °C.

At the initial stages of the experiment, the disc showed a thin bright layer outside indicative of the presence of water adsorbed on its surface, this layer was corresponded to 0.43 mm. At 180 minutes the bright layer was thicker, and the disc height was 5.2 mm, 40% larger than at the beginning of the experiment, indicative of a swelling process. The hydration rate at this time point was 7.2  $\mu\text{m}/\text{min}$ . After 210 minutes it was possible to observe erosion of the swollen disc, although the disc core was still dry. Its height at this time point was 4.8 mm and the hydrated layer corresponds to 1.7 mm on the upper and lower faces of the disc. A progressive mass loss of 0.2 mm in each face was also observed at 270 minutes, (data not shown). The mass loss is characteristic of the matrix degradation after water penetration and swelling. Finally, after 300 minutes the disc collapsed completely. Roughly, the disc hydration occurs at a rate of 13  $\mu\text{m}/\text{min}$ , or 216 nm/s, at pH 7.4.

The results obtained are in agreement with a preliminary work that showed the dissolution of PVM/MA compressed discs follow three steps characterized by (i) solvent penetration into the compressed disc and initial polymer swelling (the lag time), (ii) formation of a hydrated layer on the disc surface and the attainment of a maximum hydrated layer thickness and (iii) polymer dissolution [60]. The hydration of the polymer matrix was visible as a thin bright layer on the disc surface during the first phase of the swelling process. It was possible to follow the hydration, swollen and degradation of the outer part of the disc whereas the inner part remained dry. Afterwards, the disc matrix started to disintegrate and, finally, collapsed completely after 300 min of the experiment.

### **4.1.3. Conclusion**

ATR-FTIR spectroscopy was applied for the polymer characterization before its application to produce the colloidal formulations. The acquired spectrum showed the polymer did not have signal of hydrolysis, being in conditions to be used. The technique was useful to identify the increasingly concentration of hydrolyzed-PVM/MA in the mixture non-hydrolyzed PVM/MA and hydrolyzed PVM/MA. The set of ATR-FTIR spectra obtained by this mixture may be used as a reference for the qualitative analysis of the extent of polymer hydrolysis in the colloidal formulation.

The MRI data permit an estimation of the kinetics of dissolution of the bulk polymer under sink conditions. Although the instrument has a limited resolution, was possible to estimate the rate of the water penetration in the macroscopic disc-like structure and

extend the results to the nanoparticles predicting the rate of polymer hydrolysis in an aqueous medium. The rate hydrolysis of the polymeric nanostructure was estimated 216 nm/s, at pH 7.4, which suggests the instability of the polymeric nanoparticles at neutral conditions.

## **4.2. PVM/MA Nanoparticles – study of polymer hydrolysis**

### **4.2.1. Particle size, zeta potential, and pH measurements**

#### **4.2.1.1. Plain nanoparticles (NP)**

DLS and NTA techniques determine the diffusion coefficient of the dispersed particles under Brownian motion. From diffusion coefficient, the hydrodynamic diameter can be calculated using Stokes-Einstein equation, equation

Equation 1 
$$D_H = \frac{kT}{3\pi\eta D}$$

Where:  $D_H$  = Hydrodynamic diameter  
 $K$  = Boltzmann constant  
 $\eta$  = solvent viscosity  
 $D$  = Diffusion coefficient

DLS measures the fluctuations of the scattered light due to the motion of particles dispersed or dissolved in a liquid medium as a function of time. The theoretical background considers that the particles are spherically shaped and do not interact with each other. However, most particles are nonspherical and may be hydrated and solvated, and several algorithms are available for different kind of samples. The hydrodynamic diameter distributions obtained from DLS are intensity weighed distributions, which is highly sensitive to the volume of the particle, since the scattering power is directly proportional to the sixth power of the particle diameter. Thus, the resultant diameter can be biased by a very small amount of big particles. Given the intensity distribution, the volume distribution and the number distributions can be calculated using either the Mie or Rayleigh-Gans-Debye theories [61]–[64]. The NTA device has a high-sensitivity camera (sCMOS) coupled to an optical microscope, that can visualize the center of the scattered light correspondent to each particle individually. Each particle is recorded and tracked by the software. The analysis of the images gives the displacement coefficient which is used to calculate the particle size. This technique provides the average numbers of particles, instead the intensity weighted distribution. Although the intensity of scattered light of particles with the same refractive index is higher for larger particles, the method is less sensitive to the

presence of larger particles when compared to DLS. The NTA can also provide an estimation of particle concentration since the number of particles is counted and the sample volume is known. NTA is based on the tracking of single particles while DLS measures a bulk of particles. Consequently, DLS collect a large amount of statistical data [65]–[67].

The suitable polymer concentration of the freshly prepared nanoparticles for size determination by DLS was determined by measuring the formulation in different polymer concentrations: 0.2 mg/mL, 1 mg/mL, 2 mg/mL and 4 mg/mL. For that, immediately after preparation, the nanoparticle formulation was diluted in filtered bi-distilled water and measured at 25 °C under automatic settings, applying the general purpose algorithm, Fig. 5.

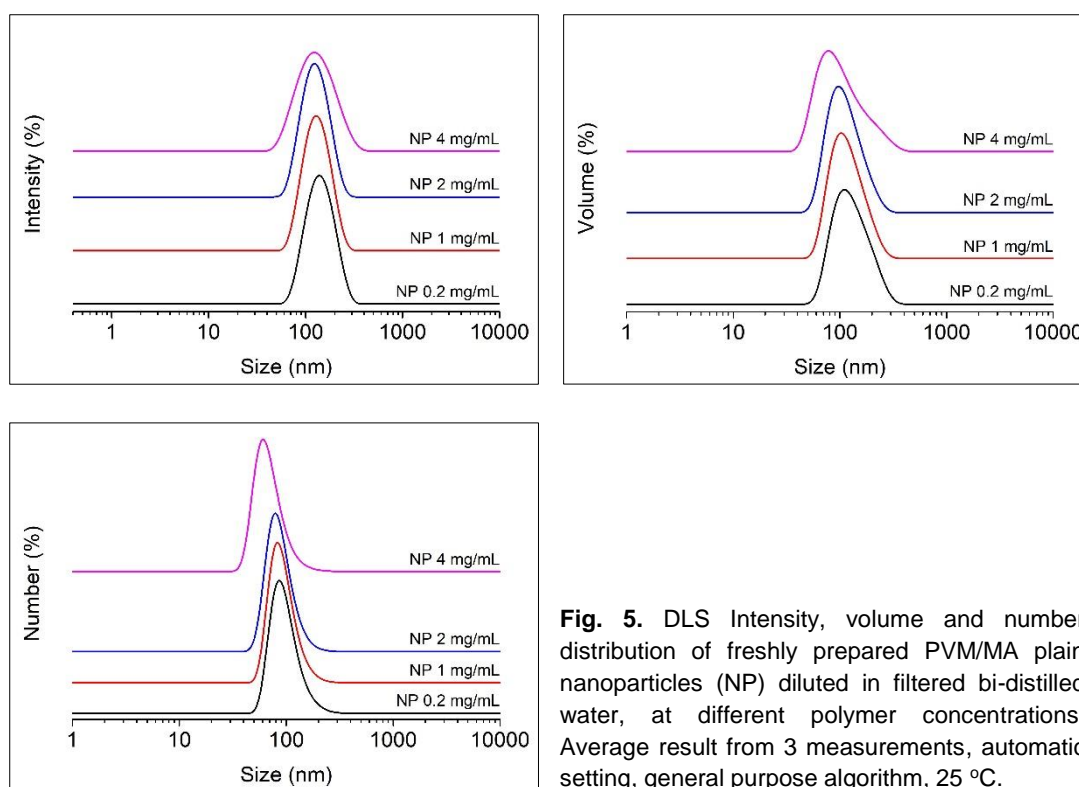


**Fig. 5.** DLS Intensity, volume and number distribution of freshly prepared PVM/MA plain nanoparticles (NP) diluted in filtered bi-distilled water, at different polymer concentrations. Average result from 3 measurements, automatic setting, general purpose algorithm, 25 °C.

No obvious effect of concentration on the particle size was observed in the range between 0.2 mg/mL and 2 mg/mL. Similar results of intensity, volume and number distributions indicates the particles are stable in this concentration range. Thus, the polymer concentration of 2 mg/mL was selected for size measurements.

For NTA measurements, it is necessary to adjust the focus of the camera to give a clear, sharp image of the particles. After a 60 seconds analysis time, at least 30 particles per frame have to be identified and no less than 200 completed tracks

recorded. Finally, the particle concentration should lie in a range between  $10^7$  and  $10^{10}$  particles/mL [67]. The final polymer concentration of freshly prepared nanoparticles that fulfilled all these conditions was  $0.1 \mu\text{g/mL}$ , a concentration 20000 times smaller than that applied to DLS measurements.

The mean particle size, zeta potential, and pH of plain PVM/MA nanoparticles were measured at the time point 0.5, 3, 6, 10, and 24 hours after preparation. Fig. 6 below shows the DLS and NTA outputs. DLS results showed that at the time point 0.5 hours the particle size was  $93 \text{ nm} \pm 12 \text{ nm}$  and the polydispersity index (Pdl) was 0.157, characteristic of a formulation with a narrow size distribution. The particle size increased progressively reaching  $283 \text{ nm} \pm 14 \text{ nm}$  after 10 hours. The Pdl was smaller than 0.2 over time. After the time point 10 hours the samples were considered too polydisperse to cumulant analysis. The results obtained with NTA showed similar tendency regarding the size,  $91 \text{ nm} \pm 23 \text{ nm}$  at time point 0.5 hours and  $213 \text{ nm} \pm 48 \text{ nm}$  after 6 hours. The standard deviation also increased from 25 nm to 100 nm, indicating the samples changed from relatively monodisperse to a polydisperse distribution. The particle concentration was stable until time point 3 hours, in a range of  $7 \times 10^8$  particles/mL, and decreased at the time point 10 hours to  $7 \times 10^7$  particles/mL. At 10 hours it was possible to detect particles and measure them only using a polymer concentration equal to  $2 \mu\text{g}$  of polymer/mL. A dilution 20 times smaller than that used at the beginning of the measurements at time point 0.5 hours. The number of particle per frame, that was higher than 30 for all measurements until 3 hours, decreased to about 4 particles/frame at time point 10 hours. (Appendix I, Table I).

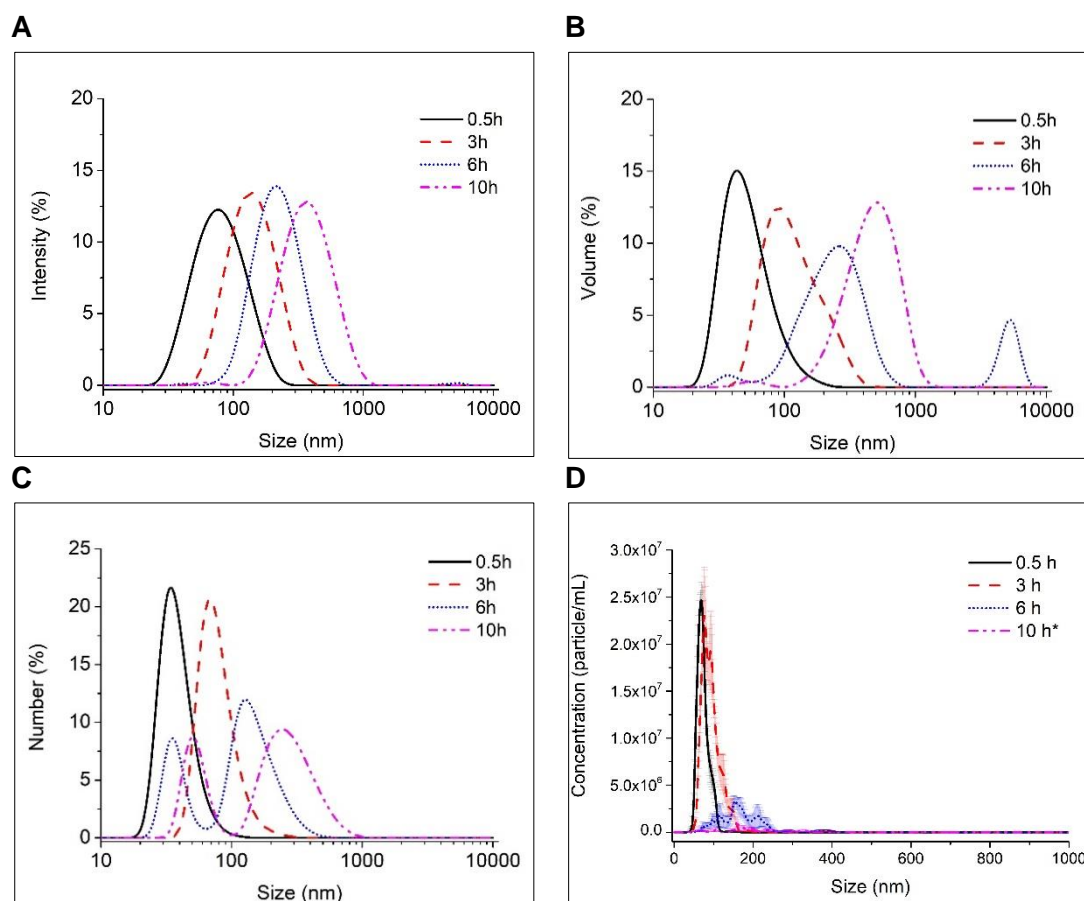


**Fig. 6.** Size distribution from DLS (A, B, and C) and NTA (D) measurements of PVM/MA plain nanoparticle (NP) at time point 0.5, 3, 6, and 10 hours after preparation. DLS: average result from 3 measurements (automatic setting, general purpose algorithm), the samples were diluted in filtered bi-distilled water at a final concentration of 2 mg polymer/mL. NTA: average result and standard error from 5 measurements, 60 s each, the samples diluted in filtered bi-distilled water; sample concentration 0.1 µg polymer/mL. \*sample concentration 2 µg polymer/mL.

The pH of the formulation dropped from  $2.76 \pm 0.16$  to  $2.29 \pm 0.01$ , even though moderate, the change can be detected and considered as an indicative of carboxylic acid formation, as already described in the literature [68]. The change in pH values was accompanied by an increase in zeta potential, from  $-30.5 \text{ mV} \pm 4.2 \text{ mV}$  to  $-21.7 \text{ mV} \pm 1.3 \text{ mV}$ , Table 2.

**Table 2.** pH and zeta potential of PVM/MA plain nanoparticles (NP) over time.

Formulation	Time (hour)	pH $\pm$ S.D.	Zeta Potential $\pm$ S.D. (mV)
NP	0.5	$2.76 \pm 0.16$	$-30.5 \pm 4.2$
	3	$2.52 \pm 0.14$	$-25.2 \pm 0.4$
	6	$2.31 \pm 0.06$	$-22.4 \pm 2.1$
	10	$2.27 \pm 0.02$	$-21.5 \pm 2.3$
	24	$2.29 \pm 0.01$	$-21.7 \pm 1.3$

Fig. 7 shows the NP formulation at three different time points, 0.5, 3 and 6 hours after preparation, the formulation that was clear whitish immediately after preparation became progressively clearer over time. The change in color is a macroscopically signal of the polymer hydrolysis.

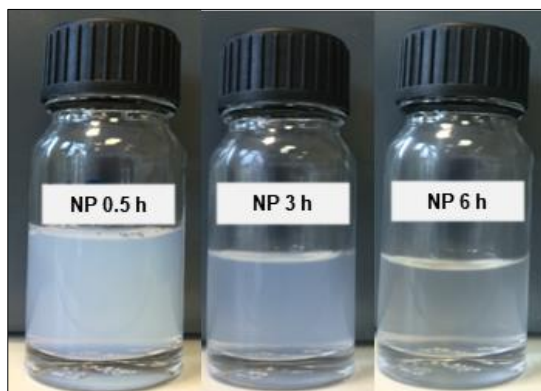


**Fig. 7.** PVM/MA nanoparticles formulation (NP) at time point 0.5, 3 and 6 hours after preparation.

The DLS results for the plain nanoparticle formulation (NP) showed an increase in the particles size until the time point 10 hours, and between 10 and 24 hours particle size remained constant. Although there were no apparent alterations on the results between 10 and 24 hours, the results did not achieve the quality criteria of the method at the latest time point. These results were expected since the needed conditions for the best DLS analysis were not fully achieved by the hydrolysed PVM/MA nanoparticles – spherical particles that do not interact with each other. The hydrolysis of the maleic anhydride yields two carboxylic acids that may promote particle interaction, depending on the pH of the medium. The formation of the carboxylic acid increases the polymer solubility in water [69] that leads to the dissolution of the nanoparticles. Thus, the polymeric chains give rise a charged net which may produce misinterpretation of the software outputs when the general purpose algorithm is applied.

The use of the NTA technique to measure particles size of the same samples analyzed by DLS is justified by the fact that NTA detection is a function of the difference between the refractive index of the sample and the refractive index of the medium, among other variables [67]. When the nanoparticles are formed, they are dense polymeric structures, which undergo dissolution in contact with water. Indeed, the NTA results showed that during the first 3 hours of the experiment the particles presented similar size, and the particle concentration was constant. However, after 6 hours the number of tracked particles was six times smaller, and at 10 hours it was not possible to detect particles, as may be seen in Fig. 6. At this time point, it was necessary to change the

samples dilution and use a concentration 20 times higher compared to that used for the time points 0.5, 3 and 6 hours, and it was still insufficient to perform the measurements.

The zeta potential of the plain nanoparticles became less negative over the first 10 hours and remained constant from 10 to 24 hours, as well as the pH of this formulation. These changes are related to the increase in free acid concentration caused by the hydrolysis of the anhydride groups. Zeta potential and pH results also suggest that the majority of polymer hydrolysis occurs during the first 6 hours of the existence of the nanoparticles in unbuffered conditions with intrinsic low pH values.

#### **4.2.1.2. Cross-linked nanoparticles (NP-DP)**

The DLS analysis showed that the mean particle size of cross-linked nanoparticles (NP-DP) at the time point 0.5 hour was  $157 \text{ nm} \pm 34 \text{ nm}$  and the Pdl was  $0.139 \pm 0.022$ . During the first 3 hours, the size of NP-DP increased to  $314 \text{ nm} \pm 81 \text{ nm}$  and the Pdl increased to 0.241, which is characteristic of a polydisperse system. Both parameters remained constant until the end of the analysis at time point 24 hours. Albeit the high polydispersity of the system, the quality of the analysis remained good over the 24 hours of the experiment. The same trending was observed with NTA – increasing in size and standard deviation during the first 3 hours. The size and standard deviation of NP-DP were  $151 \text{ nm} \pm 69 \text{ nm}$  and  $53 \text{ nm} \pm 22 \text{ nm}$ , respectively, larger than that observed for NP at the first-time point. Size and standard deviation then increased until the time point 3 hours, reaching  $320 \text{ nm} \pm 16 \text{ nm}$  and  $104 \text{ nm} \pm 7 \text{ nm}$ , respectively, and remained constant from 3 hours to 24 hours after preparation. Particle concentration was constant over time, being  $6.6 \times 10^8 \text{ particles/mL} \pm 1.5 \times 10^8 \text{ particles/mL}$  at time point 0.5 hour and  $4.9 \times 10^8 \text{ particles/mL} \pm 1.1 \times 10^8 \text{ particles/mL}$  at 24 hours, Fig. 8. (Appendix I, Table I).



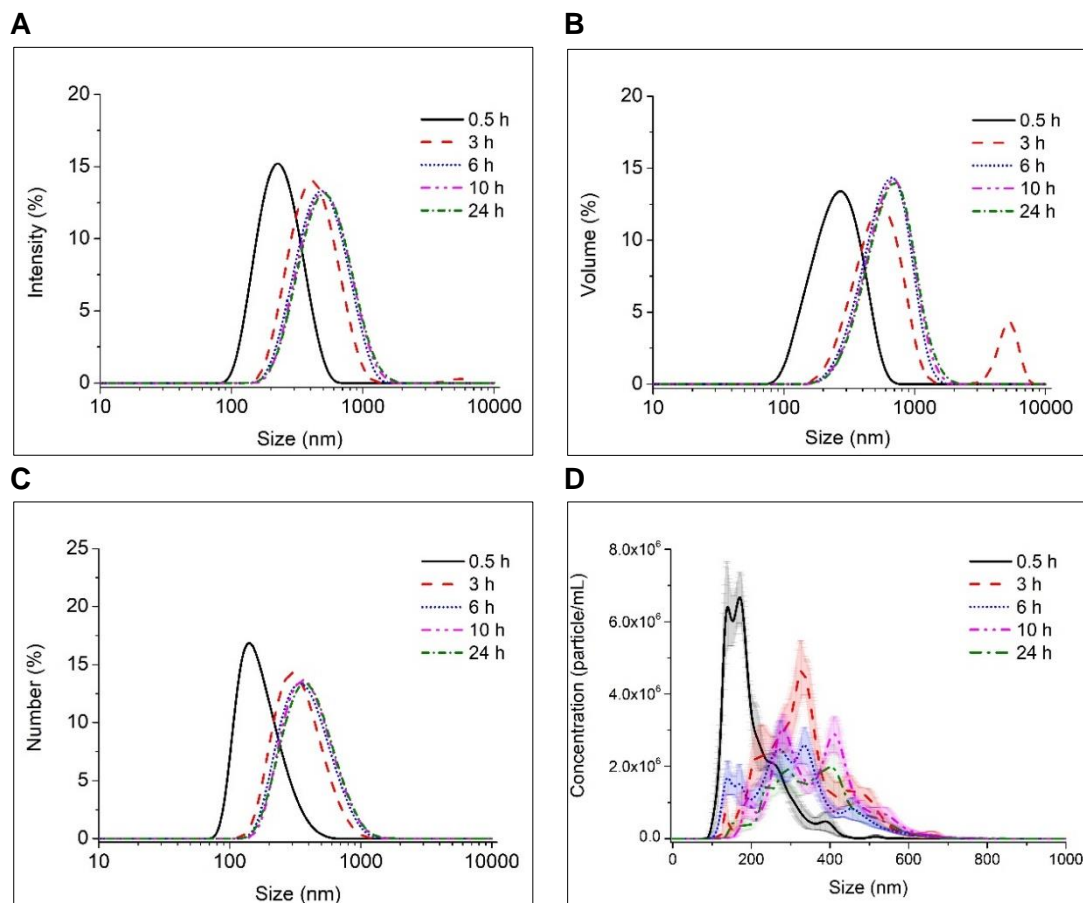


**Fig. 8.** Size distribution from DLS (A, B, and C) and NTA (D) measurements of PVM/MA-1,3-diaminopropane cross-linked nanoparticles (NP-DP) at time point 0.5, 3, 6, 10 and 24 hours after preparation. DP concentration was 0.118 mg DP/mg PVM/MA, the monomer:DP molar ratio was 4:1. DLS: average result from 3 measurements (automatic setting, general purpose algorithm) the samples were diluted in filtered bi-distilled water at a final concentration of 0.2% w/v. NTA: average result and standard error from 5 measurements, 60 s each, o the samples were diluted in filtered bi-distilled water; sample concentration 0.1  $\mu$ g polymer/mL.

The pH of NP-DP at 0.5 hours was  $4.46 \pm 0.36$ , less acidic when compared to that observed to NP, as expected after reaction of 1,3-diaminopropane with the anhydride groups. The pH at 3 hours was lower,  $3.81 \pm 0.42$ , indicating hydrolysis of remaining anhydride groups. After 3 hours, it continued constant until the end of the experiment, as well as the zeta potential, Table 3.

**Table 3.** pH and zeta potential of PVM/MA nanoparticles cross-linked with 1,3-diaminopropane (NP-DP) over time. DP concentration was 0.118 mg DP/mg PVM/MA, the monomer:DP molar ratio was 4:1.

Formulation	Time (hour)	pH $\pm$ S.D.	Zeta Potential $\pm$ S.D. (mV)
NP-DP	0.5	4.46 $\pm$ 0.36	-30.3 $\pm$ 1.4
	3	3.81 $\pm$ 0.42	-32.3 $\pm$ 3.4
	6	3.78 $\pm$ 0.33	-28.9 $\pm$ 3.1
	10	3.74 $\pm$ 0.37	-28.7 $\pm$ 2.5
	24	3.74 $\pm$ 0.32	-26.7 $\pm$ 2.3

Fig. 9 shows the plain nanoparticles (NP) and the cross-linked (NP-DP) formulations at 0.5 and 6 hours after preparation. The formulation containing cross-linked particles (NP-DP) maintains the same appearance after 6 hours. Even after 24 hours, it was not possible to visualize difference in the turbidity of the formulation.

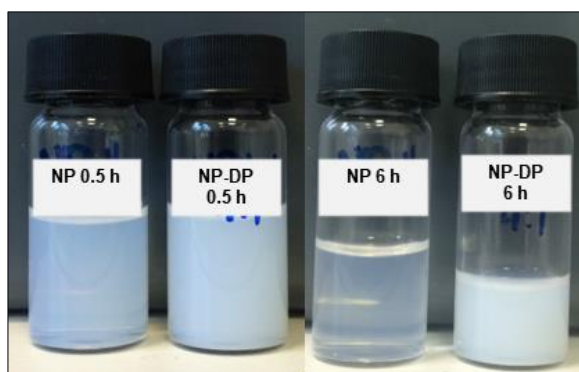


**Fig. 9.** PVM/MA plain (NP) and cross-linked nanoparticles (NP-DP) at time point 0.5, 3 and 6 hours after preparation. DP concentration was 0.118 mg DP/mg PVM/MA, monomer:DP molar ratio 4:1.

The particle size of NP-DP formulation increased during the first 3 hours and remained constant after this time point until the end of the measurements. The NTA data shows the system became more polydisperse during the first 3 hours and a decrease in the particle concentration until the time point 6 hours, however, it was still possible to detect the particles over the whole experiment. The mean diameter of the NP-DP formulation was larger than that observed for NP formulation at the initial time point. This observation may be explained by the rearrangement of the polymer chains after the reaction with the cross-linker agent, followed by the hydrolysis of the lasting maleic anhydride groups, as suggested by the pH and zeta potential results.

#### **4.2.2. Impact of pH of the medium on the plain and cross-linked nanoparticles**

The effect of pH of the medium on plain and cross-linked nanoparticles was evaluated after the dilution (50% v/v) of the freshly prepared formulation in three different buffers solutions - HCl/KCl buffer at pH 1.2 (NP:pH 1.2), citric acid/phosphate buffer pH 5.0 (NP:pH 5.0) and PBS pH 7.4 (NP:pH 7.4 and NP-DP:pH 7.4). NP:pH1.2 presented pH value about 1.3 from the beginning until the end of the experiment. The pH of NP:pH 5.0 was  $4.51 \pm 0.05$  at time point 0.5 and  $4.0 \pm 0.03$  at 3 hours. The pH of NP:pH7.4 was adjusted to  $7.4 \pm 0.7$  by addition of NaOH 1M.

##### ***Plain nanoparticles***

Particle size was analyzed by NTA and DLS, Fig. 10. The DLS results showed that the particles of NP:pH 1.2 formulation was smaller than that observed for the formulation in its intrinsic pH, being  $78 \text{ nm} \pm 11 \text{ nm}$  at 0.5 hours and  $180 \text{ nm} \pm 26 \text{ nm}$  at 10 hours. The Pdl was below 0.15 at the time point 0.5 and 3 hours; at 6 hours it was above 0.2, and at 10 hours it was higher than 0.3. From NTA data the distribution at 0.5 hours was narrower and sharper when compared to NP. Nevertheless, the particle concentration was a half that observed for the NP. The tendency was the same observed for the NP - increasing in size and standard deviation and decreasing of particle concentration over time. Besides the smaller particle concentration,  $3.2 \times 10^8$  particles/mL at 0.5 hour, the number of detected particles was also smaller at the same dilution, about 20 particle/frame. After 10 hours the particle concentration was 0.9 particles/mL, and only 4 particles/frame were detectable.

DLS results for NP:pH 5.0 at 0.5 hours were  $152 \text{ nm} \pm 14 \text{ nm}$  and Pdl equal to 0.101. At 3 hours the mean diameter was  $279 \text{ nm} \pm 36$  and the Pdl 0.273. Particle size measured by NTA was  $142 \text{ nm} \pm 39 \text{ nm}$  at 0.5 hours and  $239 \text{ nm} \pm 19 \text{ nm}$  at 3 hours after preparation. The particle concentration was  $14 \times 10^8$  particles/mL at 0.5 hour and  $7.5 \times 10^8$  particles/mL at the time point 3 hours.

Particles at pH 7.4 (NP:pH 7.4) were almost 300 nm and Pdl higher than 0.3 at time point 0.5 h. Following the same dilution applied for the other formulation was not possible to detect particles by NTA. In an attempt to detect particles and determine their size, a dilution of 1:10000 ( $2 \mu\text{g}$  of polymer/mL, as previously described for the NP) was applied and even in this condition was not possible to determine the particle size by NTA, since less than 10 particles/frame were recorded. (Appendix I, Table II).

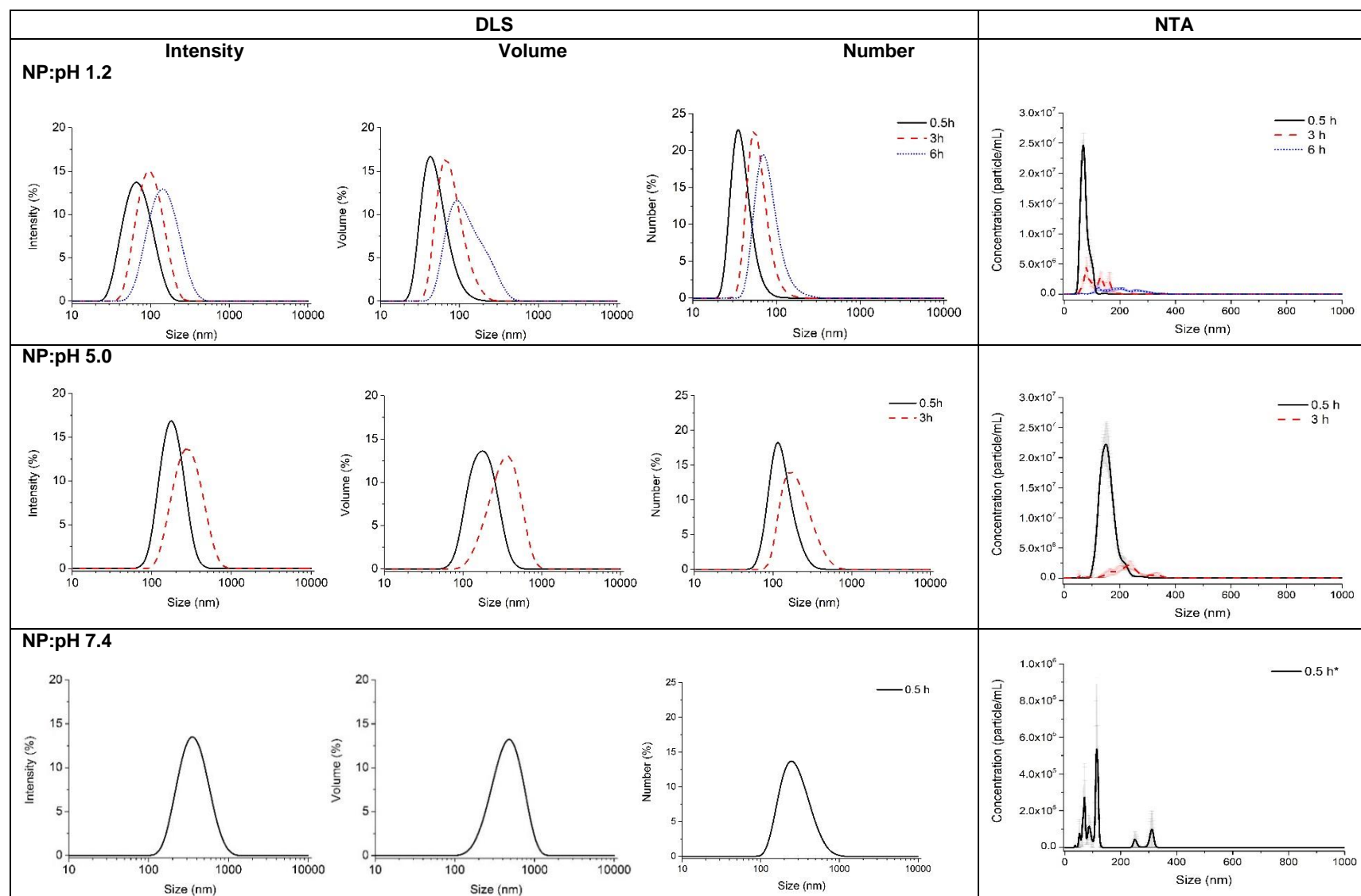


**Fig. 10.** Size distribution from DLS and NTA measurements of PVM/MA plain nanoparticle (NP) diluted in HCl/KCl buffer pH 1.2 (NP:pH1.2), in citric acid/phosphate buffer pH 5.0 (NP:pH 5.0), or in PBS pH 7.4 (NP:pH 7.4). Final polymer concentrations equal to 10 mg/mL. Time point 0.5, 3, 6, and 10 hours. DLS: average result from 3 measurements (automatic setting, general purpose algorithm), the samples were diluted in filtered bi-distilled water; sample concentration 1 mg polymer/mL. NTA: average result and standard error from 5 measurements (60 seconds each), the samples were diluted in filtered bi-distilled water; sample concentration 0.1  $\mu$ g polymer/mL. \*sample concentration 2  $\mu$ g polymer/mL.

Zeta potential of NP:pH1.2 was  $-10.0 \text{ mV} \pm 1.2 \text{ mV}$  at 0.5 hours and remained constant over the 10 hours of experiment. For the NP:pH 5.0 it varied from  $-47.9 \text{ mV} \pm 2.9 \text{ mV}$  at 0.5 hour to  $-40.5 \text{ mV} \pm 4.9 \text{ mV}$  at 3 hours. NP:pH 7.4 presented zeta potential equal to  $-54.2 \text{ mV} \pm 1.0 \text{ mV}$ . The numbers reflect the protonation of the hydroxyl groups, being more positive at acidic medium when compared to the formulation at neutral pH.

A macroscopic comparison between the NP formulations at the different pH conditions over time can be seen below, Fig. 11. Formulations diluted in pH 5.0 and 7.4 (NP:pH 5.0 and NP:pH 7.4) showed lower turbidity 3 hours after dilution, when compared with the formulation diluted in water and that at pH 1.2 (NP:H<sub>2</sub>O and NP:pH 1.2). At the time point 10 hours all samples have a similar appearance, which is a macroscopic signal of the polymer hydrolysis.

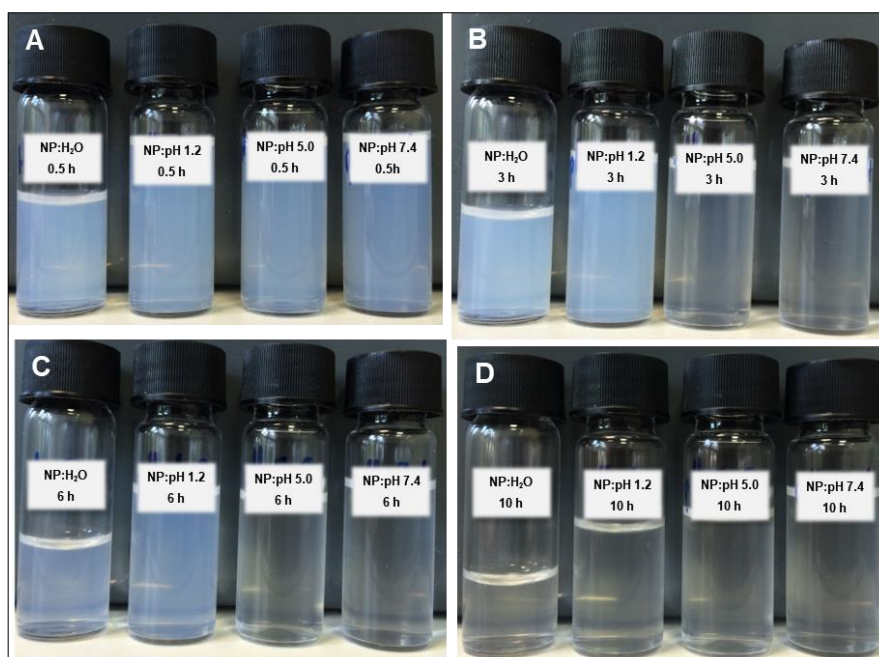


**Fig. 11.** PVM/MA plain nanoparticle diluted in bi-distilled water - NP:H<sub>2</sub>O, in HCl/KCl buffer pH 1.2 - NP:pH1.2, in citric acid/phosphate buffer pH 5.0 - NP:pH 5.0, and in PBS pH 7.4 -NP:pH 7.4 at time point 0.5 (A), 3 (B), 6 (C), and 10 (D) hours. Final polymer concentrations equal to 10 mg/mL.

The DLS results indicate the presence of particles until the later time points for all pH conditions tested. Although the size distribution became more polydisperse at earlier time points. For the formulation NP:pH 1.2 a pronounced change in polydispersity was observed at 6 hours. For NP:pH 5.0 it was observed at the time point 3 hours, and for NP:pH 7.4 at the very beginning of the experiment, at 30 minutes after preparation. The mean hydrodynamic diameter of NP:pH 1.2 was smaller than that observed for NP, remaining below 200 nm during the whole period of experiment. For the other two

pH conditions, the particle size was similar to that observed for NP at the later time points. The NTA data show that at all applied pH conditions accelerated the dissolution of the particles when compared to the formulation at its intrinsic pH. It may be seen by the decrease in the number of particles per frame and in the particle concentration at earlier time points. The rate of dissolution was accelerated as the pH increases, occurring in less than 30 minutes when the nanoparticles were submitted to a pH 7.4.

### **Cross-linked nanoparticles**

Cross-linked nanoparticles were analyzed after dilution in PBS pH 7.4 (NP-DP pH 7.4). The DLS results showed that the size and Pdl were constant over the whole experiment period, about 210 nm and 0.12, respectively. The NTA results also showed constant size and standard deviation over time – size 150 nm and standard deviation 50 nm, respectively Fig. 12, (and Appendix I, Table II).

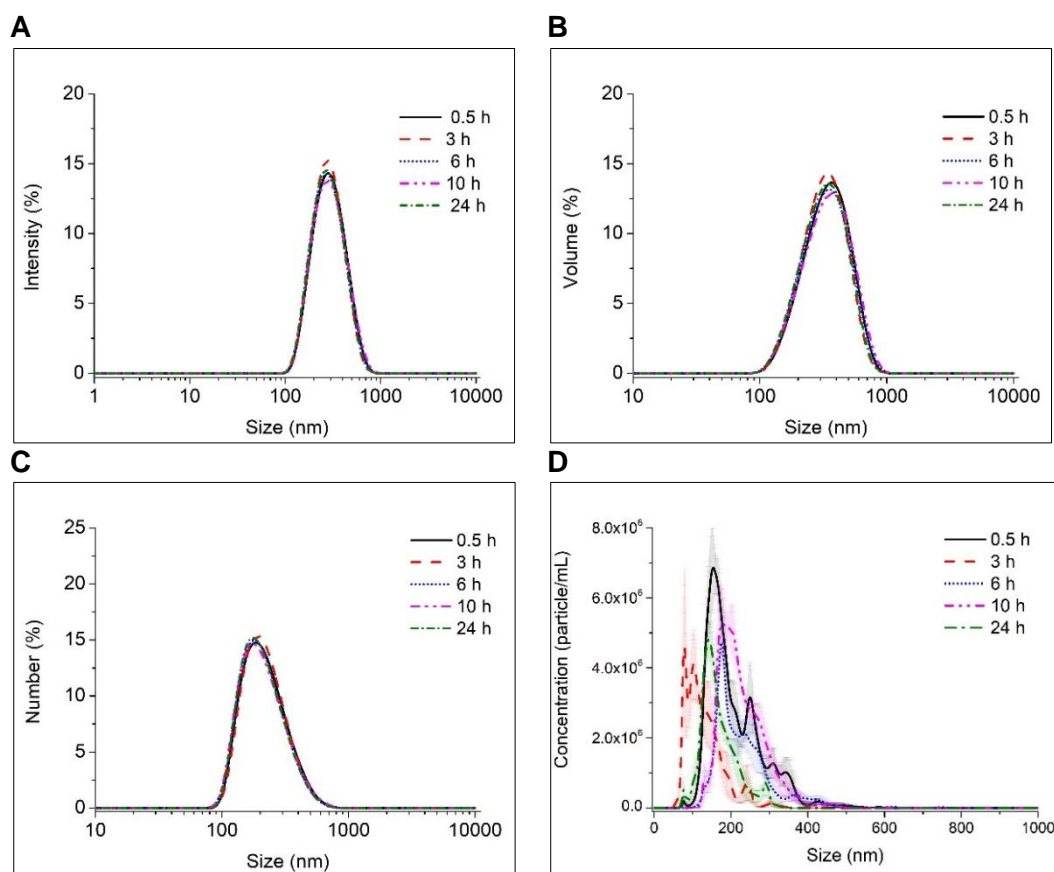


**Fig. 12.** Size distribution from DLS and NTA measurements of PVM/MA-1,3-diaminopropane cross-linked nanoparticles (NP-DP) diluted in PBS pH 7.4 (NP-DP:pH 7.4), at time point 0.5, 3, 6, 10, and 24 hours after preparation. Final polymer concentrations equal to 10 mg/mL. DP concentration was 0.118 mg DP/mg PVM/MA, the monomer:DP molar ratio was 4:1. DLS: average result from 3 measurements (automatic setting, general purpose), sample concentration 1 mg polymer/mL. NTA: average result and standard error from 5 measurements, 60 s each; sample concentration 0.1  $\mu$ g polymer/mL. The samples were diluted in filtered bi-distilled water.

When these results of NP-DP:pH 7.4 are compared to those obtained for NP-DP is possible to observe the particles are bigger at the first-time point, indicating, as expected, the hydrolysis of the remaining anhydride groups due to the pH of the medium. The hydrolysis reaction was accelerated and, gave at the first moment, the final particles size. The particles size of NP-DP:pH 7.4 is clearly different of NP:pH 7.4, the particles on latter were diluted immediately after the pH adjustment and was not possible to determine their size or even record a reliable number of particles by NTA. In conclusion, the polymer hydrolysis is a very fast process at neutral pH.

#### ***4.2.3. Impact of polymer concentration on the DLS results of nanoparticles***

The NTA analysis of the plain nanoparticle formulation strongly suggests that at the later time points, as 10 and 24 hours after preparation, the particles were solubilized. Similar results were observed when the particles were in acidic pH – 1.2 and 5.0, or in a neutral medium – pH 7.4. However, the DLS data suggests the presence of particles during the whole period of experiment, although the particles became larger and the size distribution broader.

In order to elucidate these results a formulation containing hydrolyzed polymer at low concentration (0.2 mg/mL) was analyzed by DLS. For that, a nanoparticle formulation was prepared and left at room temperature for 24 hours in order to hydrolyze the polymer. Immediately before the DLS measurements, the hydrolyzed nanoparticles were diluted in filtered (200 µm) bi-distilled water, or in filtered HCl/KCl buffer solution pH 1.2 or in PBS pH 7.4 to achieve a final polymer concentration equal to 0.2 mg/mL. The final pH of the diluted samples was 1.2 for those diluted in HCl/KCl buffer solution, 3.5 for those diluted in bi-distilled water and 7.4 for those diluted in PBS. The measurements followed the protocol already described. However, multiple narrow mode algorithm was used [63].

The use of low concentrated polymer solution intended to access what occurs with the polymer chain when it was in the different media. It is expected an interaction of the polymer chains with the solvent and with other polymer chains due to polyelectrolyte character of the polymer, and these interactions might be affected by the pH of the medium and by the polymer concentration. Using DLS technique is possible to estimate the polymeric chain size and its state of aggregation, thus clarifying the results obtained for hydrolyzed nanoparticles. The results are shown below in Fig. 13.

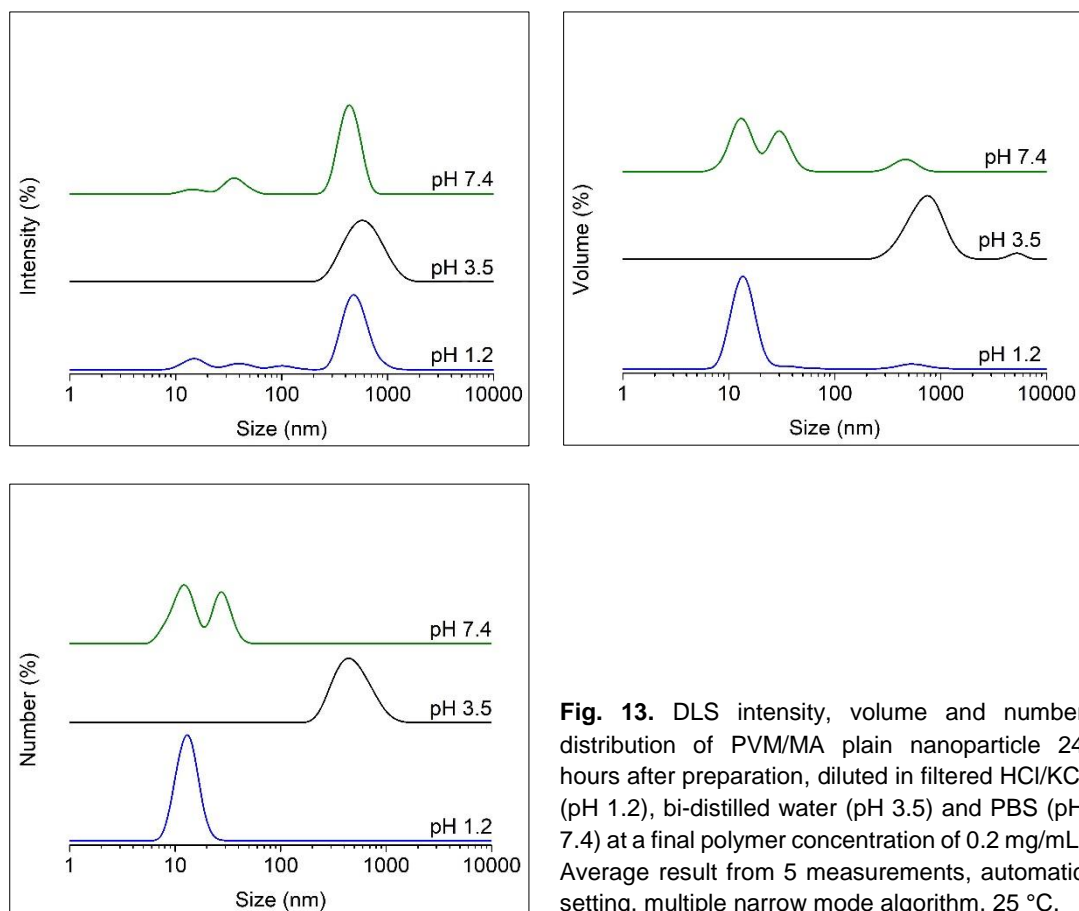


**Fig. 13.** DLS intensity, volume and number distribution of PVM/MA plain nanoparticle 24 hours after preparation, diluted in filtered HCl/KCl (pH 1.2), bi-distilled water (pH 3.5) and PBS (pH 7.4) at a final polymer concentration of 0.2 mg/mL. Average result from 5 measurements, automatic setting, multiple narrow mode algorithm, 25 °C.

Volume and number distributions show that the major part of the particles is in the range of 10 nm when at pH 1.2. While in pH 7.4, the size distributions show two peaks, in the range 10 nm and 200 nm. The sample diluted with water, pH 3.5, presents a shift of the mean size to the range of 500 nm, in this pH condition also volume and number size distributions are in the same range, about 500 nm.

The extension of the protonation of the hydrolyzed polymer certainly interferes on the interactions between the chains. In different pH conditions, different intra- and intermolecular interaction may occur. When the polymer is at pH 1.2, the carboxylic acid groups are protonated, Table 4. The absence of charge allows the carbon chain to assume the 'compact coil' conformation, folding over itself. The interactions of the polymer with the medium and with adjacent chains are minimized. For the polymer at pH 3.5 and pH 7.4, the protonated carboxylic acid groups are able to form hydrogen bonds giving rise to interactions between the polymer chains, and also intramolecular interactions. It was already described that the hydrolyzed polymer in its intrinsic pH conditions in 95% DMSO/5% water solution, at 20% of dissociation, forms stable aggregates and the chains are parallelly oriented [59]. The degree of dissociation of the polymer at pH 3.5 is similar to that described by Ladaviere and co-workers and,



although the medium here was different, the water may also interact with the polymer chain by means of hydrogen bonds. In this condition, the polymer chain can, therefore, forms aggregates, whose size may fall in the range of 200 and 1000 nm. When at pH 7.4, the extension of the polymer protonation is smaller, and the polymer interaction due to hydrogen bonds is consequently also smaller. Indeed, at pH 7.4, there are two peaks in the region between 5 and 50 nm. This may mean the existence of particle aggregation and elongated or rod structures whose dimensions are not adequately solved by DLS.

**Table 4.** Protonation of hydrolyzed PVM/MA in different pH conditions according to the Henderson-Hasselbalch equation.

	Deprotonation	
	1 <sup>st</sup> COOH pK <sub>a1</sub> 3.5	2 <sup>nd</sup> COOH pK <sub>a2</sub> 7.5
<b>pH 1.2 (HCl/KCl)</b>	0.5%	5 x 10 <sup>-5</sup> %
<b>pH 3.5 (H<sub>2</sub>O)</b>	50%	0.01%
<b>pH 7.4 (PBS)</b>	98.8%	44%

The estimation of the chain size of the hydrolyzed polymer may be roughly given by the mean-square end-to-end distance,  $(Re^2)^{1/2}$ , corrected by Flory's characteristic ratio,  $C_{\infty}$ , which can be seen as a measure of the stiffness of the polymer in a given ideal model. For chains with  $n$  bonds and bond angle  $\theta$ , the end-to-end distance can be calculated using Equation 2:

**Equation 2.**  $Re^2 = nl^2 C_{\infty}$

Where:  $n$  = number of steps  
 $l$  = vector describing a single step  
 $C_{\infty} = (1 - \cos \theta) / (1 + \cos \theta)$

The length of the repeat unit (the mer) is 5 carbons and the degree of polymerization is 1402 repeat units, the number of steps,  $n$ , is equal to 7010 steps. A single step is 154 pm – the length of the carbon-carbon bond, and the angle  $\theta$ , of the carbon bond, is 109.5°. Considering these numbers, the estimation of the size of one single chain of PVM/MA  $M_w$  216000, is 18 nm. The radius of gyration,  $R_g$ , which is based on the end-to-end distance of a freely-jointed chain is equal to 31 nm. The estimated end-to-end distance of the polymer chain is in agreement with the results obtained at pH 1.2, a condition in which intra- and intermolecular interaction are hindered by the protonation of the charged moieties. The results are also in agreement with the data published by Ladaviere and co-workers aforementioned [59].

#### 4.2.4. Transmission electronic microscopy – Freeze-Fracture and Cryo

Freshly prepared plain and cross-linked nanoparticles (DP and NP-DP) were submitted to freeze-fracture TEM. Representative photomicrographs are shown in Fig. 14. The nanoparticles present round structures with a rough surface in the range of 100 nm.

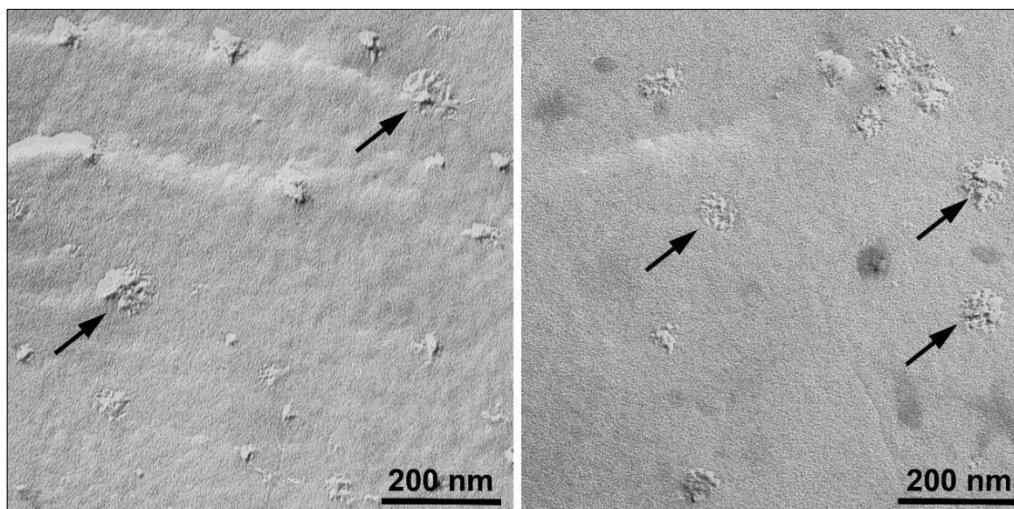


**Fig. 14.** Freeze-fracture-TEM micrographs of freshly prepared PVM/MA nanoparticles (arrows). (A) Plain nanoparticles (NP) and (B) cross-linked nanoparticles (NP-DP). DP concentration was 0.118 mg DP/mg PVM/MA, monomer:DP molar ratio was 4:1.

Cryo – TEM of nanoparticles after 20 hours of preparation, kept at room temperature in its intrinsic pH was also performed. The images, which are presented below in Fig. 15, show that at this time point it is not possible to observe nanoparticles, but agglomerates of the polymer without well-defined structures. These agglomerates present size in a broad range, from about 40 nm to about 100 nm.

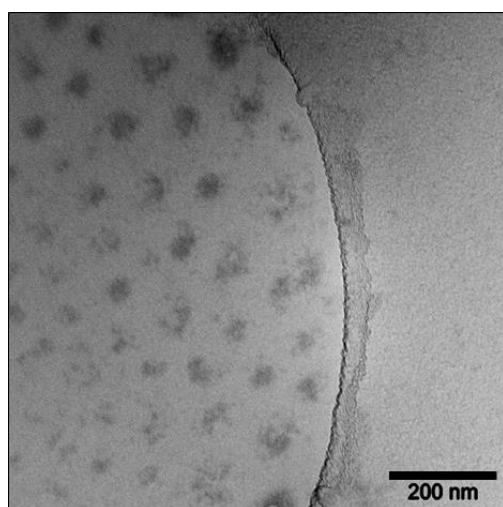


**Fig. 15.** Cryo-TEM micrographs of plain PVM/MA nanoparticles after 20 hours of preparation. Formulation at its intrinsic pH and kept at room temperature.

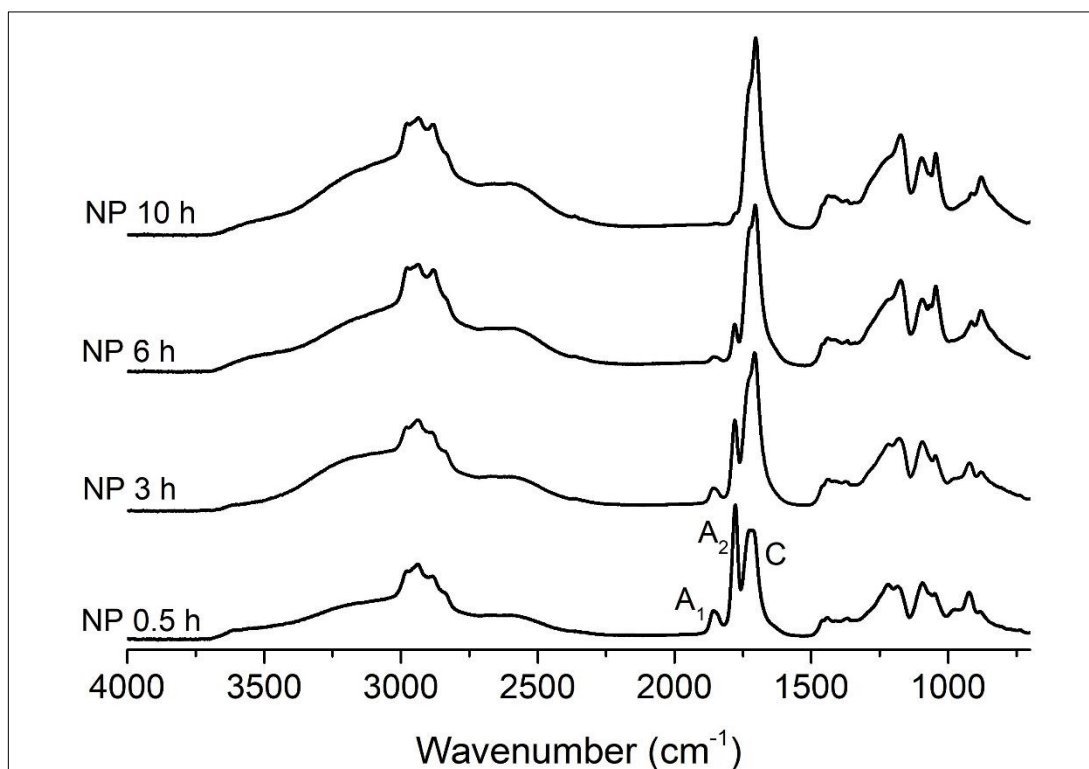
The combination of cryo- and freeze-fracture-TEM images provide additional information about the ultrastructure of the nanoparticles. The freeze-fracture images show round structures with a rough surface, which are almost parallel to the fracture plane. Generally, the fractured plane develops predominantly along areas of the samples with weak molecular interactions [70]. This fact may explain the flat and rough surface, considering the polymeric chains are interacting by weak electrostatic attractions. It is reasonable to propose the polymeric chains were split from each other at the level of the fracture plane.

The results obtained by Cryo-TEM are in agreement with the previous data obtained by DLS and NTA, that suggests the polymer in its intrinsic pH, at later time points, is already hydrolyzed and the particles do not exist anymore as a dense structure, but as aggregates. It is important to note that electron microscopy gives images in two dimensions of three-dimensional structures, for this reason, the interpretation of the results should be carefully analyzed and considered, for example, the different spatial orientation and overlapping of structures may lead to important misinterpretation.

#### **4.2.5. ATR-FTIR spectroscopy**

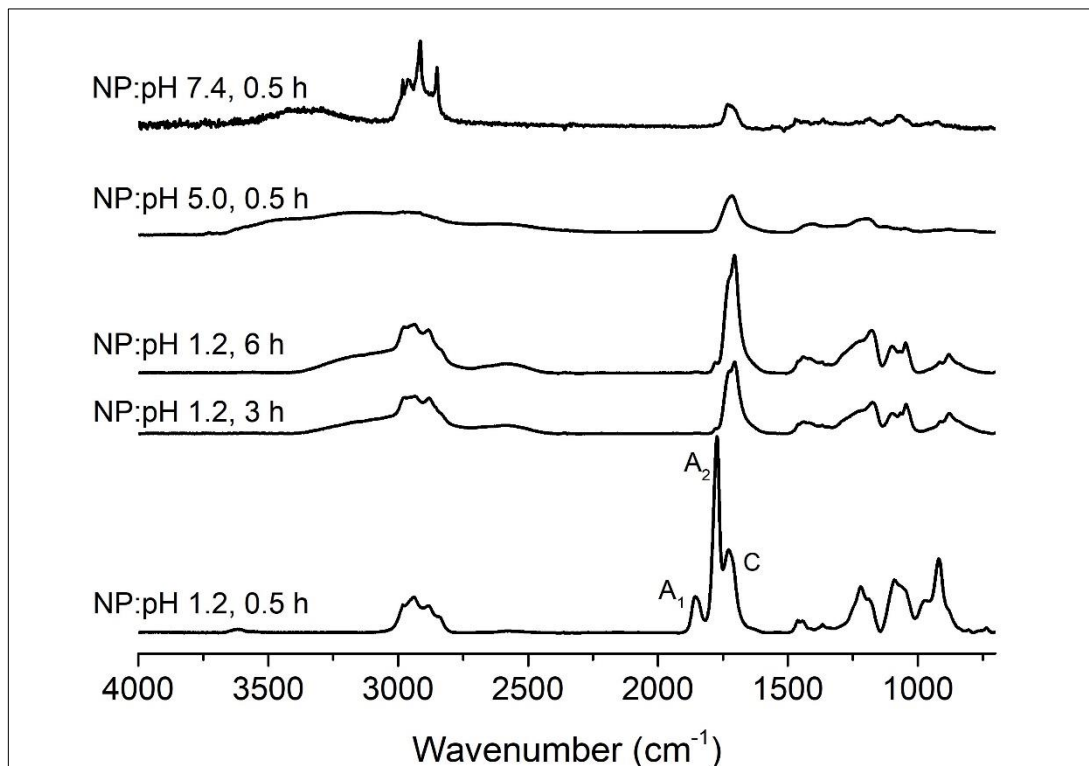
ATR-FTIR spectroscopy was applied to elucidate the progression of the PVM/MA hydrolysis of the formulation in its intrinsic pH and the effect of the pH on it. Infrared spectrum of PVM/MA has two characteristic bands of anhydride groups,  $A_1$  and  $A_2$ , at 1860 and 1780  $\text{cm}^{-1}$  respectively, as discussed before on the topic 4.1.1.

Fig. 16 shows the ATR-FTIR spectra of NP at different time points after preparation. The spectra of NP in its intrinsic pH show that at first time point, 30 minutes after nanoparticle preparation, the characteristic bands of carboxylic acid groups are already present. These bands arise from stretching vibration of carbonyl groups (C=O) at 1710  $\text{cm}^{-1}$  (C), and of hydroxyl groups (OH), between 2400 and 3400  $\text{cm}^{-1}$ . The carboxylic acid bands became strong with time, while the anhydride signal became smaller until completely disappear at the time point 10 hours.



**Fig. 16.** ATR-FTIR spectra of PVM/MA nanoparticles at its intrinsic pH (NP). At the defined time point the formulations were dried under vacuum and, immediately before the infrared analysis, solubilized in THF. C=O stretching vibration: Anhydride: 1860 and 1780  $\text{cm}^{-1}$  ( $A_1$  and  $A_2$ ) Carboxylic acid: 1710  $\text{cm}^{-1}$  (C). O-H stretching vibration: Carboxylic acid: 2400-3400  $\text{cm}^{-1}$ .

After dilution of the freshly prepared nanoparticle formulation (NP) in the three different buffer solutions at pH 1.2 (NP:pH 1.2), 5.0 (NP:pH5.0) and 7.4 (NP:pH7.4), according to the protocol already described, the final colloidal suspensions were dried under vacuum at the specified time points and the infrared spectra obtained. The results are shown in the Fig. 17. When the formulation was in pH 1.2 (NP:pH 1.2) a residual band of anhydride group can be seen at the time point 3 hours, this small signal is still visible until 6 hours after preparation. For the formulation NP:pH 5.0 or NP:pH7.4 only the carboxylic group bands can be seen at the first time point 0.5 hours.



**Fig. 17.** ATR-FTIR spectra of PVM/MA nanoparticles diluted in HCl/KCl buffer pH 1.2 (NP:pH 1.2), citric acid/phosphate buffer pH 5.0 (NP:pH5.0) or PBS pH 7.4 (NP:pH 7.4). At the defined time point the formulations were dried under vacuum and solubilized in THF immediately before the infrared analysis. C=O stretching vibration: Anhydride: 1860 and 1780 cm<sup>-1</sup> (A<sub>1</sub> and A<sub>2</sub>) Carboxylic acid: 1710 cm<sup>-1</sup> (C). O-H stretching vibration: Carboxylic acid: 2400-3400 cm<sup>-1</sup>.

Although the infra-red technique is difficult to use for quantitative determination, it is possible to compare the spectra of nanoparticle formulation to that spectra obtained from the analysis of progressively hydrolyzed polymer, showed in the first part of this work, in Fig. 3. An estimation of the polymer degradation is then possible by the comparison between the intensity of the signals of the anhydride and carboxylic acid bands. For NP at 0.5 hours after preparation, the intensity of the signal of anhydride and carboxylic groups are similar to that observed in 40% hydrolyzed PVM/MA. At the time point 3 hours, the signal of carboxylic acid groups is stronger than the anhydride group, and are comparable to the signal of 70% hydrolyzed PVM/MA. It is possible to see a weak signal of the anhydride band until 6 hours, roughly comparable to 80% or 90% of hydrolyzed PVM/MA.

A clear impact of the pH on the formulations was seen. NP:pH 1.2 showed a weak signal for anhydride band already at time point 3 hours, while NP:pH 5.0 and NP:pH 7.4 exhibited only the carboxylic acid bands at the time point 0.5 hours. This is an evidence that the polymer hydrolysis and, consequently, particle dissolution was

completed at the earliest moment after dilution of the nanoparticle formulation in those buffered media.

#### **4.2.6. Nanoparticle Titration**

The maleic anhydride groups of PVM/MA undergo hydrolysis in aqueous media forming carboxylic acid, and the polyacid formed decreases the pH of the medium. Moreover, the velocity of the hydrolysis reaction changes with the pH of the medium, being faster at higher pH values, as already discussed above. Employing the auto-titration was possible to investigate pH sensitivity of the polymer and the velocity of its hydrolysis at different pH values, which is a simple experiment to evaluate the kinetic of polymer hydrolysis.

For that purpose, the formulation was pre-titrated to pH 2.9 (NaOH 0.01M), a value slightly above the pH of the freshly prepared formulation ( $2.76 \pm 0.16$ ) and also to pH 5.0 and 7.4 (NaOH 0.1M). Afterwards, the formulation was auto-titrated with small amounts of NaOH (0.01M or 0.1 M) to neutralize the carboxylic acid yielded by the hydrolysis reaction until no more consumption of NaOH was registered.

The curves showed on Fig. 18 present three different phases: the first is related to the pre-titration to the required initial pH that was about 7 minutes for pH 7.4, 3 minutes for pH 5.0 and 2 minutes for pH 1.2. The second phase corresponds to the polymer hydrolysis and consequent consumption of NaOH to neutralize the yielded acid. Finally, the plateau that characterizes the end of the hydrolysis reaction. The time required to reach the plateau was 15 minutes for the formulation pre-titrated to pH 7.4 and 120 minutes for that pre-titrated to pH 5.0. For the formulation kept at the intrinsic pH, pH 2.9, it was necessary 400 minutes.

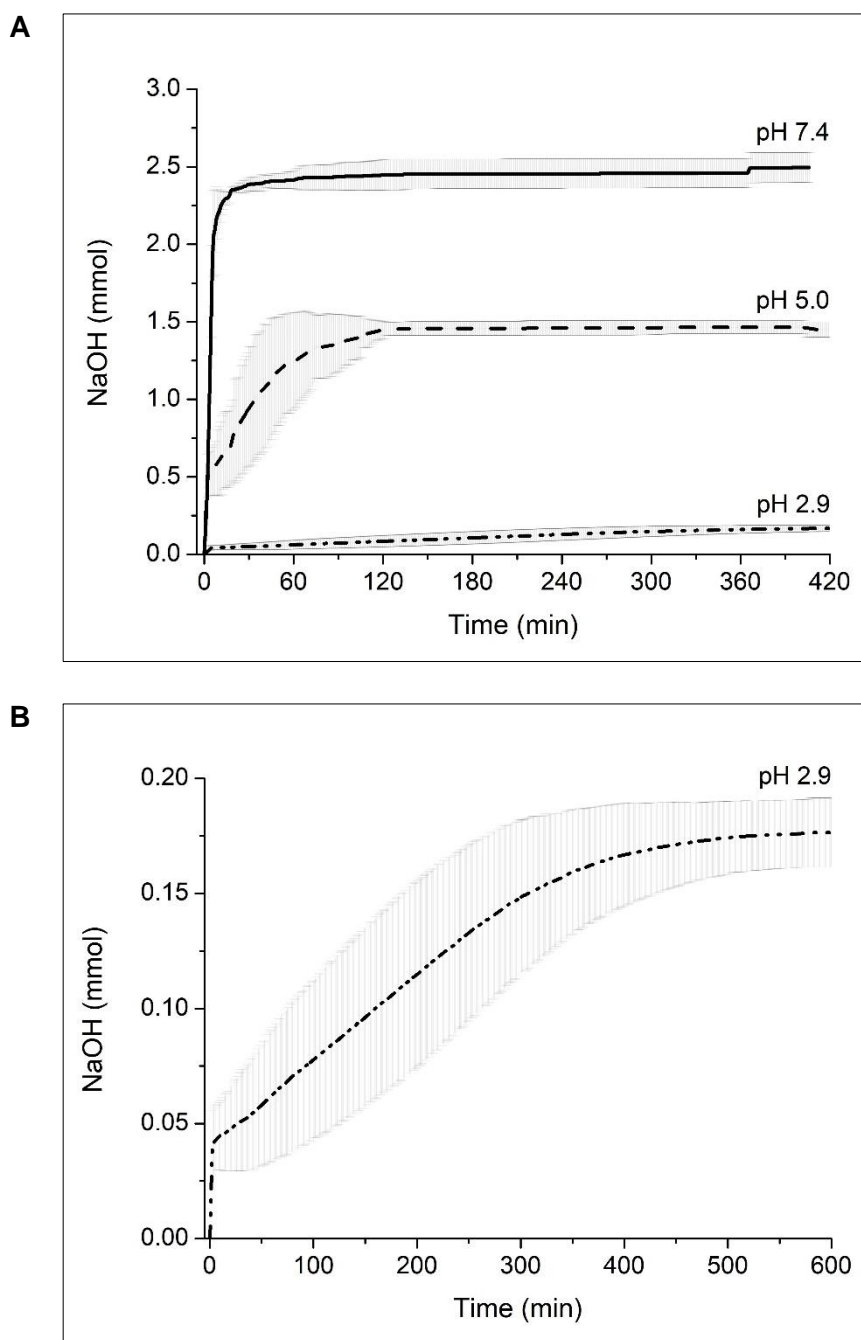


**Fig. 18.** Titration curve of PVM/MA Nanoparticles (A) and detailed curve of NP titration to pH 2.9 (B). The Nanoparticles were pre-titrated to pH 2.9 with NaOH 0.01 M and to 5.0 or 7.4 with NaOH 0.1 M and then titrated until no more consumption of NaOH was registered.

The titration curves indicate the hydrolysis of the polymer is faster at higher pH values. The consumption of NaOH was different for the analyzed pH values. The carboxylic acid groups are only ascertained by the pH-stat method when they are dissociated. The dissociation of an acid is determined by its  $pK_a$ . The estimated intrinsic  $pK_a$  of the hydrolyzed PVM/MA are  $pK_{a1} = 3.5$  and  $pK_{a2} = 7.5$  [71]–[73]. Thus, considering the total consumption of NaOH and the stoichiometry of the reaction, at pH 2.9 the dissociated

acid was 4%, at pH 5.0 it was about 30% and 60% at pH 7.4 when the plateau was reached. The results clearly show the fast hydrolysis of the polymer when it is at pH 7.4, being in agreement with NTA and ATR-FTIR results.

#### 4.2.7. EPR spectroscopy – Nanoparticles loaded with TEMPO-benzoate

Nanoparticles formulation loaded with the spin probe TB (NP - TB), at a final concentration of TB equal to 1 mM, was prepared following the previously described protocol and the EPR spectra were acquired at 5 minutes, 1 and 24 hours after preparation. Additionally, the freshly prepared formulation was diluted (1:1) in PBS pH 7.4, and the EPR spectra acquired immediately after dilution and after 1 hour of preparation.

The spin probe TEMPO-Benzoate, Fig. 19, is a lipophilic stable nitroxyl radical, its octanol-water partition coefficient is greater than 100 [74], presenting the log P value of 2.46. Thus, it can be considered a poorly water-soluble model drug [74], [75].

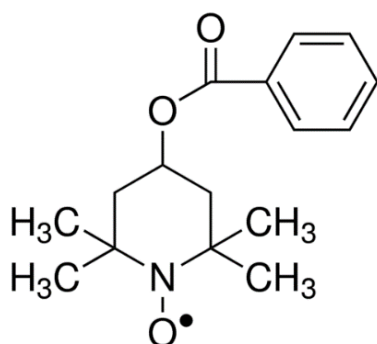


**Fig. 19.** Chemical structure of TEMPO-Benzoate TB. (representation of its the mesomeric form in a nonpolar environment)

The nitroxyl radicals are sensitive to the charge density of the milieu. Therefore, in a polar environment, the unpaired electron will be closer to the nitrogen atom whereas in a nonpolar environment it will be more localized at the oxygen atom, as shown above in Fig. 19. The hyperfine interaction of the unpaired electron of nitroxyl radicals with the nuclear spin of nitrogen nuclei produces three lines hyperfine splitting. The strength of the interaction between the unpaired electron and the nitrogen nuclei and consequently the spin density on the nitrogen atom is directly proportional to the distance between the first and the third peaks in an EPR spectrum ( $2a_N$ ). Hence, the micropolarity can be estimated by  $2a_N$  – more polar environments give larger hyperfine splitting or larger  $2a_N$ . The rotation correlation time,  $\tau_C$ , calculated from the signal amplitude and the peak-to-peak line width obtained from the EPR spectra, estimates the mobility of the spin-probe, giving the microviscosity of the medium.



The EPR spectrum of TB in MCT has a characteristic shape: a decreasing height of the three peaks of the hyperfine splitting. It happens because TB molecules are not spherical and experience a reduced mobility in two of three directions, and it is more pronounced when the spin probe is in a viscous environment - the higher the viscosity, the lower the mobility [58], [76], [77].

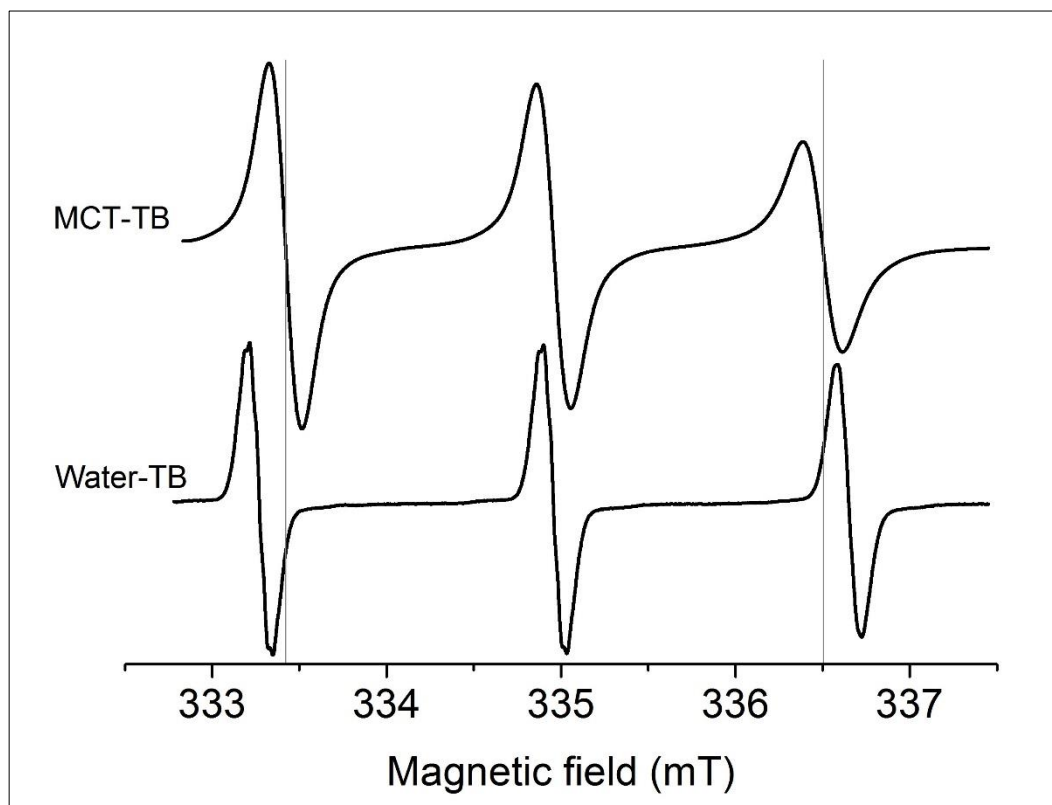
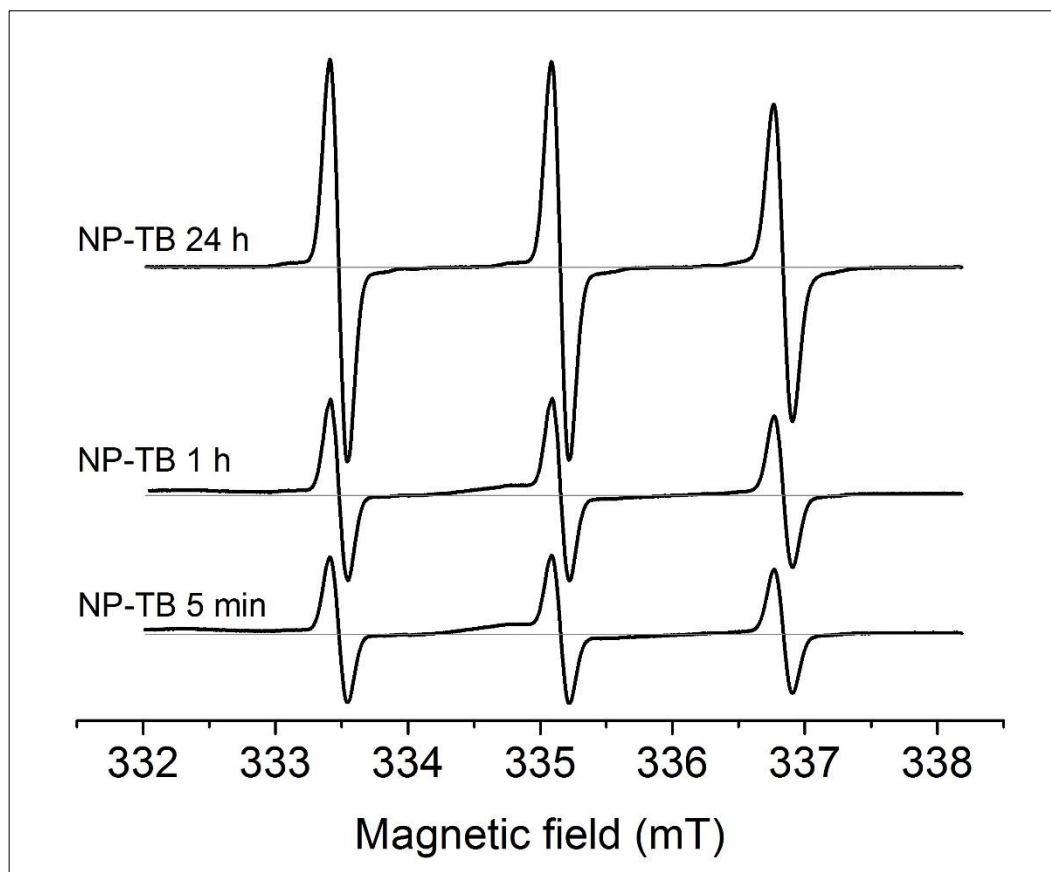


Fig. 20. EPR spectra of TEMPO-benzoate in water (Water-TB) and in MCT (MCT-TB).

Fig. 20 above shows the experimental spectra of TB in water and in MCT. The vertical gray lines cross the MCT-TB spectrum on the center of the first and third lines, hyperfine splitting -  $2a_N$ . It is clear that the hyperfine splitting of TB is larger in water than in MCT. It is also shown the characteristic decreasing height of the peaks in the MCT-TB spectrum.

The spectra of TB in nanoparticles exhibited below in Fig. 21, show the alteration of the microenvironment of nanoparticles over time. The spectrum of NP-TB 5 minutes presents a broader peak, this deflection from the horizontal line of the hyperfine splitting indicates the presence of immobilized spin-probe. The broader peak is still present after 1 hour. At 24 hours the acquired spectrum does not show the broader peak. The flat horizontal line indicates the spin probe is not immobilized as at the beginning. At this time point the NP-TB spectrum is similar to Water-TB spectrum.

When the spectra of the three different time points are graphically compared, it is not possible to detect a difference in  $2a_N$  value that was equal to 3.3606 mT, which suggests the micropolarity remained constant over time.



**Fig. 21.** EPR spectra of PVM/MA nanoparticles, NP-TB, at 5 min, 1 hour, and 24 hours after preparation. NP - TB polymer concentration 2% w/v, TB concentration 1 mM.

The presence of immobilized spin-probe at the earliest time point suggest its movement was hindered by the polymeric chains inside a dense nanoparticle structure. The immobilized spin-probe disappears with time, being the latest acquired spectrum similar to that acquired for TB in water. As already discussed in this work, when the PVM/MA nanoparticles are in their intrinsic pH, the polymer was hydrolyzed, and the nanoparticles were gradually solubilized within 10 hours. As shown by infrared and NTA, the maleic anhydride moieties were hydrolyzed and it was not possible to identify the structure of the particles 10 hours after nanoparticle preparation. The results obtained by EPR spectroscopy are in agreement with those data.

The freshly prepared NP - TB formulation was diluted (1:1) in PBS pH 7.4 and the spectra acquired 5 minutes and 1 hour after dilution. The pH effect on PVM/MA nanoparticles loaded with TB is shown below, Fig. 22. The spectrum of NP-TB pH 7.4

at 5 minutes does not show the broader lines indicative of immobilized spin-probe and it is similar to the spectrum acquired after 1 hour of dilution.

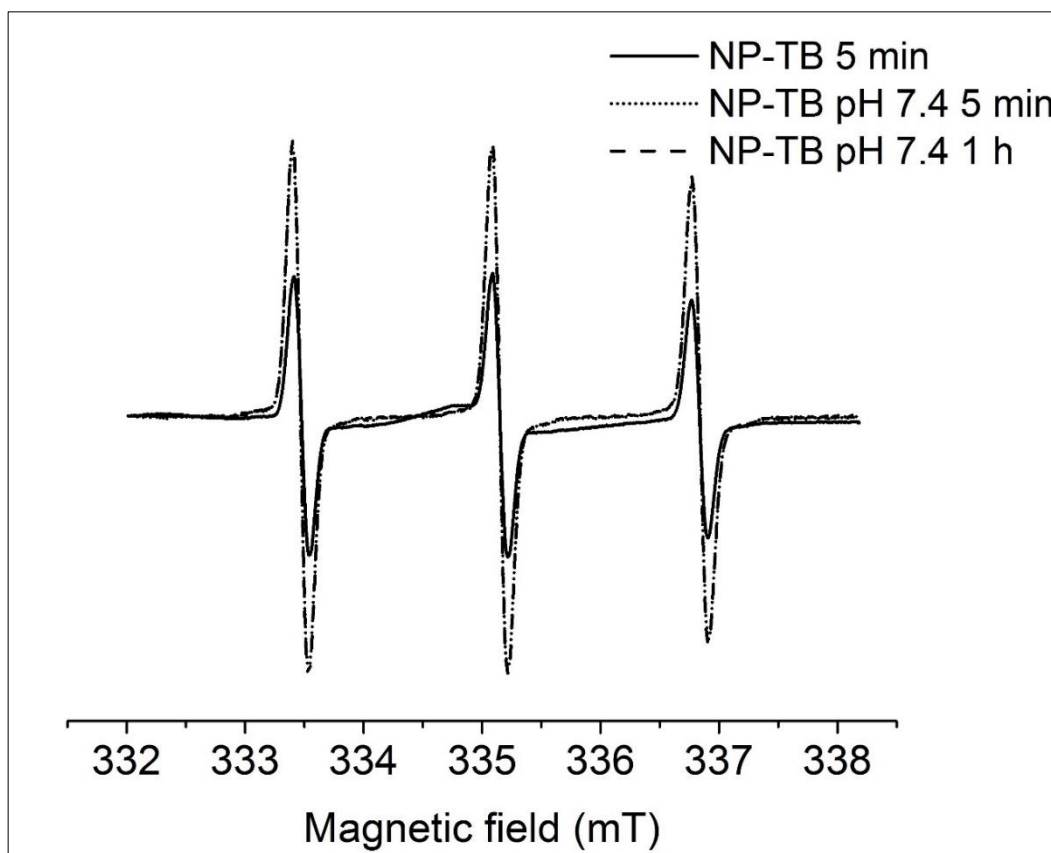


**Fig. 22.** EPR spectra of freshly prepared PVM/MA nanoparticles formulation NP-TB at 5 min and freshly prepared NP-TB diluted (1:1) in pH 7.4 at 5 min and 1 hour after preparation. NP - TB polymer concentration 2% w/v, TB concentration 1 mM.

As observed for NP-TB at its intrinsic pH, the micropolarity does not change over time. The mobility of the spin probe, however, reaches high amplitude at 5 minutes, and it is not possible to observe the presence of immobilized particles at this early time point. The spectrum of NP - TB at 1 hour is not different from that acquired at 5 minutes, which is indicative of the fast change in the structure of the nanoparticles, as discussed previously.

The results suggest the PVM/MA nanoparticles are solubilized immediately after the dilution, and the spin-probe was not protected inside the nanoparticle, contrary to what was observed for NP-TB 5 minutes. The microenvironment where the spin probe is located remains constant during the following hour of experiment, as expected.

#### **4.2.8. Conclusion**

DLS and NTA techniques were applied to determine the size distributions of the yielded plain and cross-linked nanoparticles and their evolution over 24 hours. The data obtained for the plain nanoparticles formulation by both methods were in agreement until the time point 3 hours after preparation. The presence of dense polymeric particles was also determined by freeze-fracture TEM. At later time points, DLS results indicated the presence of particles that, although more polydisperse than at the beginning of the experiment, presented a monodisperse size distribution. NTA output, however, showed a sharp decrease in the particle concentration after 6 hours and an absence of particles at time point 10 hours, indicating the dissolution of those particles. The NTA results are in agreement with the results of the ATR-FTIR spectroscopy. ATR-FTIR analysis showed the progressive hydrolysis of PVM/MA by the decrease of the characteristic anhydride bands and the concomitant increase of the carboxylic acid bands. Six hours after nanoparticles preparation only a residual amount of the anhydride moieties was still detectable. Further DLS analysis employing hydrolyzed polymer in lower concentration and at different pH conditions showed the behavior of the polymeric chains were strongly dependent on the pH of the medium. The extension of the protonation has a direct influence on the interaction of the polymer chains, leading to their aggregation. The aggregation was solved by the DLS algorithms as larger particles.

The employment of a cross-linker agent is an attempt to maintain the structure of the particles. However, the remaining anhydride groups still undergo hydrolysis. The hydrolysis changes the polymer conformation and, consequently, the final particle structure. Fig. 23, below, illustrates the dissolution of the plain and cross-linked nanoparticles over time.

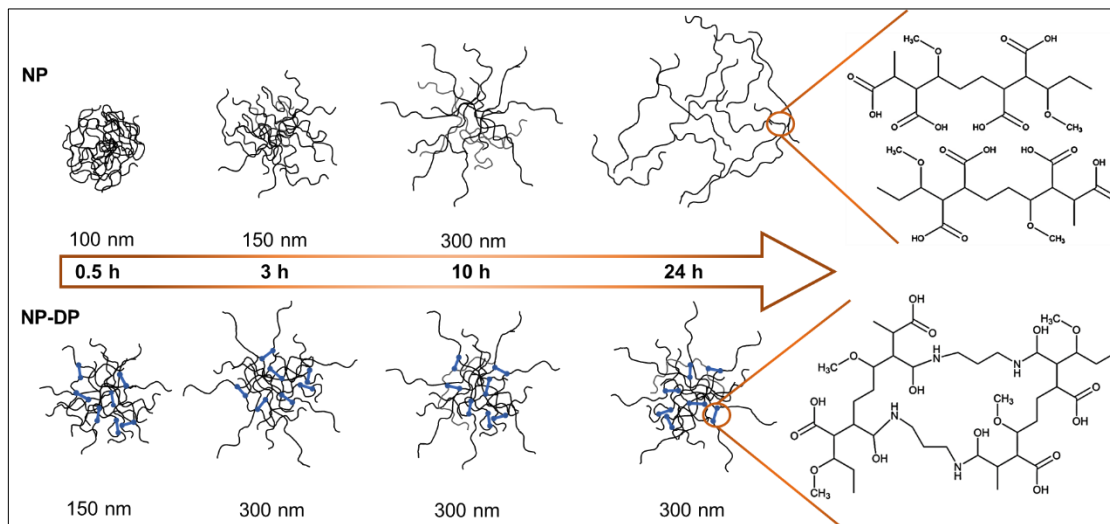


**Fig. 23.** Schematic representation of the plain (NP) and cross-linked nanoparticles (NP-DP) behavior over time. NP evolved from well-defined structures composed by insoluble anhydride-based polymer to bigger structures formed by entangled carboxylic acid polymer chains. Hydrogen bonds maintain the polymer chains interaction and alignment. Although larger and more polydisperse NP-DP kept its size, and PDI, over time. The covalent bond between polymer chain and the cross-linker (diaminopropane) maintain the hydrolysed polymeric chains together.

When pH conditions similar to that observed in the different portions of the gastrointestinal tract are applied, the hydrolysis of the nanoparticles was accelerated. The acidic condition tested, pH 1.2, accelerated the reaction, this result is in agreement with the literature. Higuchi and co-workers have reported that acidic conditions, especially pH lower than 2, can accelerate the hydrolysis since it is subject to proton catalysis [78]. Moreover, increasing the pH of the medium leads to faster hydrolysis, and at neutral pH, the nanoparticles are immediately hydrolyzed. The effect of the pH particles structure was clearly demonstrated by NTA, ATR-FTIR spectroscopy, and titration of the nanoparticles.

The EPR results suggest the presence of dense polymeric structures at the first-time points by the presence of immobilized spin-probe. The signal of immobilized probe decreased over time and was not detectable at the latest time points. This signal was also absent when the nanoparticles were in neutral pH. These results confirm those data obtained by the other employed techniques. That the polymer is sensitive to the pH and the nanoparticles are quickly solubilized at neutral pH.

### 4.3. PVM/MA-MCT Nanocapsules: development and characterization

#### 4.3.1. Particle size, zeta potential, and pH measurements

##### 4.3.1.1. Plain nanocapsules (NC I, NC II and NC III)

Three different nanocapsules formulations composed by PVM/MA and MCT were prepared. The final polymer-oil concentrations were 0.37%, 0.74% and 1.11% w/v and the formulations were named as NC I, NC II and NC III, respectively. Dynamic and static light scattering techniques (DLS and SLS) were applied to determine the particle size distribution of the nanocapsules formulations immediately after their preparation and to monitor the size after 1, 2 and 7 days. While the DLS can give particle sizes from about 1 nm to 6  $\mu\text{m}$ , the SLS works in a broader range, from 0.05  $\mu\text{m}$  to about 800  $\mu\text{m}$ . Combining the both methods, it is possible to evaluate the presence of large particles and the formation of aggregates over time.

The DLS results indicate that particle size increased with the polymer-oil concentration, being 195 nm  $\pm$  8 nm for NC I, 229 nm  $\pm$  11 nm for NC II and 266 nm  $\pm$  17 nm for NC III. The Pdl of NC I, 0.087, was similar to that observed for NC II, 0.1, and for NC III, 0.106. The same tendency was observed in SLS measurements: NC I was 154 nm  $\pm$  7 nm; NC II was 160 nm  $\pm$  6 nm; NC III was 181 nm  $\pm$  14 nm in size, while NC III showed a broader distribution when compared with NC I and NC II, Fig. 24.

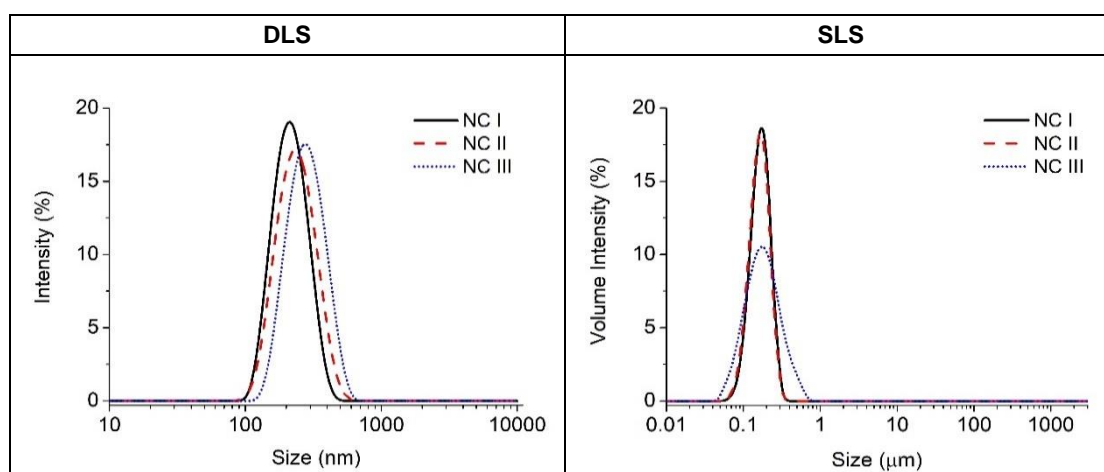


**Fig. 24.** Size distribution from DLS and SLS measurements of PVM/MA-MCT nanocapsules NC I (0.37% w/v), NC II (0.74% w/v), and NC III (1.11% w/v) immediately after preparation. DLS: average result from 3 measurements (automatic setting, general purpose algorithm), the samples were diluted in filtered bi-distilled water. SLS: average result from 5 measurements, 10 s each, with optical obscuration of 5%.

In addition to size distribution, pH and zeta potential of the formulations were measured and the result is shown below in Table 5. The pH of NC I and NC II were similar, being

$3.32 \pm 0.1$  for the former and  $3.26 \pm 0.12$  for the latter. NC III showed pH  $3.12 \pm 0.06$ . The zeta potential was  $-63.7 \text{ mV} \pm 3.9 \text{ mV}$ ,  $-60.2 \text{ mV} \pm 2.2 \text{ mV}$  and  $-56.1 \text{ mV} \pm 1.9 \text{ mV}$  for NC I, NC II and NC III, respectively. The pH of formulations decreased with the increase of polymer-oil concentration, while the zeta potential became higher.

**Table 5.** pH and zeta potential of the PVM/MA-MCT nanocapsules formulations NC I, NC II and NC III at time point 1 hour.

Formulation	pH $\pm$ S.D.	Zeta Potential $\pm$ S.D. (mV)
NC I	$3.32 \pm 0.10$	$-63.7 \pm 3.9$
NC II	$3.26 \pm 0.12$	$-60.2 \pm 2.2$
NC III	$3.12 \pm 0.06$	$-56.1 \pm 1.9$

As shown in Fig. 25 below, when evaluated over time by DLS, the mean diameter and Pdl of the formulation NC I was stable during the first day, being  $196 \text{ nm} \pm 7 \text{ nm}$  and 0.086. After 2 days the particle size and Pdl were  $208 \text{ nm} \pm 2$  and 0.115. After 7 days the particle size was  $208 \text{ nm} \pm 7 \text{ nm}$  and the Pdl 0.113. The results obtained by SLS showed the particle size was constant over the 7 days. The largest difference observed for size and pH of NC II and NC III occurred during the first 24 hours. After this time point the parameters remained stable until the time point 7 days. DLS data showed the mean diameter of NC II increased from  $229 \text{ nm} \pm 11 \text{ nm}$  at the time point 1 hour, to  $252 \text{ nm} \pm 10 \text{ nm}$  after 1 day. NC III increased from  $266 \text{ nm} \pm 17 \text{ nm}$  at 1 hour, to  $314 \text{ nm} \pm 6 \text{ nm}$  at day 1. The same trend was observed for the Pdl of both formulations: for NC II it was 0.1 at 1 hour, and 0.125 at 1 day. For NC III it was 0.106 and 0.132 at 1 hour and 1 day, respectively. The SLS results remained constant over time (Appendix II, Table I).

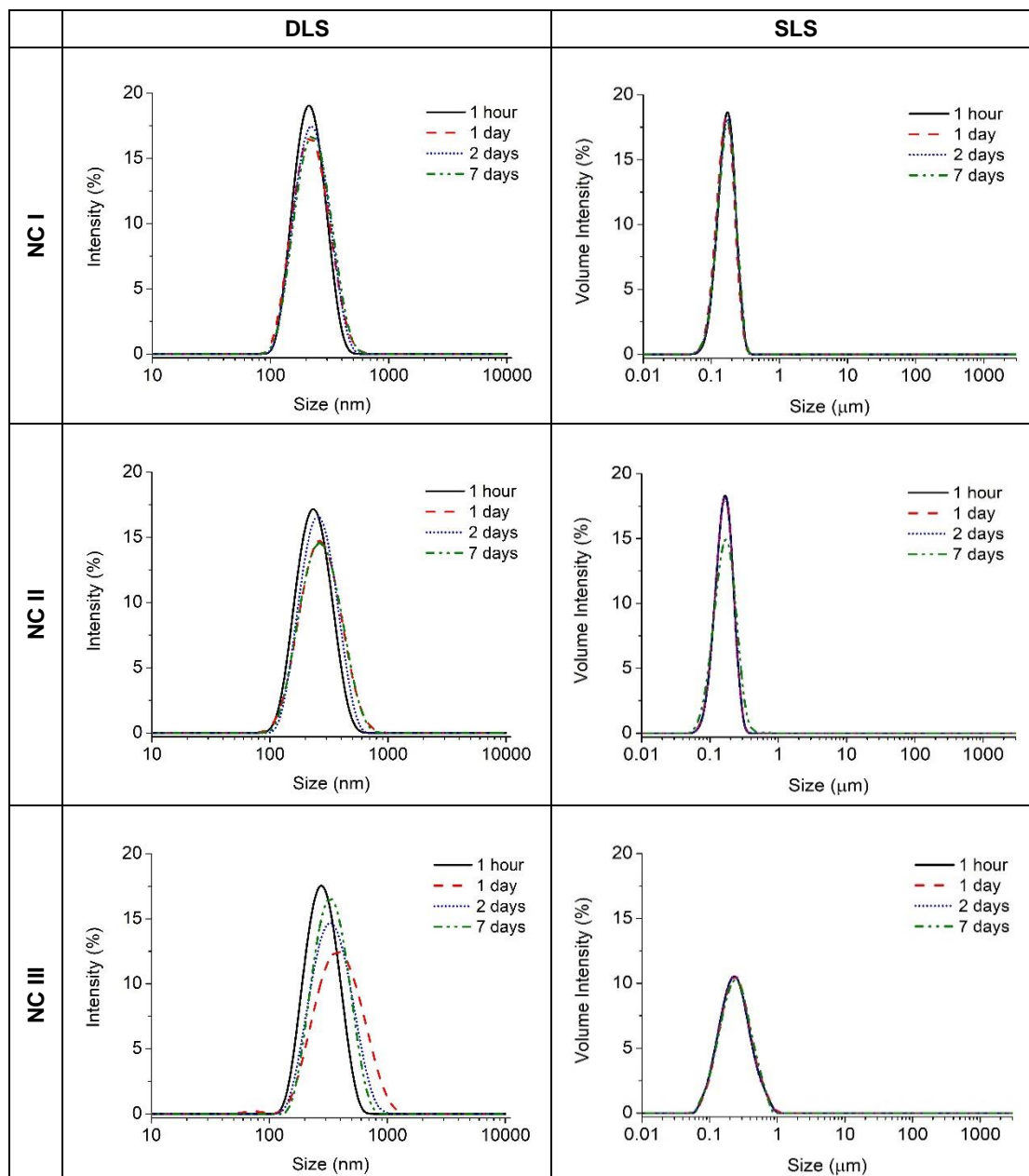


**Fig. 25.** Size distribution from DLS and SLS measurements of PVM/MA-MCT nanocapsules NC I (0.37% w/v), NC II (0.74% w/v), and NC III (1.11% w/v) at time point 1 hour, 1,2 and 7 days after preparation. DLS: average result from 3 measurements (automatic setting, general purpose algorithm), the samples were diluted in filtered bi-distilled water. SLS: average result from 5 measurements, 10 s each, with optical obscuration of 5%.

Zeta potential and pH were measured after 1, 2 and 7 days after preparation. The pH and zeta potential of NC I formulation were not affected over time. The pH of the formulation NC II and NC III became smaller with time, while the zeta potential remained constant, Table 6.



**Table 6.** pH and zeta potential of the PVM/MA-MCT nanocapsules formulations NC I, NC II and NC III over time.

Formulation	Time	pH ± S.D.	Zeta Potential ± S.D. (mV)
NC I	1 h	3.32±0.10	-63.7±3.9
	1 d	3.32±0.03	-67.2±4.1
	2 d	3.31±0.03	-67.5±1.3
	7 d	3.31±0.06	-64.1±5.1
NC II	1 h	3.26±0.12	-60.2±2.2
	1 d	3.11±0.04	-58.9±3.0
	2 d	3.08±0.03	-60.6±3.2
	7 d	3.08±0.02	-61.9±2.2
NC III	1 h	3.12±0.06	-56.1±1.9
	1 d	2.92±0.03	-55.8±0.6
	2 d	2.93±0.01	-56.2±0.2
	7 d	2.95±0.02	-56.7±1.4

NC I was the most stable formulation showing the smallest particle size with a monodisperse distribution over time. The particle size distribution of NC III was larger when compared to NC I, but its Pdl was below 0.155 even after 7 days of evaluation. For all formulation, the results obtained from SLS were constant over time. Although the DLS and SLS results suggest the all the yielded nanocapsules were stable over time, macroscopically both NC II and NC III formulations showed oil droplets onto their surfaces after the first day; the amount and size of those droplets increased over time, especially for NC III.

#### ***4.3.1.2. Comparison between the particles prepared using magnetic stirring and rotor-stator mixer***

To achieve the best method to produce the nanoparticles the formulations were initially prepared using magnetic stirring instead of the rotor-stator mixer for mixing the aqueous and organic phases. The polymer-oil concentrations tested were 0.74 and 1.11%w/v, NC II and NC III, respectively. The comparison of the results obtained by both methods are shown below, Fig. 26. The DLS outputs showed the particle size and Pdl of NC II prepared using magnetic stirring – NC II (MS), was equal to 243 nm ± 9 nm and 0.108, while the particles produced using rotor-stator mixer – NC II (UT) were

229 nm  $\pm$  11 with Pdl equal to 0.1. The particle size of NC III (MS) was 266 nm  $\pm$  17 nm and its Pdl were 0.106. NC III (UT) presented particle size 258 nm  $\pm$  29 nm and Pdl equal to 0.105. SLS results were 174 nm  $\pm$  16 nm for NC II (MS) and 160 nm  $\pm$  6 nm for NC II (UT). For NC III (MS) was obtained 196 nm  $\pm$  18 nm, and 181 nm  $\pm$  14 nm for NC III (UT). Zeta potential and pH results were not different for the formulations prepared by magnetic stirring or rotor-stator methods. (Appendix II, Table II).

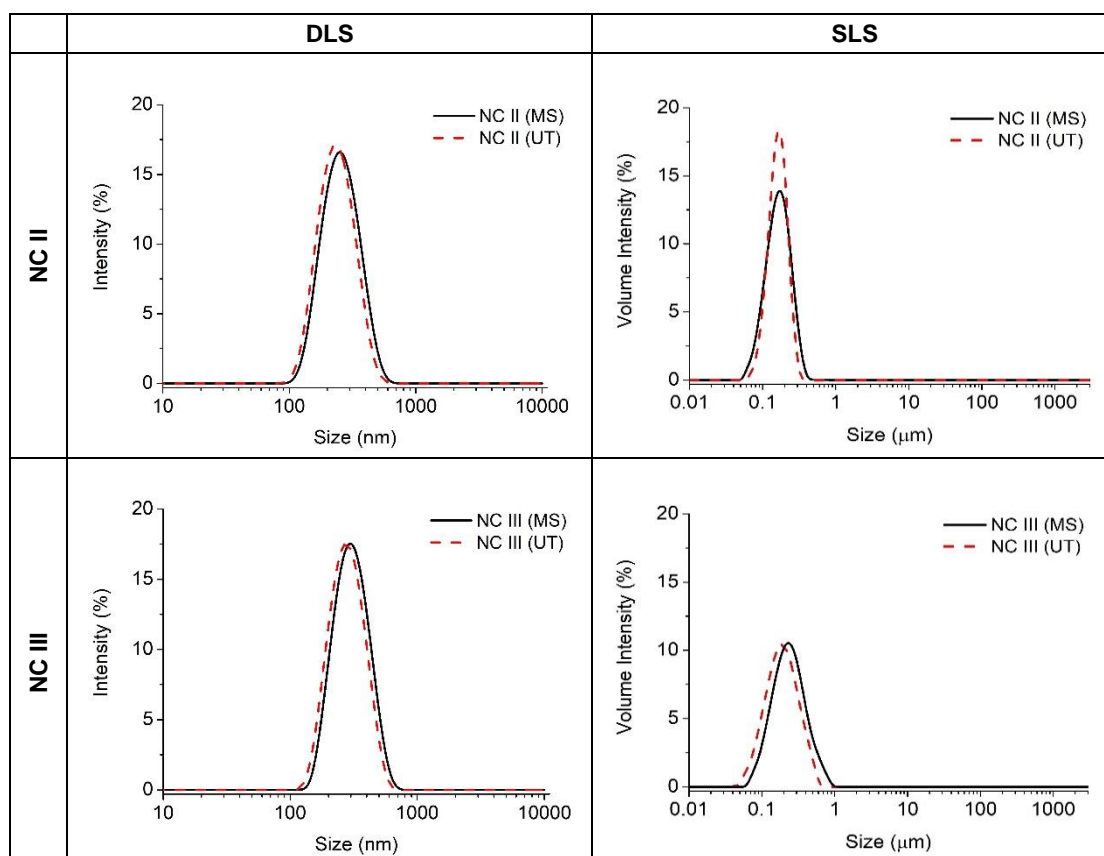


**Fig. 26.** Size distribution determined by DLS and SLS of PVM/MA-MCT nanocapsules NC II (0.74% w/v) and NC III (1.11% w/v) prepared using magnetic stirring (MS) or rotor-stator mixer – Ultra TURRAX (UT) at time point 1 hour after preparation. DLS: average result from 3 measurements (automatic setting, general purpose algorithm), the samples were diluted in filtered bi-distilled water. SLS: average result from 5 measurements, 10 s each, with optical obscuration of 5%.

The particle size of the formulations prepared using the rotor-stator mixer was in all cases smaller than that observed for the formulations that were prepared with magnetic stirring. In addition, the size distribution obtained by SLS for NC II (UT) was narrower when compared to NC II (MS). For this reason, the rotor-stator mixer was the method selected to produce the particles in the next step of the development – the cross-linked nanocapsules.

#### **4.3.1.3. Cross-linked nanocapsules (NC + DP)**

All formulations (NC I, NC II and NC III) were cross-linked with 1,3-diaminopropane (DP) at final Polymer:DP molar ratio equal to 4:1 (NC I + DP 4:1, NC II + DP 4:1 and NC III + DP 4:1) or equal to 2:1 (NC I + DP 2:1, NC II + DP 2:1 and NC III + DP 2:1). Fig. 27 shows the comparison of the size distributions (DLS and SLS) between the plain and cross-linked formulations immediately after preparation. All cross-linked formulations were similar in size when compared with the plain nanocapsules. The mean diameter and Pdl of NC I + DP 2:1 were 195 nm  $\pm$  10 nm and 0.121. NC I + DP 4:1 were 213 nm  $\pm$  11 nm in size with Pdl equal to 0.094. For NC II + DP 2:1 were found 232 nm  $\pm$  14 nm and Pdl 0.135, while for NC II + DP 4:1 were found 241 nm  $\pm$  7 nm and 0.093. The size and Pdl of NC III + DP 2:1 were 284 nm  $\pm$  13 nm and 0.11, respectively. NC III + DP 4:1 were 289 nm  $\pm$  26 nm in size and its Pdl was 0.099. (Appendix II, Table III and Table IV).

The zeta potential of formulations cross-linked at PVM/MA:DP molar ratio 4:1 were between -47 mV and -45 mV, and pH were in the range of 4.4. For those formulations cross-linked at PVM/MA:DP molar ratio 2:1 zeta potential was about -42 mV and pH about 5.2, Table 7.

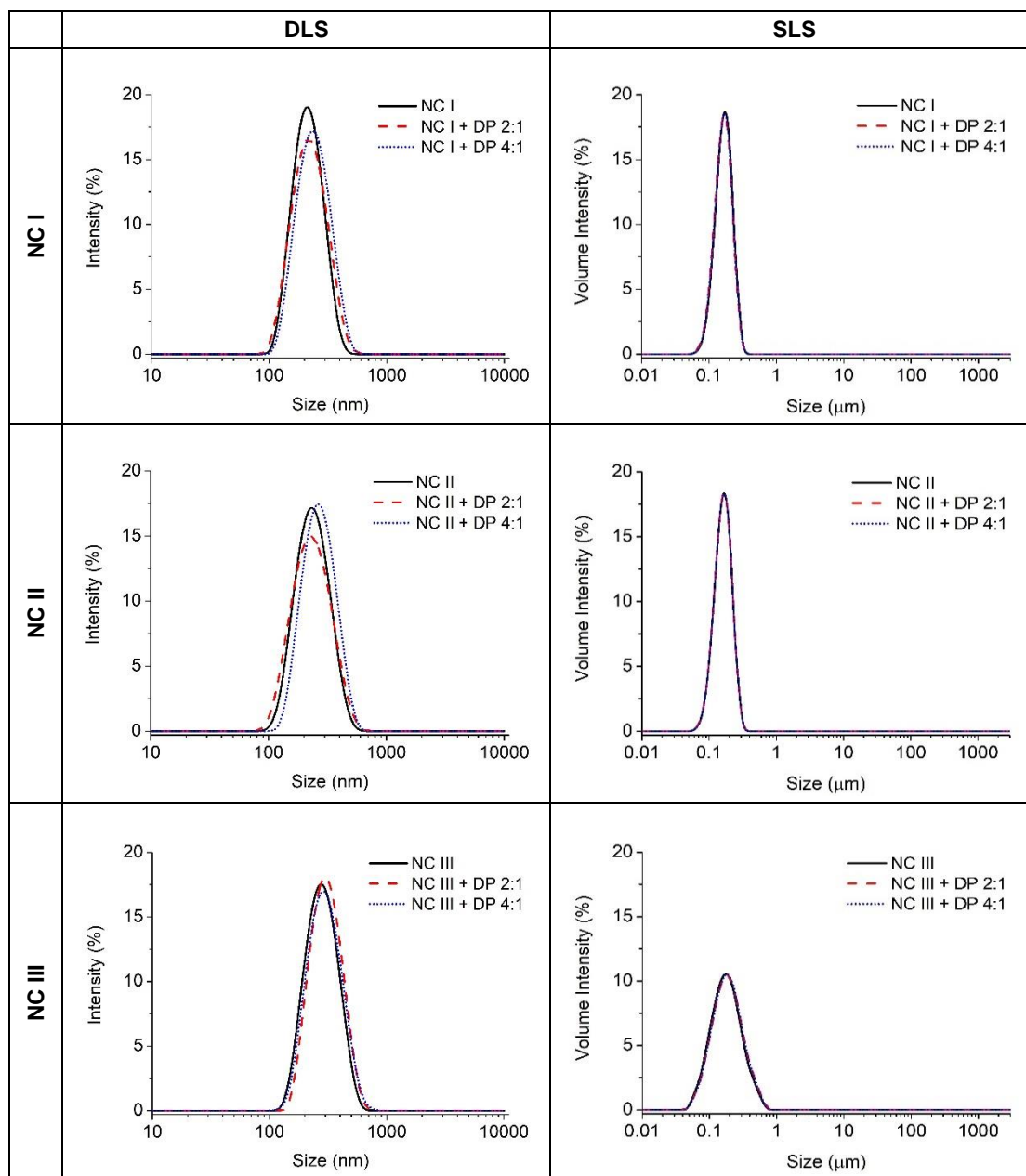


**Fig. 27.** Size distribution determined by DLS and SLS of PVM/MA-MCT nanocapsules NC I (0.37% w/v), NC II (0.74% w/v), and NC III (1.11% w/v) cross-linked with 1,3-diaminopropane (DP) at time point 1 hour after preparation. PVM/MA monomer:DP molar ratio was 4:1 (0.118 mg DP/mg PVM/MA) or 2:1 (0.237 mg DP/mg PVM/MA). DLS: average result from 3 measurements (automatic setting, general purpose algorithm), the samples were diluted in filtered bi-distilled water. SLS: average result from 5 measurements, 10 s each, with optical obscuration of 5%.

The stability of cross-linked formulations was evaluated over 7 days, size, pH, and zeta potential were measured after 1, 2 and 7 days of preparation. For the formulations cross-linked at PVM/MA:DP molar ratio equal to 2:1, SLS results showed the particle size remained constant over time. The same trend was observed for DLS results,

except for NC III + DP 2:1, which the particles size distribution became broader after 1 day, Fig. 28.

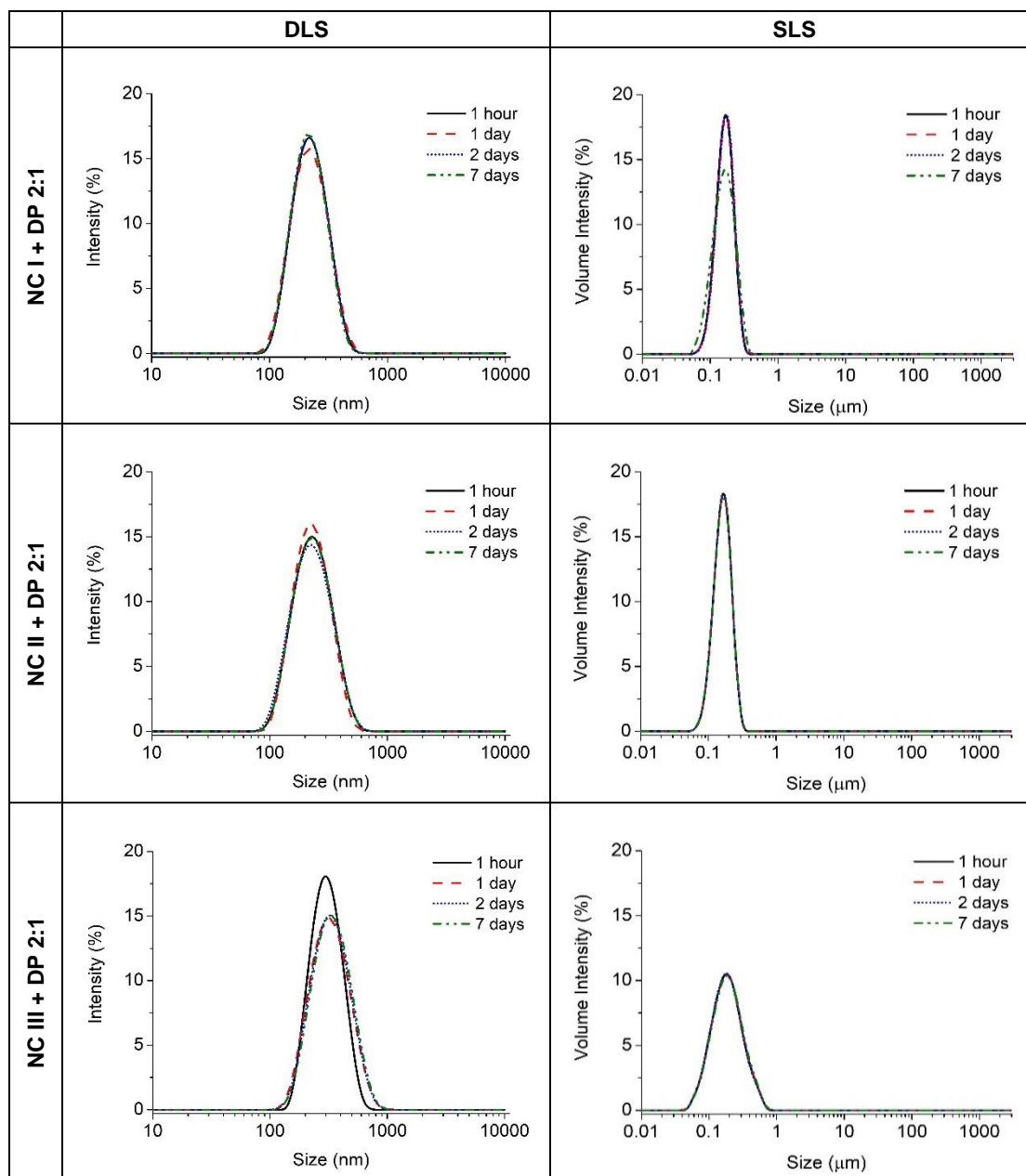


**Fig. 28.** Size distribution determined by DLS and SLS of PVM/MA-MCT nanocapsules NC I (0.37% w/v), NC II (0.74% w/v), and NC III (1.11% w/v) cross-linked with 1,3-diaminopropane (DP) at time point 1 hour after preparation. PVM/MA monomer:DP molar ratio 2:1 (0.237 mg DP/mg PVM/MA). DLS: average result from 3 measurements (automatic setting, general purpose algorithm), the samples were diluted in filtered bi-distilled water. SLS: average result from 5 measurements, 10 s each, with optical obscuration of 5%.

SLS results showed the particle size of formulations cross-linked at PVM/MA:DP molar ratio equal to 4:1 was constant over time. DLS results, however, shows the particle size and Pdl became higher especially after the first 24 hours. For the formulation NC III + DP 4:1 the increase in size and Pdl was more pronounced than for the other two formulations, Fig. 29.

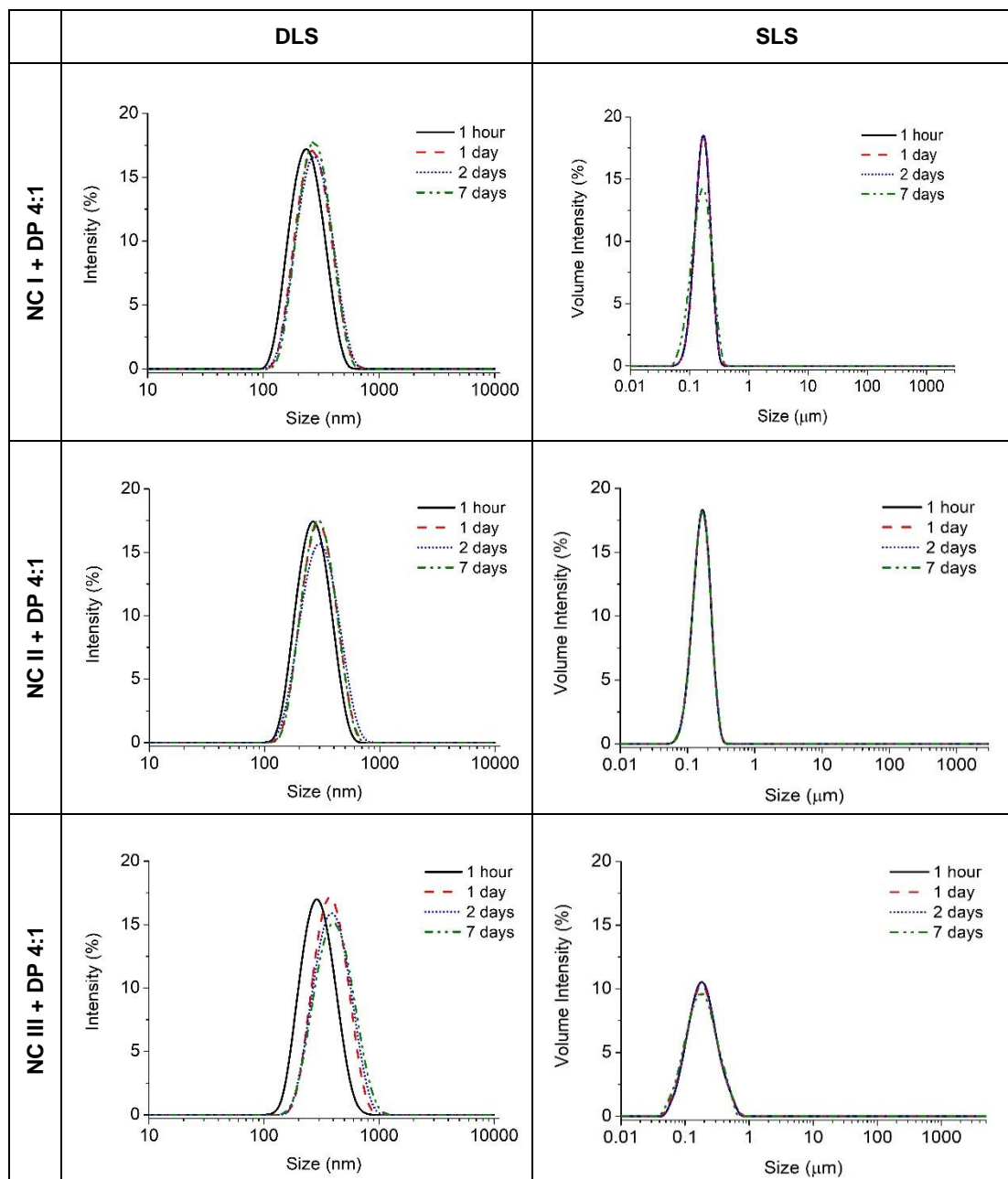


**Fig. 29.** Size distribution determined by DLS and SLS of PVM/MA-MCT nanocapsules NC I (0.37% w/v), NC II (0.74% w/v), and NC III (1.11% w/v) cross-linked with 1,3-diaminopropane (DP) at time point 1 hour after preparation. PVM/MA monomer:DP molar ratio 4:1 (0.118 mg DP/mg PVM/MA). DLS: average result from 3 measurements (automatic setting, general purpose algorithm), the samples were diluted in filtered bi-distilled water. SLS: average result from 5 measurements, 10 s each, with optical obscuration of 5%.

The pH was stable for NC I cross-linked formulations over time, being 4.3 for PVM/MA:DP 4:1 and 5.3 for PVM/MA:DP 2:1. The most pronounced change in pH was observed for the nanocapsules formulations cross-linked with PVM/MA:DP molar ratio equal to 4:1, as can be seen below in Table 7. Zeta potential remained constant about

-45 mV for the formulations cross-linked with PVM/MA:DP molar ratio equal to 4:1, and -42 mV for the formulations cross-linked with PVM/MA:DP molar ratio equal to 2:1.

**Table 7.** pH and zeta potential of NC I (0.37% w/v), NC II (0.74% w/v), and NC III (1.11% w/v) cross-linked with 1,3-diaminopropane (DP) at time point 1 hour after preparation. PVM/MA monomer:DP molar ratio was 4:1 (0.118 mg DP/mg PVM/MA) or 2:1 (0.237 mg DP/mg PVM/MA).

Formulation	Time	pH ± S.D.	Zeta Potential ± S.D. (mV)
NC I + DP 4:1	1 h	4.37±0.11	-47.4±0.9
	1 d	4.30±0.08	-47.7±1.0
	2 d	4.36±0.01	-47.7±0.4
	7 d	4.37±0.02	-47.7±0.5
NC I + DP 2:1	1 h	5.26±0.20	-42.9±0.5
	1 d	5.22±0.22	-44.2±3.0
	2 d	5.30±0.03	-41.9±1.5
	7 d	5.35±0.07	-41.0±1.2
NC II + DP 4:1	1 h	4.43±0.20	-45.1±1.0
	1 d	4.12±0.07	-45.9±0.3
	2 d	4.13±0.06	-48.0±1.7
	7 d	4.12±0.04	-47.6±0.9
NC II + DP 2:1	1 h	5.22±0.15	-42.3±0.8
	1 d	5.01±0.14	-43.3±0.8
	2 d	5.06±0.18	-43.2±1.1
	7 d	5.05±0.18	-42.7±0.9
NC III + DP 4:1	1 h	4.48±0.20	-45.7±0.4
	1 d	4.24±0.45	-46.3±1.1
	2 d	4.02±0.08	-46.0±1.3
	7 d	4.03±0.09	-46.6±1.4
NC III + DP 2:1	1 h	5.15±0.16	-42.1±1.5
	1 d	5.05±0.31	-41.4±0.7
	2 d	4.92±0.17	-41.0±1.1
	7 d	4.93±0.17	-40.8±1.4

Comparing the results obtained DLS and SLS techniques it is possible to observe that the formulation NC I is the most stable one, there is only a small increase in the particle size and polydispersity after 7 days. For the NC III, the change in size is more pronounced as well as in its polydispersity. Besides the relative stability throughout the

experimental period, cross-linked NC II and NC III formulations also showed oil droplets on their surface after the first day.

#### 4.3.2. Transmission electronic microscopy – Freeze-Fracture and Cryo

Representative photomicrographs of the freeze-fractured nanocapsules NC I, NC II and NC III are shown in Fig. 30, the particles present a nanocapsules structure with a shell (arrow) and a well-defined core (arrowhead). The average diameter of NC I was about 160 nm with the core ranging about 60 nm. The average diameter of NC II was 195 nm, and its core was about 70 nm. For NC III were found 267 nm for the whole capsule and 100 nm for its core.

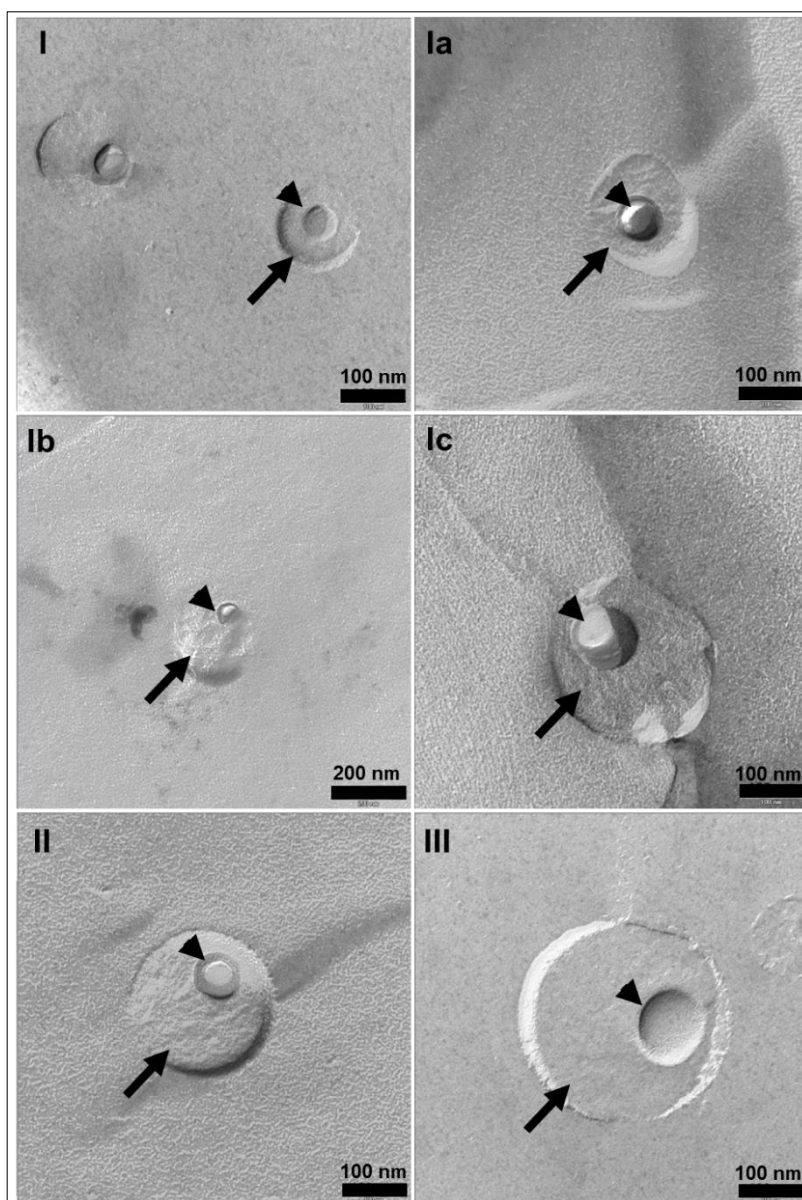




**Fig. 30.** TEM micrographs of PVM/MA-MCT nanocapsules after freeze-fracture. (I) NC I (0.37% w/v); (Ia) NC I 24 hours after preparation; (Ib) NC I + DP 4:1 (PVM/MA:DP molar ratio 4:1); (Ic) NC I + DP 2:1 (PVM:DP molar ratio 2:1); (II) NC II (0.74% w/v) and (III) NC III (1.11% w/v). Arrow polymeric shell and arrowhead oil core.

Freeze-fracture TEM gives useful information about nanocapsules structure, including estimation of the shell thickness. Although not common, nanocapsules showing thicker shells were already described before in the literature, one example is the 100 nm to 200 nm stearic acid styrene/methyl methacrylate nanocapsules, prepared by Wang and co-workers, that showed shell sizing about 30 nm, [79].

A typical cryo-TEM photomicrograph of nanocapsules NC I are shown in Fig. 31, the particles present spherical structure with average diameter around 120 nm.

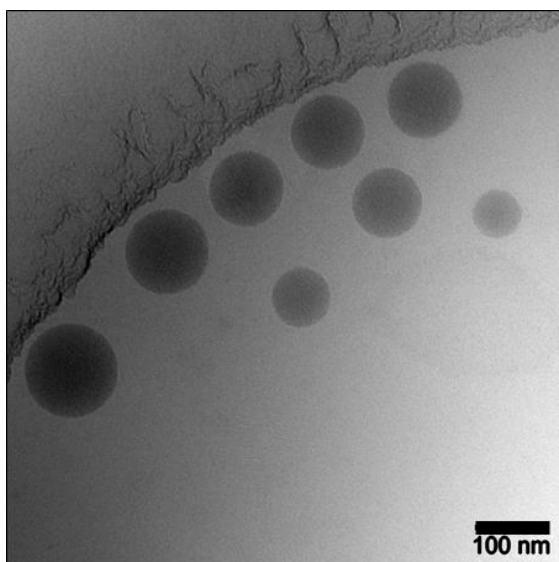


**Fig. 31.** Cryo-TEM micrograph of cross-linked NC I, 24 hours after preparation. Formulation at its intrinsic pH and kept at room temperature.

The cryo-TEM images revealed spherical structures, which have the same appearance of emulsion droplets. The absence of contrast between the core and shell may be explained by the low contrast of the polymer when compared to the contrast of the oil core, as observed in colloidal emulsions stabilized by different polymers [70], [80]–[82]. The size of the nanocapsules seen in the freeze-fractured and cryo-TEM images appeared to be smaller than that measured by DLS and similar to that measured by SLS. This result is expected considering the sensitivity of DLS to the larger particles to the determination of the hydrodynamic diameter.

#### **4.3.3. Impact of pH of the medium on the on the nanocapsules size**

The sensitivity of the polymer to the pH of the medium was already discussed in the previous chapter. When at its intrinsic pH, about 2.9, the polymer is hydrolyzed and the nanoparticles are almost totally solubilized in less than 10 hours. Acidic pH, pH 1.2, accelerates the hydrolysis reaction and the nanoparticles are solubilized in 6 hours. However, at higher pH values as pH 5.0 or pH 7.4, the solubilization of the nanoparticles occurs in less than 1 hour.

To evaluate the stability of the nanocapsules and the hydrolysis of the polymer on the surface of them, plain and cross-linked nanocapsules were evaluated at pH 1.2 (HCl/KCl buffer solution) and at pH 7.4 (PBS). For that purpose, 24 hours after preparation the nanocapsules formulation were diluted (1:10) and incubated for 5 minutes in the different buffer solutions. Finally, the particle size was measured using DLS. The pH of the diluted formulation was controlled over the experiments and varies from  $1.22\pm 0.03$  to  $1.26\pm 0.03$  for samples diluted in HCl/KCl buffer solution and from  $7.36\pm 0.01$  to  $7.45\pm 0.01$  in samples diluted in PBS. As a control, all formulations were also sized in filtered bi-distilled water, following the same protocol described before.

The particle size of PVM/MA-MCT nanocapsules remained constant over the first 24 hours, as observed on the initial characterization. The results of the formulations diluted in buffered solutions showed that the size and Pdl of NC I remained constant at both pH conditions when compared with the control (NC I:Water, 1:10), Fig. 32. Cross-linked NC I formulations had similar size when compared with the control. The Pdl of the formulations at pH 7.4 was also similar to that observed for the control, while the formulations at pH 1.2 presented smaller Pdl.

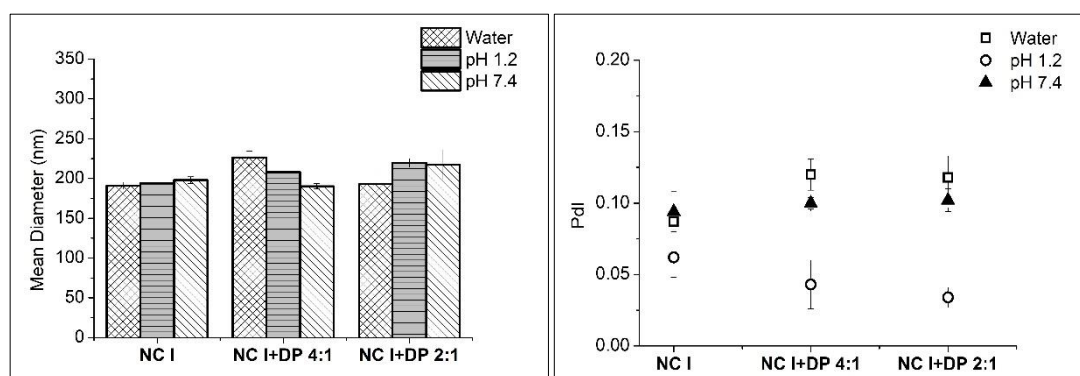


**Fig. 32.** Particle size and Pdl of plain and cross-linked NC I nanocapsules, 1 day after preparation, diluted (1:10) and incubated for 5 minutes in water, HCl/KCl buffer pH 1.2 or in PBS pH 7.4. NC I (0.37% w/v), PVM/MA monomer:DP molar ratio 4:1 (0.118 mg DP/mg PVM/MA) or 2:1 (0.237 mg DP/mg PVM/MA). DLS: average result from 3 measurements (automatic setting, general purpose algorithm).

The results of NC II showed the particle size was slightly smaller when the formulations were in the buffered conditions, and Pdl of the formulation at pH 1.2 was smaller than that observed for the control. The size of cross-linked NC II formulations was similar in both pH conditions, while the Pdl was smaller only for formulations at pH 1.2, Fig. 33.

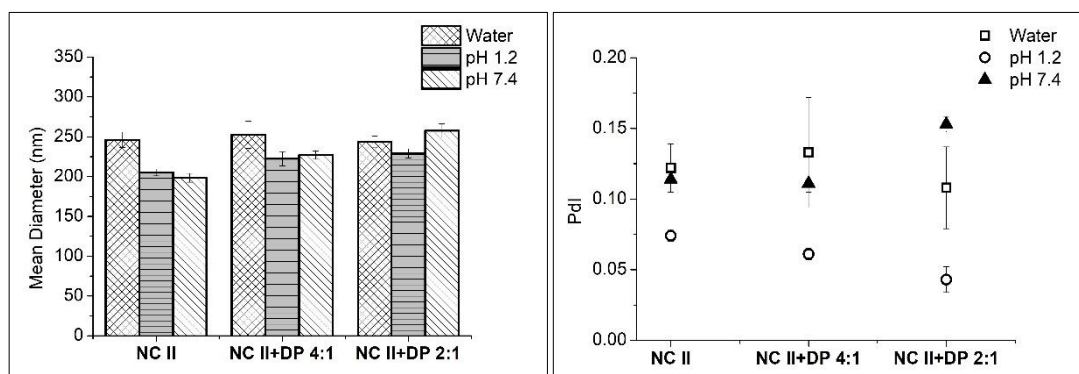


**Fig. 33.** Particle size and Pdl of plain and cross-linked NC II nanocapsules, 1 day after preparation, diluted (1:10) and incubated for 5 minutes in water, HCl/KCl buffer pH 1.2 or in PBS pH 7.4. NC II (0.74% w/v) PVM/MA monomer:DP molar ratio 4:1 (0.118 mg DP/mg PVM/MA) or 2:1 (0.237 mg DP/mg PVM/MA). DLS: average result from 3 measurements (automatic setting, general purpose algorithm).

Fig. 34 below, shows the data obtained for NC III. The plain nanocapsules in buffered media were smaller than the control, and the Pdl values were similar in all conditions. The cross-linked formulations were similar in size and the Pdl values were smaller only for formulations at pH 1.2.

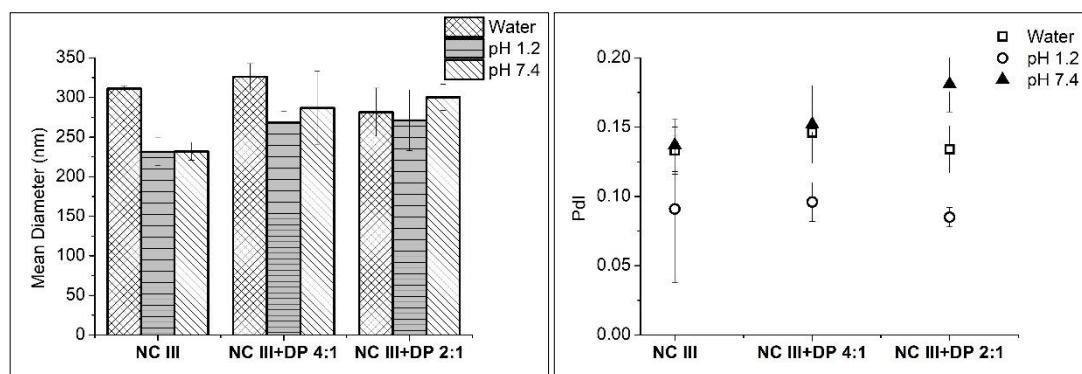


**Fig. 34.** Particle size and Pdl of plain and cross-linked NC III nanocapsules, 1 day after preparation, diluted (1:10) and incubated for 5 minutes in water, HCl/KCl buffer pH 1.2 or in PBS pH 7.4. NC III (1.11% w/v), PVM/MA monomer:DP molar ratio 4:1 (0.118 mg DP/mg PVM/MA) or 2:1 (0.237 mg DP/mg PVM/MA). DLS: average result from 3 measurements (automatic setting, general purpose algorithm).

The formulation NC I is the only one where the size and Pdl remained constant at both pH conditions, suggesting the medium does not affect the nanocapsule structure. The more pronounced change in the size of plain NC II and NC III suggests the polymer is exposed at the capsule surface, being more accessible to interaction with the aqueous medium and, consequently to hydrolysis of the exposed groups. Moreover, the size

stability of cross-linked formulations is also in agreement with this observation and can be explained by the fact the cross-linker stabilized the polymer at the nanocapsule surface. Hence, as a general feature, the particle size did not change at buffered media. The Pdl of all formulations at pH 1.2 was smaller when compared to the control. It can be explained by the protonation and protection of the oxygens of carboxylic acid groups reducing the repulsion of negatively charged oxygen atoms. This accommodation of the polymer could reduce the variability of the particle size that may occur due to the interaction of hydrolyzed polymer with the aqueous medium. On the other hand, the pH 7.4 favors the swelling of the polymer at the very external layer of the nanocapsules shell, increasing the variability of the particle size. The more pronounced change of plain NC II and NC III suggests the polymer is more exposed at the capsule surface, being more accessible to interaction with the aqueous medium. The Pdl was always smaller than 0.2 suggesting the formulations remain monodisperse over time, although some degree of polymer hydrolysis may be observed. (Appendix II, Table V).

#### ***4.3.4. EPR Spectroscopy - Nanocapsules loaded with TEMPO-benzoate***

Nanocapsule formulation loaded with the spin probe TEMPO-benzoate (NC I - TB), at a final concentration of TB equal to 0.15 mM, was prepared following the protocol previously described. NC I - TB was also dialyzed over 24 hours against HCl/KCl buffer pH 1.2 or PBS pH 7.4. The spectra were acquired immediately after nanocapsule preparation and after 1 day for non-dialyzed and dialyzed samples.

The formulation loaded with TB, presented particle size and zeta potential similar to that observed for NC I. Particle size remained constant over time, while Pdl increased from 0.083 to 0.155. For the dialyzed samples the size and Pdl were similar to that observed for the control, 0.171 for pH 7.4 and 0.131 for pH 1.2. The zeta potential was -70 mV after the dialysis in pH 7.4, and -14 mV after the dialysis in pH 1.2.

Fig. 35 below shows the experimental EPR spectra of TB in MCT and in the nanocapsule formulation NC I - TB, the latter at 1 hour and 1 day after preparation. It is possible to observe that the spectra of TB in NC I and in MCT are similar in shape, suggesting the TB molecules in NC I - TB are in a lipophilic environment. The overlapping of the NC I - TB spectra at 1 hour and 1 day suggests that TB molecules are still in the same condition after 24 hours, although it is possible to observe a decrease in signal amplitude, which is related to spin probe concentration [58].

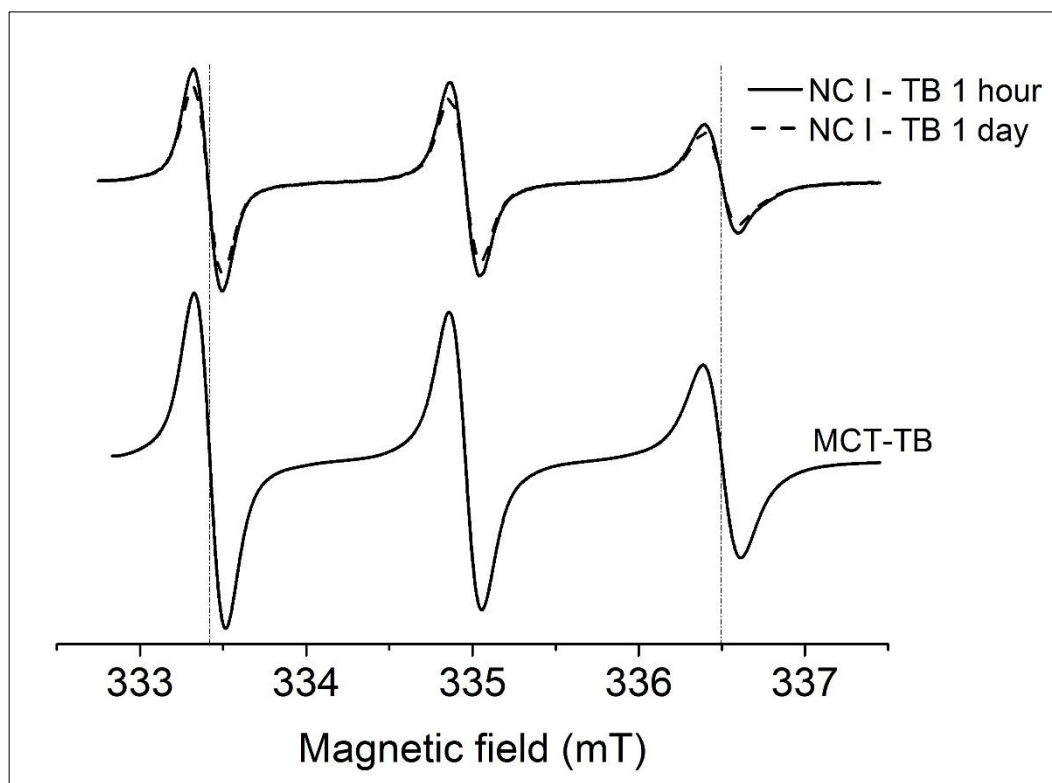


**Fig. 35.** EPR spectra of MCT-TB and PVM/MA-MCT nanocapsules loaded with Tempo-Benzoate, NC I - TB at 1 hour and 1 day after preparation. NC I - TB: polymer-oil concentration 0.37% w/v; TB concentration 0.15 mM.

From the experimental data, a simulation of EPR spectra of MCT, water, and NC I - TB 1 hour was performed to determine the micropolarity and microviscosity of the medium where TB was located. The polarity in MCT was equal to 1.016 and  $\tau_c$  equal to 0.229 ns. For water, polarity and  $\tau_c$  were 1.111 and 0.024 ns, respectively. The simulation also indicates the presence of 2 species in NC I - TB. The species I, which had a contribution of 55.5% to the spectrum, showed polarity equal 1.019 and rotation correlation time 0.186 ns. The species II showed polarity 1.054 and rotation correlation time of 0.867 ns, Table 8.

**Table 8.** Data obtained from simulation of EPR spectra of TB in water, MCT and NC I at 1 hour after preparation.

Medium	Polarity <sup>a</sup>	Rotation Correlation Time <sup>b</sup> (ns)	Partition <sup>c</sup>
Water	1.111	0.024	1
MCT	1.016	0.229	1
NC I	Species I	1.019	0.555
	Species II	1.054	0.445

<sup>a</sup> Standard deviation =  $\pm 0.005$ ; <sup>b</sup> Standard deviation =  $\pm 0.001$ ; <sup>c</sup> percentage of normalized AUC obtained from integrated of spectra. AUC is a function of spin-probe concentration.

The data above indicates the two TB species in NC I - TB 1 hour was in a hydrophobic environment. The data of the second species indicated the environment is slightly more polar and considerably more viscous than the MCT itself. Regarding the equilibrium between the nanocapsules and the aqueous medium, it is possible to assume the existence of a third environment – the water, in which a small amount of TB could be found, considering its solubility in water is in the millimolar range. Therefore, it is not possible to acquire its spectrum or simulate data due to the low concentration of the spin probe in the external medium.

Twenty-four hours after preparation the spectrum shape of NC I - TB was not different from that observed at 5 minutes. The simulated results obtained from the spectra of NC I - TB 1 day are shown and compared to the data of NC I - TB 1 hour in Table 9 below.

The polarity of the species I remained constant after 24 hours. Species II, however, showed an increase in it, from 1.054 to 1.090. Rotation correlation time,  $\tau_c$ , of the species II, although smaller than that observed at 1 hour, 0.707 ns, remained higher in comparison to  $\tau_c$  of species I and MCT environment. The area under the curve of a double-integrated spectrum is proportional to the spin-probe concentration. Therefore it can give an estimation of the movement of TB molecules inside the different media. Considering the area obtained for NC I - TB at 5 minutes after preparation as a reference, it was possible to conclude that after 24 hours 10% of the spin-probe signal was lost. The more lipophilic environment, species I, showed an increase of relative TB concentration, from 55% to 63%. The environment represented by the species II, showed a decrease in TB concentration, from about 44% to 26.3% of the total signal.

**Table 9.** Data obtained from simulation of EPR spectra of TB in water, MCT and NC I at 1 hour and 1 day after preparation.

Medium	Time Point	Polarity <sup>a</sup>	Rotation Correlation Time <sup>b</sup> (ns)	Partition <sup>c</sup>	Double integral <sup>d</sup>	Normalized AUC	Normalized partition	
Water	-	1.111	0.024	1	-	-	-	
MCT	-	1.016	0.229	1	-	-	-	
NC I	1 hour	Species I	1.019	0.186	0.555	1073.9	1	0.555
		Species II	1.054	0.867	0.445			0.445
	1 day	Species I	1.015	0.203	0.706	961.1	0.895	0.632
		Species II	1.090	0.707	0.294			0.263

<sup>a</sup> Standard deviation =  $\pm 0.005$ ; <sup>b</sup> Standard deviation =  $\pm 0.001$ ; <sup>c</sup> percentage of normalized AUC obtained from integrated of spectra. AUC is a function of spin-probe concentration; <sup>d</sup> Standard deviation =  $\pm 0.01$ .

These findings suggest the existence of an interfacial area where the movement of the TB molecules is disturbed, showing a reduced mobility. This environment with a high viscosity still present after 24 hours of nanocapsules preparation, but a smaller amount of TB molecules is present on it. In addition, an increase in the polarity of this environment was observed. A decrease in signal of the spin probe in the interfacial area (species II) may be explained by the loss of TB from this area to the external medium due to the equilibrium and, also, by the increased TB concentration in the oily phase, as depicted in the figure below, Fig. 36.

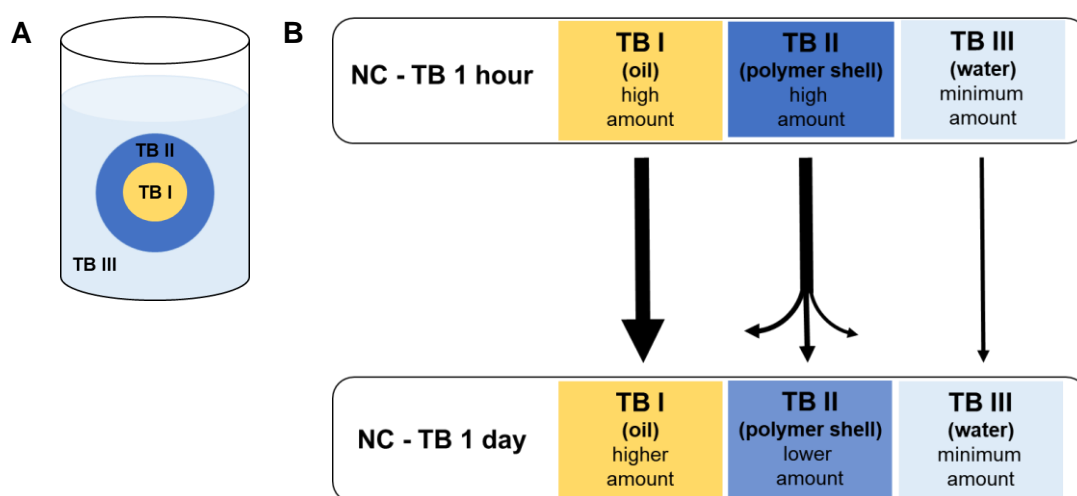


**Fig. 36.** (A) Schematic representation of the different environment that tempo-benzoate (TB) experiences in the nanocapsules formulation: TB I represents the oily phase - species I, TB II represents the interfacial area – species II and TB III the external aqueous medium. (B) Represents the distribution of TB over the three environments after 1 day of preparation.

After 24 hours of dialysis against HCl/KCl buffer solution pH 1.2 or PBS pH 7.4 it was possible to observe that the shape of the spectra is alike that observed for the parent formulation NC I - TB 1 day, suggesting the majority of TB molecules still present in the lipophilic environment, Fig. 37. It was also possible to observe a decrease in signal amplitude of both dialyzed formulation, especially for that at pH 1.2.



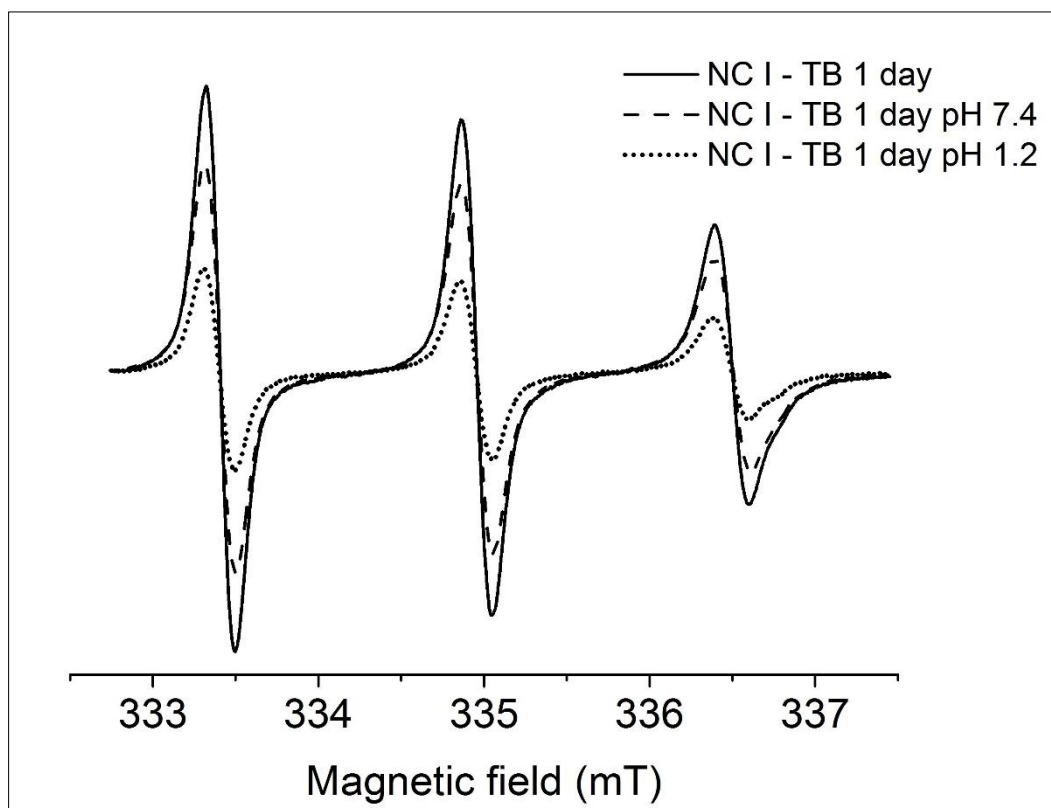


**Fig. 37.** EPR spectra of PVM/MA-MCT nanocapsules loaded with Tempo-Benzoate, NC I - TB at 1 day after preparation. NC I - TB 1-day pH 7.4 and NC I TB 1day pH 1.2 were dialyzed against PBS pH 7.4 or HCl/KCl buffer solution for 24 hours. NC I - TB: polymer-oil concentration 0.37% w/v; TB concentration 0.15 mM.

The EPR spectra of dialyzed formulations were also subject of simulation, and the obtained data indicates the TB molecules are divided into two different environments, as observed for the parent non-dialyzed formulation. For both formulation 92% of TB molecules were located in the lipophilic environment, presenting same polarity and viscosity of MCT, species I. The second species showed polarity similar to that observed for water, 1.117. Moreover, the  $\tau_c$  of the formulation at pH 1.2 was 0.115 ns, five times higher than  $\tau_c$  of water (0.024 ns) and the  $\tau_c$  of the formulation at pH 7.4 was 0.245 ns, 10 times higher. The nanocapsules submitted to dialysis lost about 17% of the TB signal at pH 7.4 and 58% at pH 1.2, when compared with the parent formulation NC I - TB 1 day. A comparison between the simulation data of all conditions is shown in Fig. 38. (Appendix II, Table VI).

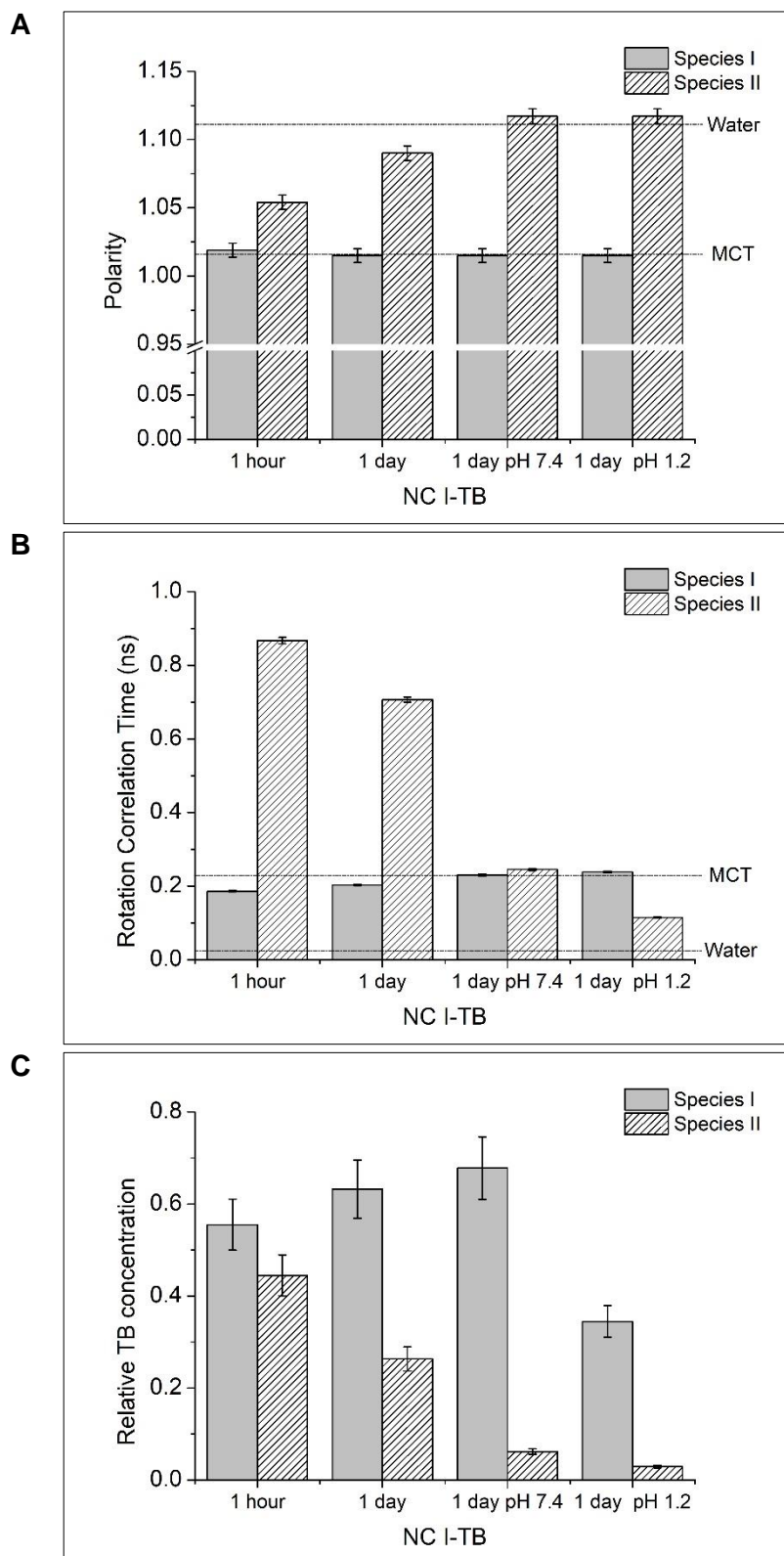


**Fig. 38.** Comparison between the data obtained from simulation of EPR spectra of NC I-TB at 1 hour and 1 day after preparation without dialysis and of NC I-TB after 24 hours of dialysis against PBS pH 7.4 or HCl/KCl buffer solution pH 1.2. Polarity (A), Rotation correlation time (B) and Relative TB concentration (C).

It is worth to mention the pronounced difference in the polarity of the species II of the different samples. At the beginning of the experiment, it was 1.054, an intermediate value between MCT and water. After 1 day at intrinsic pH conditions, this milieu became more polar, reaching a value equal to 1.090. After dialysis, the polarity of species II was similar to the polarity of water.

Regarding the rotation correlation time,  $\tau_c$ , species II presented a value about four times higher than that observed for the species I at the time point 1 hour and, although smaller, after 1 day it was still high. However, for the samples dialyzed against PBS pH 7.4, the  $\tau_c$  of species II was similar to that observed for species I and, for the formulation at pH 1.2, it was smaller.

The relative concentration of species I was higher after 1 day, the same trend was observed for the dialyzed samples, although a loss of its signal was observed. The decrease of TB signal was more pronounced for the samples dialyzed against pH 1.2 buffered solution.

The different buffered media seems to accelerate the changes in the external polymeric layer, as suggested by the change in the polarity of the species II. Those alterations may be related to de formation of carboxylic acid. The decrease in signal of the spin probe in the interfacial area (species II) is expected since the more polar milieu expels the TB molecules, to external aqueous medium or to the internal oil phase. Considering the chemical characteristics of tempo-benzoate, it is expected to concentrate in the oily phase, as depicted in Fig. 39.

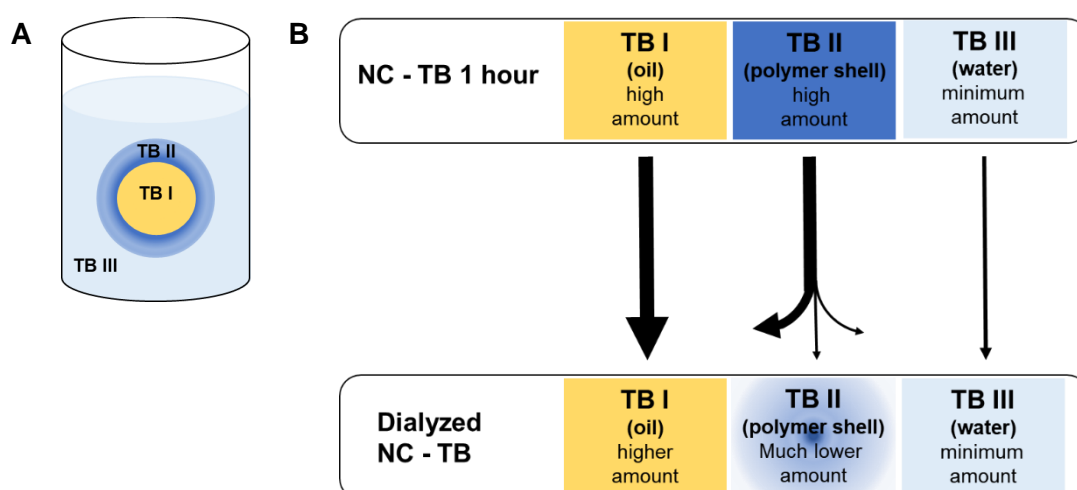


**Fig. 39.** (A) Schematic representation of the different environment that tempo-benzoate (TB) experiences in the nanocapsules formulation after dialysis. TB I represents the oily phase - species I, TB II represents the interfacial area – species II and TB III the external aqueous medium. (B) Represents the distribution of TB over the three environments after 1 day of dialysis.

Considering that the force that governs the drug release from nanocapsules is mainly the partition coefficient of the drug in the oil and external medium, the loss of TB signal may be partially explained by the release of TB in the medium. Furthermore, the acidic medium is capable of quenching the spin probe signal by the acid induced disproportionation reaction. The nitroxyl free radicals piperidine can undergo the reversible disproportionation reaction when in acidic conditions, according to the general chemical equation below, Fig. 40. The disproportionation reaction of a piperidine (I) forms the diamagnetic compounds oxammonim (II) and hydroxipiperidinium (III) that are silent for EPR spectroscopy. At pH values below 2 the rate of disproportionation is greater than the rate of the reverse reaction – comproportionation, which is negligible. However, at pH values greater than 3, the equilibrium is shifted to the left maintaining the paramagnetic characteristics of the compounds [83]–[85]. This condition explains the data obtained for the system at pH 1.2.

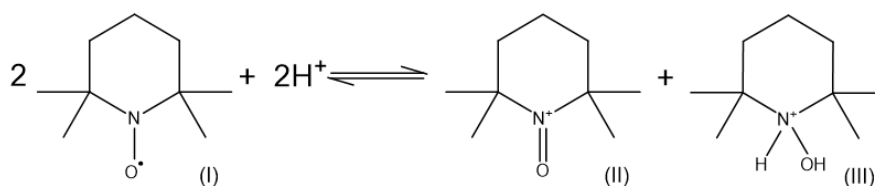


**Fig. 40.** Chemical equation of piperidine disproportionation in acidic medium.

There is also an important difference between the rotation correlation time of the capsules at pH 1.2 and at pH 7.4. These observations may be explained by the fact that at pH 1.2 the hydrolyzed polymer groups are protonated, ( $pK_{o1} = 3.5$ ;  $HA/A^- = 199/1$ ), lowering the interaction between the polymer chains. At pH 7.4, by contrast, the hydrolyzed groups are deprotonated ( $pK_{o2} = 7.5$ ;  $HA/A^- = 1/2.5$ ). In this condition, polymer chains are charged and interact with each other by means of hydrogen bonds at the very external layer of the nanocapsules shell. The gel-like environment may disturb the mobility of the spin-probe.

At this point, it is possible to compare the EPR results obtained for nanoparticles and nanocapsules loaded with TEMPO-benzoate. Fig. 41 below shows the normalized spectra of NC -TB and NP - TB at 5 minutes after preparation.

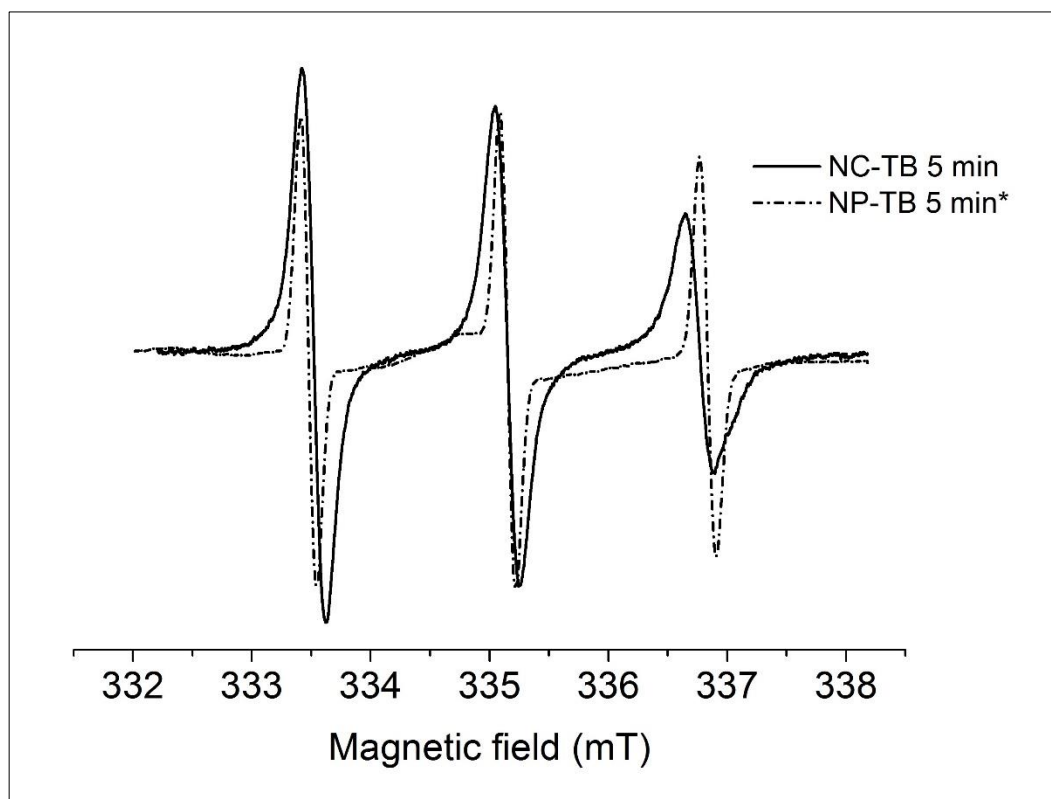


**Fig. 41.** EPR spectra of PVM/MA-MCT nanocapsules loaded with Tempo-Benzoate, NC I – TB, and of PVM/MA nanoparticles, NP-TB at 5 min immediately after preparation. NC I - TB: polymer-oil concentration 0.37% w/v; TB concentration 0.15 mM. NP - TB polymer concentration 2% w/v, TB concentration 1 mM. \*Spectrum normalized against the central line of the NC – TB spectrum.

When the TB was incorporated in nanoparticles it experienced polarity and mobility different from that observed in nanocapsules immediately after preparation. Although the simulation is not possible for the nanoparticles, due to the presence of immobilized species, it is possible to see the difference in the hyperfine splitting graphically. The micropolarity was higher for the nanoparticles, as can be seen by the values of  $2a_N$ , which was equal to 3.3606 mT for NP-TB 5 minutes and 3.0937 mT for NC I-TB 5 minutes. The difference in mobility may be observed from the width of the lines and the height of the three lines of the spectra, the sample NC I-TB 5 minutes shows the typical decrease of the height of the three peaks when the TB is in a viscous medium.

Hence, comparing both PVM/MA colloidal systems, nanoparticles and nanocapsules, the EPR spectroscopy results suggest the nanocapsules offer a more protective environment for the drug model TB than the nanoparticles

#### **4.3.5. Conclusion**

The size of the three different developed PVM/MA-MCT nanocapsules NC I, NC II and NC III, was characterized by the employment of the combination of light scattering

techniques and electron microscopy. The data obtained by DLS and SLS were used initially to select among magnetic stirrer and rotor-stator mixer the best method to perform the mixing of organic and aqueous phases. The particle size distribution of the formulations prepared using the rotor-stator mixer was in all cases slightly smaller, and this was, hence, the selected method. The DLS and SLS results were in agreement for the three formulations, and the higher the polymer-oil concentration, the larger the mean diameter of particles. Moreover, NC III showed also a broader distribution when compared with NC I and NC II. Besides size determination pH and zeta potential were also measured. The pH of formulations became moderately smaller with the increase of polymer-oil concentration, while the zeta potential became higher.

Electron microscopy results revealed the ultrastructure of the nanocapsules, whereas cryo-TEM images showed spherical structures without contrast between the polymeric shell and the oil core, the freeze-fracture showed the particles had a nanocapsules structure with shell and a well-defined core. The mean particle size observed in freeze-fractured and cryo-TEM micrographs was in agreement to that measured by SLS and smaller than that measured by DLS, which is expected considering the sensitivity of DLS to the larger particles. Interestingly, the polymeric shell revealed was thicker than that usually described on literature for solvent displacement method, which is about 10 – 20 nm. However, the characteristics of each system – polymer, oil, and production protocol applied might interfere with the final structure of the nanocapsule [18].

The stability of the formulations was monitored during 7 days after preparation. NC I was the most stable formulation, presenting the same size and Pdl over time. A small variation in size was observed for NC II and NCIII, but it remained as a monomodal size distribution during the period of evaluation. Even though the DLS and SLS results suggested that all formulations were stable over time, NC II and NC III formulations showed oil droplets onto their surfaces after the first day. The pH and zeta potential of NC II and NC III also changed after 1 day of preparation. The decrease of pH values of the NC II and NC III over time suggests the polymer is near the capsule surface, at the interface of oil and water phases. The leakage of oil, observed by the presence of oil droplets on the surface of these formulations, may expose part of the polymer to the water phase permitting the hydrolysis of these moieties. Thus, the decrease of pH can be related to the formation of carboxylic acids after the hydrolysis of the maleic anhydride groups that was in contact with the aqueous medium. The drop of pH values was more pronounced for NC III than for NC II, while it remained unchanged for NC I.

In an attempt to stabilize the polymeric shell, the nanocapsules formulations were cross-linked with 1,3-diaminopropane (DP) in two different concentrations (0.118 mg DP/mg PVM/MA and 0.237 mg DP/mg PVM/MA). These formulations were also characterized and their stability evaluated over 7 days. Cross-linked NC I presented only a small increase in the particle size and polydispersity after 7 days. For the cross-linked NC III, the change in size was more pronounced as well as its polydispersity. The changes observed for the nanocapsules cross-linked at polymer:DP molar ratio 4:1 (0.118 mg DP/mg PVM/MA) were more pronounced than that observed for polymer:DP molar ratio 2:1 (0.237 mg DP/mg PVM/MA). It could be related to the change in the backbone conformation after cross-linking reaction and the consequent exposition of anhydride groups to the aqueous medium, followed by the hydrolysis of these groups during the first 24 hours. Comparatively, the cross-linked formulations at a higher concentration of DP do not show this behavior, which may be explained by the larger amount of cross-linker that was high enough to stabilize the polymer structure immediately after cross-linking reaction and, consequently, stabilize the size of the nanocapsules. Even after cross-linking, formulations NC II and NC III presents oil leakage 1 day after preparation. The cross-linking process seemed to interfere strongly neither on the size nor the stability of the nanocapsules formulations, as was shown by the freeze-fracture TEM of cross-linked NC I formulations.

To evaluate the hydrolysis of the polymer on the surface of the nanocapsules and the consequences of it on the stability of the formulations, 24 hours after preparation plain and cross-linked nanocapsules were diluted in buffer solutions at pH 1.2 and at pH 7.4, incubated for 5 minutes and then sized by DLS. NC I was the most stable formulation, its size and Pdl remained constant at both pH condition. NC II and NC III experienced more changes in size and Pdl, while the cross-linked formulations were similar in size. However, the Pdl of all formulations at pH 1.2 was smaller when compared to the control. These more pronounced variations of the size of NC II, NC III, and cross-linked formulations are in agreement with characterization data (DLS, pH and zeta potential results), suggesting the polymer is exposed at the capsule surface on these formulations, being more prone to hydrolysis of the exposed anhydride groups. The change in Pdl suggests the medium may interfere in the protonation of the hydrolyzed groups at the particle surface, as observed for nanoparticles. When totally protonated, at pH 1.2, the polymer chains shrink and when at pH 7.4, electrostatic repulsion forces provoke the swelling of the polymer, interfering on the Pdl results.

The EPR results demonstrated the TEMPO-benzoate experienced different environmental conditions in the formulation, inside the nanocapsules and in water. The first species had similar polarity and viscosity of the MCT, whereas the second species indicated the environment is slightly more polar and considerably more viscous than the MCT itself, suggesting a presence of an interfacial area between the oily and aqueous phases. The more viscous environment was present after 24 hours of nanocapsules preparation, but with a lower TB signal. Interestingly the relative concentration of TB in the lipophilic environment increased during this period.

When the formulation was dialyzed against buffer solutions at pH 1.2 and 7.4 the polarity and viscosity of the lipophilic environment remained constant. The polarity of the interfacial area was similar to that observed for water in both media, however the rotation correlation time,  $\tau_c$  of the formulation at pH 1.2 was five times higher than  $\tau_c$  of water and the  $\tau_c$  of the formulation at pH 7.4 about 10 times higher.

The results show that the polymeric shell releases the spin probe in the medium, due to the equilibrium of the probe in both compartments but, also, lose TB to the oil phase, since it was observed an increase of TB in the lipophilic phase. This condition was more pronounced when the formulation was exposed to different pH conditions in the dialysis process. The different pH conditions seemed to interfere and change the external polymeric layer, disturbing the mobility of the spin probe. And these findings are in agreement with the data obtained by DLS experiments. The decrease of the TB signal on dialyzed samples may be explained by the partition of the spin probe in both media, and also by the disproportionation reaction that quenches the piperidines in acidic medium.

For the first time, a stable nanocapsules formulation based in PVM/MA and MCT, without stabilizers and employing only acetone as an organic solvent, was developed. Considering all presented results, it is possible to conclude that the nanocapsules were able to retain the drug model, even in a severe condition as pH 1.2 for 24 hours, when about 40% of the initial concentration was still in the lipophilic medium.



## **5. Summary and Perspectives**

### **5.1. PVM/MA nanoparticles – study of polymer hydrolysis**

Poly(methyl vinyl ether-alt-maleic anhydride) – PVM/MA is a known commercial available polymer widely employed by the cosmetic and healthcare industries in topical and oral formulations due to its capacity to develop bioadhesiveness with mucosa, ability to form films, and increase the viscosity of the medium. Its application to produce nanoparticle for drug delivery has been stimulated by recent research, especially by the group of Prof. Dr. Juan M. Irache from the University of Navarra. PVM/MA is a water-insoluble polymer that in the aqueous medium is hydrolyzed forming two carboxylic acids, acquiring a polyelectrolyte character and becoming water-soluble [72]. PVM/MA is considered a pre-activated polymer due to the presence of maleic anhydride moieties, which is very reactive to primary amines and less reactive to alcohols [28].

Several publications describing the use of PVM/MA to prepare nanoparticles for oral delivery have been published during the last years. The employment of PVM/MA relies on its capacity to develop non-specific bioadhesiveness to mucosal layer along the gastrointestinal tract and, therefore, increase drug absorption. Regarding the instability of PVM/MA in an aqueous medium, the use of a cross-linking agent was proposed to stabilize the nanoparticle structure. The improvement of the loading efficiency and adhesiveness capacity of nanoparticles was necessary. And its association to different substances such as cyclodextrins, PEG or to proteins was reported on the majority of the works [29], [30], [33], [35], [39], [40], [42]–[44], [41]

The first part of this work was dedicated to evaluate and determine the poly-anhydride hydrolysis under different pH conditions and its consequences on the plain or cross-linked nanoparticles structures. Investigation of the kinetics of polymer hydrolysis and understanding the behavior of the polymeric matrix of the nanoparticles can lead to the more successful application of this polymer in developing a more efficient drug delivery system for oral and topic administration.

The behavior of the PVM/MA nanoparticles in different pH conditions was determined by the combination of several techniques. Dynamic light scattering (DLS), nanoparticle tracking analysis (NTA) and electron microscopy after freeze-fraction were used together to determine the particle size of the freshly prepared plain and cross-linked

nanoparticles. DLS, NTA, and cryo-TEM were also employed to evaluate the evolution of the nanostructures over 24 hours after preparation. ATR-FTIR spectroscopy was used to determine the qualitative conversion of the anhydride in carboxylic acid and auto-titration was employed to measure the velocity of formation of carboxylic acid in different pH.

DLS and NTA results for the plain nanoparticle formulation (NP) showed an increase in the particles size until the time point 6 hours. After this time point the results obtained from both techniques differed considerably, while DLS results showed the presence of particles with a broader size distribution, the NTA showed the dissolution of the particles. The explanation of this fact was achieved by the understanding of the theoretical background of both techniques. Considering the polyelectrolyte character of the hydrolyzed polymer, the needed conditions for DLS analysis, applying the general purpose algorithm, were not fully achieved by the PVM/MA nanoparticles – spherical particles that do not interact with each other. On the other hand, NTA detection depends on the difference between the refractive index of the sample and the refractive index of the medium, and also on the particle size that has to be larger than 20 nm. The refractive index of the dense polymeric structures changes when they undergo dissolution in contact with water. The effect of the polymer chains interaction on the DLS results was demonstrated by the analysis of a hydrolyzed-polymer solution at low concentration. Applying the high-resolution DLS analysis, which uses the multiple narrow mode algorithm, was possible to show that the polymer chains interact to one another and this interaction depends on the pH of the medium, changing the DLS output. The polyelectrolyte character of the hydrolyzed polymer explains the DLS results that suggest the presence of the particles at the latest time points. The extension of the protonation of the carboxylic acid groups determines the polymer-polymer and polymer-medium interactions. When protonated, the measured size is smaller suggesting the polymer chain was folded over itself, acquiring the compact coil conformation. While under conditions in which hydrogen bonds are present the measured size became bigger due to self-association of the polymeric chains, which is in agreement with previous work [59].

The stabilization of zeta potential and the pH after 6 hours suggested the majority of polymer hydrolysis occurs until this time point. Those results were confirmed by ATR-FTIR spectroscopy that showed only a residual signal of anhydride groups at that time point. All these data strongly indicate the progressive dissolution of the PVM/MA nanoparticles and its complete solubilization observed by NTA.

The mean diameter of cross-linked nanoparticles (NP-DP) was larger than that observed for NP formulation at the initial time point, and increased during the first 3 hours of experiment, remaining constant after this time point until the end of the measurements. The zeta potential of the particles increased during the first 3 hours while the pH decreased during this period. These observations may be explained by the rearrangement of the polymer chains after the reaction with the cross-linker agent, followed by the hydrolysis of the lasting maleic anhydride groups. DLS and NTA outputs were similar along the whole experiment, showing the presence of particles until the latest time point analyzed, even though the size distribution was very broad. The alteration of the structure of cross-linked nanoparticles may justify the necessity of association of PVM/MA with other substances like cyclodextrins, and PEG to improve its load capacity and efficiency [33], [35].

The investigation of the effect of the pH of the medium on the polymer hydrolysis and on the nanoparticle structure, showed that all applied pH conditions – pH 1.2, pH 5.0 and pH 7.4, accelerated the polymer hydrolysis and the dissolution of plain nanoparticles. The results have evidenced the fast nanoparticle dissolution when it is at neutral pH. The cross-linked nanoparticles were also affected by the neutral pH, assuming the final size at the earliest moment after dilution in the neutral medium.

The auto-titration of the nanoparticle formulation gave a more accurate insight about the velocity of the polymer hydrolysis in the nanoparticles. The results showed the polymer undergo hydrolysis faster when at higher pH values, and, as showed by NTA and ATR-FTIR, the hydrolysis reaction was finished in less than 20 minutes when in pH 7.4.

For the EPR spectroscopy, the nitroxyl radical TEMPO-benzoate (TB) was the employed spin-probe. TB is a hydrophobic molecule with log P about 2.46 that may be used as a lipophilic model drug. The EPR results suggest the existence of dense polymeric structures at the first-time points by the presence of immobilized spin probe. The signal of this immobilized probe decreased over time and was not detectable at the latest time points, suggesting the dissolution of the protective environment that was present at the beginning of the experiment. The signal of immobilized TB was also absent at the earliest time points of nanoparticles at neutral pH, which corroborates the statement that the nanoparticles are immediately solubilized, releasing the loaded drug, when in neutral pH.

For the first time was demonstrated the kinetic of dissolution of the PVM/MA nanoparticles due to the hydrolysis reaction of the polymer. Although the hydrolysis is slow when the nanoparticles are in their intrinsic pH, it is very fast when in moderately acidic or in neutral conditions. Considering these results, it is questionable if the nanoparticles remain as a useful system for controlled release when it faces the environmental conditions of gastrointestinal tract.

## **5.2. PVM/MA Nanocapsules: development and characterization**

The second part of this work was dedicated to the development and characterization of a new nanocapsules system employing PVM/MA. Nanocapsules can circumvent PVM/MA-nanoparticle drawbacks enhancing the drug loading and encapsulation efficiency and keeping the ability of the PVM/MA to develop adhesiveness with the mucous membranes. Medium-chain triglycerides (MCT) was the chosen oil. It has been used in a variety of pharmaceutical formulations for oral, parenteral and topical applications, is already reported as an enhancer of drug absorption of orally administered drugs and does not interact chemically with the polymer [52], [86], [87].

PVM/MA-MCT nanocapsules were developed employing only acetone as an organic solvent and without the need of any type of stabilizers, applying the well-known solvent displacement method. The best formulation was selected for a screening of three different polymer-oil concentration and two different mixing methods, magnetic stirrer and rotor-stator mixer. The characterization and stability evaluation of the yielded colloidal formulations were made by the combination of various techniques including DLS, SLS, cryo and freeze-fracture TEM and EPR spectroscopy.

The final polymer-oil concentration of the three different nanocapsules formulations was 0.37% w/v (NC I), 0.74% w/v (NC II) and 1.11% w/v (NC III), they were produced using the rotor-stator mixer. The combination of light scattering techniques and electron microscopy allowed to determine the particle size and the ultrastructure of the yielded nanocapsules. DLS and SLS brought out the polymer-oil concentration had an impact on the particle size. The higher the concentration, the larger the particles. The mean particle size obtained by freeze-fracture and cryo-TEM were in agreement with the results obtained by DLS and SLS. The freeze-fracture TEM revealed a spherical core-shell structure with an uncommon thick shell, and the cryo-TEM results showed spherical structures without contrast between polymer and oil.

The formulations were evaluated over a period of 7 days. Light scattering techniques, pH, and zeta potential results showed the formulations were stable over this period and the changes were more pronounced for NC II and NC III. Even though stable accordingly DLS and SLS results, a leakage of oil was observed for NC II and NC III after the first day of storage.

To achieve more stable nanocapsules by the stabilization of the polymeric shell, the three different formulations were cross-linked with DP in 2 different concentrations 0.118 mg and 0.237 mg DP/mg PVM/MA (Polymer:DP molar ratio 4:1 and 2:1, respectively). The results showed the formulations cross-linked with the lower amount of DP had the most important changes in size distribution, Pdl, pH and zeta potential. And, the cross-linked NC II and NC III formulations presented leakage of oil, as observed for the plain formulations. The cross-linking processes did not interfere strongly on particle size and in stability of the nanocapsules formulations.

All the described results, namely the decrease in pH values and the increase in the zeta potential, strongly suggest the polymer at the nanocapsule surface may interact with the medium, being partially hydrolyzed. The only exception is the formulation NC I for which the results remained constant over time. These observations were corroborated by the results obtained from the study of the influence of the pH of the medium on the size of nanoparticles after 24 hours of preparation. These data showed the pH of the medium did not change the particle size, but it had an important effect on the Pdl of samples at pH 1.2, decreasing it to values below 0.1. The change on Pdl suggests the medium may interfere in the protonation of the hydrolyzed groups at the particle surface, shrinking the polymer chains when at pH 1.2, as demonstrated for the nanoparticles.

EPR spectroscopy was applied to investigate the microenvironment of the nanocapsules and their capacity to retain the model drug TEMPO-benzoate. The results demonstrated the presence of two distinct milieus in the nanocapsules formulation. The first showed polarity and rotation correlation time are similar to that observed for the pure MCT – species I. The second, called species II, showed polarity value between MCT and water, and rotation correlation time four times higher than that observed for MCT and more than 30 times higher than that observed for water. This second microenvironment can be, therefore, considered as an interfacial are. The same observations were made after 24 hours of preparation. Interestingly the relative concentration of TB in the lipophilic environment increased during this period. When

the formulations were exposed to pH 1.2 and 7.4, polarity and viscosity of the lipophilic environment remained constant. The polarity of the interfacial area was similar to that observed for water in both media. The viscosity, however, was five times higher than water viscosity when the formulation was at pH 1.2 and 10 times higher when at pH 7.4. The results suggest the change in the external polymeric phase expels the spin probe increasing its concentration in the lipophilic phase. The different pH conditions interfered and changed the interfacial environment. These findings corroborate the data obtained by DLS experiments. Moreover, the acquired spectra presented the same shape under the different conditions analyzed, varying only in amplitude. Therefore, it was possible to conclude that the nanocapsules were able to retain the drug model, even in a severe condition as that applied by the dialysis.

The development of PVM/MA and MCT nanocapsules without stabilizers and employing only acetone as an organic solvent was described for the first time. The applied technique yielded nanocapsules formulation that was stable in an aqueous medium for, at least, 7 days.

The development of nanocapsules still needs elucidative studies about its ultrastructure, enlightening the observed thick polymeric shell revealed in freeze-fracture micrographs. *In vitro* studies such as drug release in gastrointestinal media and mucosal environments, the toxicity of the formulation and capacity to enhance the drug absorption. Further, *in vivo* tests as the efficacy of the nanocapsules formulation for increasing the drug absorption and bioavailability via oral administration and its efficacy in the treatment of specific disorders are still needed.

The improvement of the nanoparticles capacity of loading lipophilic drugs using more suitable cross-linkers as, for example, di-amino-alkane with longer carbon chains is a possibility. This strategy may also be tested to improve the oil retention capacity of the NC II and NC III formulations.

Moreover, the improvement of the nanocapsules formulation for its employment as a system for EPR or fluorescent probes for *in vitro* and *in vivo* studies is also a possibility.

Explore the potential of PVM/MA as a carrier for topical drug administration is a field to be explored. The ability to develop films, the polar character of the polymer and its high solubility in acetone make it a good candidate for electrospinning and electrospinning applications. Considering that PVM/MA develops a polar environment due its polyelectrolyte character being able to retain drugs with the same chemical

characteristics. The loading of anti-inflammatory and antibiotic drugs in polymeric nanoparticles or fibers to produce wound dressing is not an unrealistic application. These techniques bring the advantage of delay the polymer hydrolysis during the preparation steps, increase drug loading and the possibility to scale up.

## 6. Appendix

### Appendix I. PVM/MA nanoparticles – study of polymer hydrolysis

#### Particle size, zeta potential, and pH of plain nanoparticles and cross-linked nanoparticles

**Table I.** DLS and NTA particle size distribution, pH and zeta potential of PVM/MA plain nanoparticles (NP) and of nanoparticles cross-linked with 1,3-diaminopropane (NP-DP) at time point 0.5, 3, 6, 10, and 24 hours. DP concentration was 0.118 mg DP/mg PVM/MA, the monomer:DP molar ratio was 4:1. n ≥ 3.

Formulation	Time (hour)	DLS			Zeta Potential ± S.D. (mV)	NTA		
		pH ± S.D.	Size ± S.D. (nm)	PDI ± S.D.		Size ± S.D. (nm)	Standard Deviation ± S.D. (nm)	Particle concentration ± S.D. (10 <sup>8</sup> particles/mL)
NP	0.5	2.76±0.16	93.3±12.5	0.157±0.029	-30.5±4.2	91.3±23.5	25.8±8.9	7.0±0.9
	3	2.52±0.14	147.1±20.3	0.134±0.027	-25.2±0.4	143.5±44.5	34.6±4.4	7.8±2.1
	6	2.31±0.06	237.6±65.3	0.172±0.058	-22.4±2.1	213.6±48.2	57.7±3.9	7.1±3.9
	10	2.27±0.02	283.3±14.5	0.131±0.013	-21.5±2.3	200.1±8.0	103.4±24	0.7±0.2**
	24*	2.29±0.01	289.6±16.2	0.147±0.016	-21.7±1.3	-	-	-
NP-DP	0.5	4.46±0.36	157.1±34.3	0.139±0.022	-30.3±1.4	151.0±69.4	53.2±22.7	6.6±1.5
	3	3.81±0.42	314.4±81.1	0.241±0.050	-32.3±3.4	320.0±16.7	104.8±7.2	6.2±2.8
	6	3.78±0.33	351.6±121.3	0.245±0.038	-28.9±3.1	290.9±20.3	116.2±7.5	5.5±0.7
	10	3.74±0.37	402.7±105.2	0.242±0.039	-28.7±2.5	340.3±34.3	111.8±11.0	5.6±1.2
	24	3.74±0.32	319.4±117.5	0.223±0.005	-26.7±2.3	358.1±35.2	101.5±12.3	4.9±1.3

DLS: average result from 3 measurements (automatic setting, general purpose algorithm), the samples were diluted in filtered bi-distilled water at a final concentration of 2 mg polymer/mL. NTA: average result and standard error from 5 measurements, 60 s each, of the same sample diluted with filtered bi-distilled water; sample concentration 0.1 µg polymer/mL. Zeta Potential: average result from 3 measurements, the samples were diluted 10 times (1:10) with KCl 0.1 mM, at 25 °C.

\*At the time point 24 h, the quality of measurement was not good. The samples were 'too polydisperse to cumulant analysis.'

\*\*sample concentration 2 µg polymer/mL.



### Impact of pH of the medium on the plain and cross-linked nanoparticles

**Table II.** DLS and NTA particle size distribution, pH and zeta potential of PVM/MA plain nanoparticle (NP) diluted in HCl/KCl buffer pH 1.2 (NP:pH1.2), in citric acid/phosphate buffer pH 5.0 (NP:pH 5.0), or in PBS pH 7.4 (NP:pH 7.4) and of nanoparticles cross-linked with 1,3-diaminopropane diluted in PBS pH 7.4 (NP-DP:pH 7.4), at a final polymer concentration equal to 10 mg/mL. Time point 0.5, 3, 6, 10 and 24 hours. DP concentration was 0.118 mg DP/mg PVM/MA, the monomer:DP molar ratio was 4:1. n ≥ 3.

Formulation	DLS				Zeta Potential ± S.D. (mV)	NTA		
	Time (hour)	pH ± S.D.	Size ± S.D. (nm)	PDI ± S.D.		Size ± S.D. (nm)	Standard Deviation ± S.D. (nm)	Particle concentration ± S.D. (10 <sup>8</sup> particles/mL)
NP:pH 1.2 (1:1)	0.5	1.33±0.11	78.4±11.7	0.121±0.011	-10.0±1.2	69.2±15.2	22.3±8.9	3.2±0.8
	3	1.33±0.08	99.0±7.7	0.110±0.018	-9.4±1.8	113.3±29.4	37.0±5.2	2.4±1.1
	6	1.36±0.07	141.7±8.0	0.230±0.106	-9.3±2.8	202.7±40.7	67.0±4.7	1.4±1.0
	10	1.35±0.12	180.0±26.0	0.728±0.132.3	-	210.9±13.8	140.3±4.4	0.9±0.7
NP:pH 5.0 (1:1)	0.5	4.51±0.05	152.2±14.6	0.101±0.021	-47.9±2.9	142.0±19.6	39.3±14.3	14.0±0.4
	3	4.00±0.03	279.9±36.1	0.273±0.105	-40.5±4.9	239.3±19.7	63±3.7	7.6±9.1
	6	4.01±0.02	384.9±81.1	0.468±0.084	-	349.3±23.6	180.6±9.3	1.1±0.9
NP:pH 7.4 (1:1)	0.5	7.4±0.07	283.0±16.0	0.313±0.104	-54.2±1.0	127.7±7.8	69.4±8.9	0.6±0.6*
	3	7.4±0.06	212.0±17.3	0.459±0.065	-	-	-	-
NP-DP:pH 7.4 (1:1)	0.5	7.4±0.07	214.7±71.2	0.119±0.018	-53.9±1.7	154.4±75.7	49.1±31.8	5.6±2.4
	3	7.4±0.11	212.5±67.6	0.104±0.018	-54.1±1.9	115.7±21.0	38.2±14.4	4.8±1.5
	6	7.4±0.08	213.2±67.5	0.121±0.030	-53.7±1.5	170.2±85.7	53.9±34.4	4.3±0.3
	10	7.4±0.09	214.8±70.4	0.118±0.038	-53.8±1.4	159.0±96.9	42.9±23.7	4.7±2.1
	24	7.4±0.07	257.6±68.6	0.135±0.035	-52.9±1.8	168.3±94.7	46.4±22.8	3.7±1.8

DLS: average result from 3 measurements (automatic setting, general purpose algorithm), the samples were diluted in filtered bi-distilled; sample concentration 1 mg polymer/mL. NTA: average result and standard error from 5 measurements (60 seconds each) of the same sample diluted with filtered bi-distilled water; sample concentration 0.1 µg polymer/mL. Zeta Potential: average result from 3 measurements, the samples were diluted 10 times (1:10) with KCl 0.1 mM, at 25 °C. \* sample concentration 2 µg polymer/mL.

## Appendix II. PVM/MA-MCT Nanocapsules: development and characterization

### Particle size, zeta potential, and pH of plain nanocapsules (NC I, NC II and NC III)

**Table I.** DLS and SLS particle size distribution, pH and zeta potential of PVM/MA-MCT plain nanocapsules (NC) at time point 1 hour, 1, 2, and 7 days after preparation. NC I (0.37% w/v), NC II (0.74% w/v), and NC III (1.11% w/v).

Formulation	Time	pH ± S.D.	Size ± S.D. (nm)	PDI ± S.D.	D10 ± S.D. (nm)	D50 ± S.D. (nm)	D90 ± S.D. (nm)	D[4,3] ± S.D. (nm)	Zeta Potential ± S.D. (mV)
NC I	1 h	3.32±0.10	195.6±8.5	0.087±0.015	102±5	150±7	210±8	154±7	-63.7±3.9
	1 d	3.32±0.03	196.8±7.6	0.086±0.017	97±3	144±4	204±4	148±4	-67.2±4.1
	2 d	3.31±0.03	208.8±2.3	0.115±0.021	104±0	155±2	216±3	158±1	-67.5±1.3
	7 d	3.31±0.06	208.9±7.5	0.113±0.014	104±1	157±2	223±4	161±2	-64.1±5.1
NC II	1 h	3.26±0.12	229.3±11.7	0.100±0.009	100±7	154±3	227±25	160±6	-60.2±2.2
	1 d	3.11±0.04	252.2±10.1	0.125±0.012	100±6	154±3	225±14	160±4	-58.9±3.0
	2 d	3.08±0.03	251.5±14.8	0.129±0.011	100±9	154±2	227±25	160±5	-60.6±3.2
	7 d	3.08±0.02	251.7±13.6	0.133±0.011	97±10	155±1	236±25	161±5	-61.9±2.2
NC III	1 h	3.12±0.06	266.6±17.6	0.106±0.021	85±3	161±9	306±42	181±14	-56.1±1.9
	1 d	2.92±0.03	314.6±6.9	0.132±0.014	87±5	166±14	312±41	185±19	-55.8±0.6
	2 d	2.93±0.01	300.3±13.9	0.151±0.012	86±3	163±12	307±40	183±17	-56.2±0.2
	7 d	2.95±0.02	299.7±18.6	0.155±0.032	89±4	173±6	335±9	195±6	-56.7±1.4

DLS: average result from 3 measurements (automatic setting, general purpose algorithm), the samples were diluted (1:10) in filtered bi-distilled water. SLS: average result from 5 measurements, 10 s each, with optical obscuration of 5%. SLS: average result from 5 measurements, 10 s each, with optical obscuration of 5%. Zeta Potential: average result from 3 measurements, the samples were diluted 10 times (1:10) with KCl 0.1 mM, at 25 °C.

**Particle size, zeta potential, and pH of plain nanocapsules [NC II (MS) and NC III (MS)] prepared applying magnetic stirring**

**Table II.** DLS and SLS particle size distribution, pH and zeta potential of PVM/MA-MCT plain nanocapsules (NC) prepared by magnetic stirring at time points 1 hour, 1, 2, and 7 days after preparation. NC I (0.37% w/v), NC II (0.74% w/v), and NC III (1.11% w/v).

Formulation	Time	pH ± S.D.	Size ± S.D. (nm)	PDI ± S.D.	D10 ± S.D. (nm)	D50 ± S.D. (nm)	D90 ± S.D. (nm)	D[4,3] ± S.D. (nm)	Zeta Potential ± S.D. (mV)
NC II (MS)	1 h	3.29±0.18	243.8±9.2	0.108±0.006	86±5	159±8	285±50	174±16	-62.5±0.7
	1 d	3.09±0.01	273.9±22.4	0.127±0.012	88±6	161±9	284±53	175±17	-60.5±1.4
	2 d	3.09±0.01	268.1±20.6	0.132±0.017	93±4	165±13	283±53	178±19	-63.5±2.2
	7 d	3.09±0.02	267.5±15.7	0.136±0.015	93±4	164±12	284±54	178±19	-62.8±1.7
NC III (MS)	1 h	3.20±0.06	258.5±29.8	0.105±0.017	86±6	166±13	343±8	196±18	-59.3±3.2
	1 d	3.02±0.02	294.4±25.5	0.126±0.016	88±4	162±15	294±49	179±21	-57.4±0.8
	2 d	3.02±0.02	286.3±28.5	0.145±0.020	89±4	166±10	322±23	191±12	-59.7±0.6
	7 d	3.02±0.03	279.9±30.7	0.151±0.021	84±9	160±17	293±49	176±22	-58.8±1.6

DLS: average result from 3 measurements (automatic setting, general purpose algorithm), the samples were diluted (1:10) in filtered bi-distilled water. SLS: average result from 5 measurements, 10 s each, with optical obscuration of 5%. SLS: average result from 5 measurements, 10 s each, with optical obscuration of 5%. Zeta Potential: average result from 3 measurements, the samples were diluted 10 times (1:10) with KCl 0.1 mM, at 25 °C.

**Particle size, zeta potential, and pH of PVM/MA-MCT cross-linked nanocapsules (NC + DP).**

**Table III.** DLS and SLS particle size distribution, pH and zeta potential of PVM/MA-MCT cross-linked nanocapsules (NC + DP) at time points 1 hour, 1, 2, and 7 days after preparation. NC I (0.37% w/v), NC II (0.74% w/v), and NC III (1.11% w/v). PVM/MA monomer:DP molar ratio 4:1 (0.118 mg DP/mg PVM/MA).

Formulation	Time	pH ± S.D.	Size ± S.D. (nm)	PDI ± S.D.	D10 ± S.D. (nm)	D50 ± S.D. (nm)	D90 ± S.D. (nm)	D[4,3] ± S.D. (nm)	Zeta Potential ± S.D. (mV)
NC I + DP 4:1	1 h	4.37±0.11	213.1±11.6	0.094±0.005	100±5	149±7	209±7	153±6	-47.4±0.9
	1 d	4.30±0.08	227.3±22.7	0.126±0.009	97±7	146±7	206±8	150±7	-47.7±1.0
	2 d	4.36±0.01	248.6±6.7	0.125±0.007	98±7	150±8	216±13	154±7	-47.7±0.4
	7 d	4.37±0.02	251.7±5.4	0.121±0.011	90±8	149±7	231±10	156±6	-47.7±0.5
NC II + DP 4:1	1 h	4.43±0.20	241.2±7.7	0.093±0.009	104±2	153±2	214±3	157±2	-45.1±1.0
	1 d	4.12±0.07	267.3±20.3	0.129±0.025	102±2	153±4	217±8	157±4	-45.9±0.3
	2 d	4.13±0.06	280.7±8.1	0.135±0.008	104±2	153±2	214±2	157±2	-48.0±1.7
	7 d	4.12±0.04	283.1±10.9	0.114±0.019	103±2	154±2	215±3	157±3	-47.6±0.9
NC III + DP 4:1	1 h	4.48±0.20	289.5±26.0	0.099±0.013	86±3	164±10	314±46	185±16	-45.7±0.4
	1 d	4.24±0.45	331.7±17.4	0.142±0.009	87±4	157±9	306±42	183±16	-46.3±1.1
	2 d	4.02±0.08	342.2±14.8	0.143±0.010	90±3	168±13	316±45	189±18	-46.0±1.3
	7 d	4.03±0.09	342.4±18.0	0.145±0.030	87±6	167±14	317±45	189±20	-46.6±1.4

DLS: average result from 3 measurements (automatic setting, general purpose algorithm), the samples were diluted (1:10) in filtered bi-distilled water. SLS: average result from 5 measurements, 10 s each, with optical obscuration of 5%. SLS: average result from 5 measurements, 10 s each, with optical obscuration of 5%. Zeta Potential: average result from 3 measurements, the samples were diluted 10 times (1:10) with KCl 0.1 mM, at 25 °C.

**Table IV.** DLS and SLS particle size distribution, pH and zeta potential of PVM/MA-MCT cross-linked nanocapsules (NC + DP) at time points 1 hour, 1, 2, and 7 days after preparation. NC I (0.37% w/v), NC II (0.74% w/v), and NC III (1.11% w/v). PVM/MA monomer:DP molar ratio 2:1 (0.237 mg DP/mg PVM/MA).

Formulation	Time	pH ± S.D.	Size ± S.D. (nm)	PDI ± S.D.	D10 ± S.D. (nm)	D50 ± S.D. (nm)	D90 ± S.D. (nm)	D[4,3] ± S.D. (nm)	Zeta Potential ± S.D. (mV)
NC I + DP 2:1	1 h	5.26±0.20	195.5±10.6	0.121±0.007	100±5	145±10	208±7	152±6	-42.9±0.5
	1 d	5.22±0.22	203.0±18.9	0.122±0.010	98±5	146±6	206±7	150±6	-44.2±3.0
	2 d	5.30±0.03	197.0±7.3	0.112±0.005	100±5	150±7	212±9	154±7	-41.9±1.5
	7 d	5.35±0.07	194.5±6.0	0.119±0.011	90±7	149±7	231±8	156±7	-41.0±1.2
NC II + DP 2:1	1 h	5.22±0.15	232.1±14.3	0.135±0.020	104±2	153±2	214±3	157±2	-42.3±0.8
	1 d	5.01±0.14	231.9±18.6	0.120±0.023	99±7	152±3	220±11	157±2	-43.3±0.8
	2 d	5.06±0.18	222.1±23.2	0.145±0.026	103±1	153±2	214±2	157±2	-43.2±1.1
	7 d	5.05±0.18	225.8±23.7	0.141±0.019	103±1	153±2	215±5	157±2	-42.7±0.9
NC III + DP 2:1	1 h	5.15±0.16	284.1±13.2	0.110±0.032	88±2	166±12	316±48	188±18	-42.1±1.5
	1 d	5.05±0.31	285.4±26.2	0.136±0.014	86±3	162±11	308±43	183±16	-41.4±0.7
	2 d	4.92±0.17	297.2±8.4	0.145±0.026	86±3	164±8	313±42	185±14	-41.0±1.1
	7 d	4.93±0.17	301.5±7.5	0.143±0.013	88±3	167±11	321±48	189±17	-40.8±1.4

DLS: average result from 3 measurements (automatic setting, general purpose algorithm), the samples were diluted (1:10) in filtered bi-distilled water. SLS: average result from 5 measurements, 10 s each, with optical obscuration of 5%. SLS: average result from 5 measurements, 10 s each, with optical obscuration of 5%. Zeta Potential: average result from 3 measurements, the samples were diluted 10 times (1:10) with KCl 0.1 mM, at 25 °C.

### ***Impact of pH of the medium on the plain and cross-linked nanocapsules***

**Table V.** Particle size distribution and pH, NC and NC +DP nanoparticles formulation determined at different media.

Formulation	Bi-distilled H <sub>2</sub> O			pH 1.2		pH 7.4	
	pH	Size (nm)	PDI	Size (nm)	PDI	Size (nm)	PDI
<b>NC I</b>	3.34±0.01	191.0±4.25	0.087±0.006	193.8±1.0	0.062±0.014	198.0±4.2	0.094±0.014
<b>NC I +DP 4:1</b>	4.24±0.07	226.3±8.13	0.120±0.011	208.0±0.4	0.043±0.017	190.2±3.4	0.100±0.004
<b>NC I +DP 2:1</b>	5.05±0.16	193.1±14.3	0.118±0.015	219.6±5.5	0.034±0.007	217.4±18.6	0.102±0.008
<b>NC II</b>	3.15±0.02	246.1±9.5	0.122±0.017	205.3±4.4	0.074±0.004	198.4±5.5	0.114±0.005
<b>NC II +DP 4:1</b>	4.08±0.03	252.6±17.0	0.133±0.039	222.4±8.9	0.061±0.004	227.0±5.2	0.111±0.006
<b>NC II +DP 2:1</b>	4.95±0.08	243.6±7.4	0.108±0.029	228.9±5.8	0.043±0.009	257.8±8.6	0.153±0.005
<b>NC III</b>	3.09±0.33	311.3±2.9	0.133±0.017	231.5±17.7	0.091±0.053	232.0±11.3	0.137±0.019
<b>NC III +DP 4:1</b>	4.30±0.53	326.2±16.7	0.146±0.003	268.4±13.9	0.096±0.14	286.7±46.3	0.152±0.028
<b>NC III +DP 2:1</b>	5.05±0.37	281.5±30.4	0.134±0.017	271.2±38.5	0.085±0.007	300.1±16.5	0.181±0.020

DLS: average result from 3 measurements (automatic setting, general purpose algorithm), the samples were diluted (1:10) and incubated in filtered bi-distilled water or in, HCl/KCl buffer pH 1.2 or in PBS pH 7.4.

### EPR Spectroscopy - Nanocapsules loaded with TEMPO-benzoate (TB)

**Table VI.** Data obtained from simulation of EPR spectra of TB in water, MCT and NC I at 1 hour and 1 day after preparation without dialysis and of NC I after 24 hours of dialysis against PBS pH 7.4 or HCl/KCl buffer solution.

Medium	Time Point	Polarity <sup>a</sup>	Rotation		Double Integral <sup>d</sup>	Normalized AUC	Normalized partition	
			Correlation Time <sup>b</sup> (ns)	Partition <sup>c</sup>				
Water	-	1.111	0.024	1	-	-	-	
MCT	-	1.016	0.229	1	-	-	-	
NC I	1 hour	Species I	1.019	0.186	0.555	1073.9	1	0.555
		Species II	1.054	0.867	0.445			0.445
NC I	1 day	Species I	1.015	0.203	0.706	961.1	0.895	0.632
		Species II	1.090	0.707	0.294			0.263
NC I	1-day pH 7.4	Species I	1.015	0.230	0.916	795.4	0.740	0.678
		Species II	1.117	0.245	0.084			0.062
NC I	1-day pH 1.2	Species I	1.015	0.238	0.922	403.5	0.375	0.346
		Species II	1.117	0.115	0.078			0.029

<sup>a</sup> Standard deviation =  $\pm 0.005$ ; <sup>b</sup> Standard deviation =  $\pm 0.001$ ; <sup>c</sup> percentage of normalized AUC obtained from integrated of spectra. AUC is a function of spin-probe concentration. <sup>d</sup> Standard deviation =  $\pm 0.01$ .

## ***7. List of abbreviations***

$a_N$	Hyperfine splitting constant
ATR-FTIR	Attenuated total reflectance – Fourier transform infrared
AUC	Area under the curve
BSA	Bovine serum albumin
BT-NMR/MRI	Bench to nuclear magnetic resonance/magnetic resonance imaging
COOH	Carboxylic acid groups
DLS	Dynamic light scattering
DMSO	Dimethyl sulfoxide
DP	1,3-diaminopropane
EHDA	Electrohydrodynamic atomization
EM	Electron microscopy
EPR	Electronic paramagnetic spectroscopy
FDA	United States Food and Drug Administration
Fig.	Figure
GHz	Gigahertz
GIT	Gastrointestinal tract
GRAS	Generally Recognized as Safe
h	Hour
K	Kelvin
KCl	Potassium Chloride



---

kV	Kilovolt
LD <sub>50</sub>	Lethal dose, 50%
log P	Logarithm partition coefficient
MCT	Medium chain triglycerides
mg	Milligram
mg/ml	Milligram per millilitre
min	Minute
ml	Millilitre
ml/min	Millilitre per minute
mm	Millimetre
mM	Millimolar
Mn	Number average molecular weight
MNM	Multiple mode algorithm
MRI	Magnetic resonance imaging
ms	Millisecond
mT	Millitesla
mV	Millivolt
Mw	Weight average molecular weight
MWCO	Molecular weight cut-off
NaOH	Sodium hydroxide
NC (MS)	Nanocapsules prepared using magnetic stirring
NC	Nanocapsules (PVM/MA-MCT nanocapsules)

---

NC+DP	Cross-linked nanocapsules
NC-TB	Nanocapsule loaded with TEMPO-benzoate
NIH	National Institute of Health (United States of America)
nm	Nanometre
nm/s	Nanometre per second
NMR	Nuclear magnetic resonance
NP	Nanoparticles
NP-DP	Cross-linked nanoparticles
NP-TB	Nanoparticle loaded with TEMPO-benzoate
ns	Nanosecond
NTA	Nanoparticle tracking analysis
o/w	Oil-in-water emulsion
OH	Hydroxyl groups
PBS	Phosphate buffer solution
PDI	Polydispersity index
PEG	Poly ethylene glycol
pH	Potential of hydrogen
pKa	Acid dissociation constant
pm	Picometer
PVM/MA	Poly(methyl vinyl ether-alt-maleic anhydride)
R <sub>g</sub>	Radius of Gyration
rpm	Revolutions per minute

---

s	Second
S.D.	Standard deviation
sCMOS	Scientific complementary metal-oxide-semiconductor sensor
SLS	Static light scattering
T <sub>1</sub>	Spin-lattice relaxation time
T <sub>2</sub>	Spin-spin relaxation time
TB	TEMPO-benzoate
T <sub>c</sub>	Rotation correlation time
TE	Echo time
TEM	Transmission electron microscopy
THF	Tetrahydrofuran
TR	Repetition time
USP	United States Pharmacopeia
v/v	volume per volume
w/o	Water-in-oil emulsion
w/o/w	Water-in-oil-in-water emulsion
w/v	Weight per volume
°C	Celsius degree
µg	Microgram
µm	Micrometer
µm/min	Micrometre per minute

## 8. Bibliography

- [1] J. Kreuter, "Nanoparticles-a historical perspective," *Int. J. Pharm.*, vol. 331, no. 1, pp. 1–10, 2007.
- [2] K. Park, "Controlled drug delivery systems: Past forward and future back," *J. Control. Release*, vol. 190, pp. 3–8, 2014.
- [3] N. Kamaly, B. Yameen, J. Wu, and O. C. Farokhzad, "Degradable Controlled-Release Polymers and Polymeric Nanoparticles: Mechanisms of Controlling Drug Release," *Chem. Rev.*, vol. 116, no. 4, pp. 2602–2663, 2016.
- [4] S. M. Moghimi, A. C. Hunter, and J. C. Murray, "Nanomedicine: current status and future prospects.," *FASEB J.*, vol. 19, no. 3, pp. 311–330, 2005.
- [5] M. L. Etheridge, S. A. Campbell, A. G. Erdman, C. L. Haynes, S. M. Wolf, and J. McCullough, "The big picture on nanomedicine: The state of investigational and approved nanomedicine products," *Nanomedicine Nanotechnology, Biol. Med.*, vol. 9, no. 1, pp. 1–14, 2013.
- [6] Y. Perrie, "Aulton's Pharmaceuticals - The design and manufacture of medicines," in *Aulton's Pharmaceuticals - The design and manufacture of medicines*, 4th ed., M. Aulton and K. M. G. Taylor, Eds. Churchill Livingstone, 2013, pp. 777–796.
- [7] V. P. Torchilin, *Nanoparticulates as Drug Carriers*, 1st ed. London: Imperial College Press, 2006.
- [8] D. Quintanar-Guerrero, E. Allémann, H. Fessi, and E. Doelker, "Preparation techniques and mechanisms of formation of biodegradable nanoparticles from preformed polymers.," *Drug Dev. Ind. Pharm.*, vol. 24, no. 12, pp. 1113–1128, 1998.
- [9] K. S. Soppimath, T. M. Aminabhavi, A. R. Kulkarni, and W. E. Rudzinski, "Biodegradable polymeric nanoparticles as drug delivery devices," *J. Control. Rel.*, vol. 70, pp. 1–20, 2001.
- [10] J. W. Vanderhoff, M. S. El-Aasser, and J. Ugelstad, "Polymer emulsification method," US 4177177 A, 1979.
- [11] M. D. Blanco and M. J. Alonso, "Development and characterization of protein-loaded poly(lactide-co-glycolide) nanospheres," *European Journal of Pharmaceutics and Biopharmaceutics*, vol. 43, no. 3, pp. 287–294, 1997.
- [12] H. Fessi, F. Puisieux, J. P. Devissaguet, N. Ammoury, and S. Benita, "Nanocapsule formation by interfacial polymer deposition following solvent displacement," *Int. J. Pharm.*, vol. 55, no. 1, pp. 1–4, 1989.
- [13] D. Quintanar-Guerrero, E. Allémann, E. Doelker, and H. Fessi, "A mechanistic study of the formation of polymer nanoparticles by the emulsification-diffusion technique," *Colloid Polym. Sci.*, vol. 275, no. 7, pp. 640–647, 1997.
- [14] K. Songsurang, N. Praphairaksit, K. Siraleartmukul, and N. Muangsin, "Electrospray fabrication of doxorubicin-chitosan-tripolyphosphate

- nanoparticles for delivery of doxorubicin," *Arch. Pharm. Res.*, vol. 34, no. 4, pp. 583–592, 2011.
- [15] M. Zamani, M. P. Prabhakaran, and S. Ramakrishna, "Advances in drug delivery via electrospun and electrosprayed nanomaterials," *Int. J. Nanomedicine*, vol. 8, pp. 2997–3017, 2013.
- [16] R. Karnik, F. Gu, P. Basto, C. Cannizzaro, L. Dean, W. Kyei-Manu, R. Langer, and O. C. Farokhzad, "Microfluidic platform for controlled synthesis of polymeric nanoparticles," *Nano Lett.*, vol. 8, no. 9, pp. 2906–2912, 2008.
- [17] C. X. Zhao, L. He, S. Z. Qiao, and A. P. J. Middelberg, "Nanoparticle synthesis in microreactors," *Chem. Eng. Sci.*, vol. 66, no. 7, pp. 1463–1479, 2011.
- [18] C. E. Mora-Huertas, H. Fessi, and A. Elaissari, "Polymer-based nanocapsules for drug delivery," *Int. J. Pharm.*, vol. 385, no. 1–2, pp. 113–142, 2010.
- [19] N. Anton, J. P. Benoit, and P. Saulnier, "Design and production of nanoparticles formulated from nano-emulsion templates-A review," *J. Control. Release*, vol. 128, no. 3, pp. 185–199, 2008.
- [20] N. Garti, "Double emulsions - Scope, limitations and new achievements," *Colloids Surfaces A Physicochem. Eng. Asp.*, vol. 123–124, pp. 233–246, May 1997.
- [21] Z. Lu, J. Bei, and S. Wang, "A method for the preparation of polymeric nanocapsules without stabilizer," *J. Control. Release*, vol. 61, no. 1–2, pp. 107–112, 1999.
- [22] H.-J. Krause and P. Rohdewald, "Preparation of gelatin nanocapsules and their pharmaceutical characterization," *Pharm. Res.*, vol. 2, no. 5, pp. 239–243, 1985.
- [23] P. Calvo, J. L. Vila-Jato, and M. J. Alonso, "Evaluation of cationic polymer-coated nanocapsules as ocular drug carriers," *Int. J. Pharm.*, vol. 153, no. 1, pp. 41–50, 1997.
- [24] C. Preetz, A. Rube, I. Reiche, G. Hause, and K. Mäder, "Preparation and characterization of biocompatible oil-loaded polyelectrolyte nanocapsules," *Nanomedicine Nanotechnology, Biol. Med.*, vol. 4, no. 2, pp. 106–114, 2008.
- [25] Darlow, Brian Benjamin, A. Ramsay, and M. Gibb, "Maleic anhydride alkyl vinyl ether copolymer," 1972.
- [26] C. L. Burnett, W. F. Bergfeld, D. V. Belsito, R. A. Hill, C. D. Klaassen, D. C. Liebler, J. G. Marks Jr, R. C. Shank, T. J. Slaga, P. W. Snyder, and F. A. Andersen, "Final Report of the Amended Safety Assessment of PVM/MA Copolymer and Its Related Salts and Esters as Used in Cosmetics," *Int. J. Toxicol.*, vol. 30, no. supp. 2, p. 128S–144S, 2011.
- [27] T. Iglesias, J. M. Irache, M. Butinar, B. Turk, A. López de Cerain, and A. Azqueta, "Genotoxic evaluation of poly(anhydride) nanoparticles in the gastrointestinal tract of mice," *Int. J. Pharm.*, vol. 530, no. 1–2, pp. 187–194, 2017.

- [28] U. Schmidt, S. Zschoche, and C. Werner, "Modification of Poly(octadecene-alt-maleic anhydride) Films by Reaction with Functional Amines," *J. Appl. Polym. Sci.*, vol. 87, pp. 1255–1266, 2002.
- [29] P. Arbós, M. Wirth, M. A. Arangoa, F. Gabor, and J. M. Irache, "Gantrez AN as a new polymer for the preparation of ligand-nanoparticle conjugates.," *J. Control. release*, vol. 83, no. 3, pp. 321–330, Oct. 2002.
- [30] P. Arbós, M. A. Arangoa, M. A. Campanero, and J. M. Irache, "Quantification of the bioadhesive properties of protein-coated PVM/MA nanoparticles.," *Int. J. Pharm.*, vol. 242, no. 1–2, pp. 129–136, Aug. 2002.
- [31] P. Arbós, M. A. Campanero, M. A. Arangoa, M. J. Renedo, and J. M. Irache, "Influence of the surface characteristics of PVM/MA nanoparticles on their bioadhesive properties," *J. Control. release*, vol. 89, pp. 19–30, 2003.
- [32] P. Arbós, M. A. Campanero, M. A. Arangoa, and J. M. Irache, "Nanoparticles with specific bioadhesive properties to circumvent the pre-systemic degradation of fluorinated pyrimidines.," *J. Control. release*, vol. 96, no. 1, pp. 55–65, Apr. 2004.
- [33] K. Yoncheva, E. Lizarraga, and J. M. Irache, "Pegylated nanoparticles based on poly(methyl vinyl ether-co-maleic anhydride): preparation and evaluation of their bioadhesive properties.," *Eur. J. Pharm. Sci.*, vol. 24, no. 5, pp. 411–419, Apr. 2005.
- [34] M. Agüeros, P. Areses, M. A. Campanero, H. Salman, G. Quincoces, I. Peñuelas, and J. M. Irache, "Bioadhesive properties and biodistribution of cyclodextrin-poly(anhydride) nanoparticles," *Eur. J. Pharm. Sci.*, vol. 37, no. 3–4, pp. 231–240, 2009.
- [35] M. Agüeros, L. Ruiz-Gatón, C. Vauthier, K. Bouchemal, S. Espuelas, G. Ponchel, and J. M. Irache, "Combined hydroxypropyl-beta-cyclodextrin and poly(anhydride) nanoparticles improve the oral permeability of paclitaxel.," *Eur. J. Pharm. Sci.*, vol. 38, no. 4, pp. 405–413, Nov. 2009.
- [36] M. Agüeros, V. Zabaleta, S. Espuelas, M. A. Campanero, and J. M. Irache, "Increased oral bioavailability of paclitaxel by its encapsulation through complex formation with cyclodextrins in poly(anhydride) nanoparticles," *J. Control. Release*, vol. 145, no. 1, pp. 2–8, 2010.
- [37] A. S. Porfire, V. Zabaleta, C. Gamazo, S. E. Leucuta, and J. M. Irache, "Influence of dextran on the bioadhesive properties of poly(anhydride) nanoparticles.," *Int. J. Pharm.*, vol. 390, no. 1, pp. 37–44, May 2010.
- [38] D. M. Benival and P. V Devarajan, "Lipomer of doxorubicin hydrochloride for enhanced oral bioavailability.," *Int. J. Pharm.*, vol. 423, no. 2, pp. 554–561, Feb. 2012.
- [39] H. H. Salman, C. Gamazo, M. A. Campanero, and J. M. Irache, "Salmonella-like bioadhesive nanoparticles," *J. Control. Release*, vol. 106, no. 1–2, pp. 1–13, 2005.
- [40] M. Estevan, J. M. Irache, M. J. Grilló, J. M. Blasco, and C. Gamazo,

- “Encapsulation of antigenic extracts of *Salmonella enterica* serovar. Abortusovis into polymeric systems and efficacy as vaccines in mice,” *Vet. Microbiol.*, vol. 118, no. 1–2, pp. 124–132, 2006.
- [41] S. Gómez, C. Gamazo, B. S. Roman, M. Ferrer, M. L. Sanz, and J. M. Irache, “Gantrez AN nanoparticles as an adjuvant for oral immunotherapy with allergens,” *Vaccine*, vol. 25, no. 29, pp. 5263–71, Jul. 2007.
- [42] H. H. Salman, C. Gamazo, M. Agüeros, and J. M. Irache, “Bioadhesive capacity and immunoadjuvant properties of thiamine-coated nanoparticles,” *Vaccine*, vol. 25, no. 48, pp. 8123–8132, 2007.
- [43] S. Gómez, C. Gamazo, B. San Roman, A. Grau, S. Espuelas, M. Ferrer, M. L. Sanz, and J. M. Irache, “A novel nanoparticulate adjuvant for immunotherapy with *Lolium perenne*,” *J. Immunol. Methods*, vol. 348, no. 1–2, pp. 1–8, 2009.
- [44] H. H. Salman, C. Gamazo, P. C. de Smidt, G. Russell-Jones, and J. M. Irache, “Evaluation of bioadhesive capacity and immunoadjuvant properties of vitamin B(12)-Gantrez nanoparticles,” *Pharm. Res.*, vol. 25, no. 12, pp. 2859–68, Dec. 2008.
- [45] R. Da Costa Martins, C. Gamazo, M. Sánchez-Martínez, M. Barberán, I. Peñuelas, and J. M. Irache, “Conjunctival vaccination against *Brucella ovis* in mice with mannosylated nanoparticles,” *J. Control. release*, vol. 162, no. 3, pp. 553–560, Sep. 2012.
- [46] E. Moreno, J. Schwartz, E. Larrañeta, P. A. Nguewa, C. Sanmartín, M. Agüeros, J. M. Irache, and S. Espuelas, “Thermosensitive hydrogels of poly(methyl vinyl ether-co-maleic anhydride) - Pluronic(®) F127 copolymers for controlled protein release,” *Int. J. Pharm.*, vol. 459, no. 1–2, pp. 1–9, Jan. 2014.
- [47] M. J. Garland, T. R. R. Singh, A. D. Woolfson, and R. F. Donnelly, “Electrically enhanced solute permeation across poly(ethylene glycol)-crosslinked poly(methyl vinyl ether-co-maleic acid) hydrogels: Effect of hydrogel crosslink density and ionic conductivity,” *Int. J. Pharm.*, vol. 406, no. 1–2, pp. 91–98, 2011.
- [48] L. R. de Souza, L. A. Muehlmann, M. S. C. Dos Santos, R. Ganassin, R. Simón-Vázquez, G. A. Joanitti, E. Mosiniewicz-Szablewska, P. Suchocki, P. C. Morais, Á. González-Fernández, R. B. Azevedo, and S. N. Báó, “PVM/MA-shelled selol nanocapsules promote cell cycle arrest in A549 lung adenocarcinoma cells,” *J. Nanobiotechnology*, vol. 12, pp. 1–17, 2014.
- [49] M. E. Aulton and K. M. G. Taylor, Eds., *Aulton’s Pharmaceutics The design and manufacture of medicines*, 4th ed. Churchill Livingstone, 2013.
- [50] J. Calvo, J. L. Lavandera, M. Agüeros, and J. M. Irache, “Cyclodextrin/poly(anhydride) nanoparticles as drug carriers for the oral delivery of atovaquone,” *Biomed. Microdevices*, vol. 13, no. 6, pp. 1015–1025, Dec. 2011.
- [51] K. W. Y. Lee, C. J. H. Porter, and B. J. Boyd, “The effect of administered dose of lipid-based formulations on the In Vitro and In Vivo performance of cinnarizine as a model poorly water-soluble drug,” *J. Pharm. Sci.*, vol. 102, no. 2, pp. 565–

- 578, 2013.
- [52] C. J. H. Porter, C. W. Pouton, J. F. Cuine, and W. N. Charman, "Enhancing intestinal drug solubilisation using lipid-based delivery systems," *Adv. Drug Deliv. Rev.*, vol. 60, no. 6, pp. 673–691, 2008.
- [53] J. C. Richardson, R. W. Bowtell, K. Mäder, and C. D. Melia, "Pharmaceutical applications of magnetic resonance imaging (MRI)," *Advanced Drug Delivery Reviews*, vol. 57, no. 8, pp. 1191–1209, 2005.
- [54] K. Mäder and H. Metz, "Benchtop-NMR and MRI-A new analytical tool in drug delivery research," *Int. J. Pharm.*, vol. 364, no. 2, pp. 170–175, 2008.
- [55] K. P. Nott, "Magnetic resonance imaging of tablet dissolution," *Eur. J. Pharm. Biopharm.*, vol. 74, no. 1, pp. 78–83, 2010.
- [56] K. Mäder, G. Bacic, A. Domb, O. Elmalak, R. Langer, and H. M. Swartz, "Noninvasive in vivo monitoring of drug release and polymer erosion from biodegradable polymers by EPR spectroscopy and NMR imaging.," *J. Pharm. Sci.*, vol. 86, no. 1, pp. 126–134, 1997.
- [57] K. Mäder, B. Bittner, Y. Li, W. Wohlauf, and T. Kissel, "Monitoring microviscosity and microacidity of the albumin microenvironment inside degrading microparticles from poly(lactide-co-glycolide) (PLG) or ABA-triblock polymers containing hydrophobic poly(lactide-co-glycolide) A blocks and Hydrophilic poly(ethylene)," *Pharm. Res.*, vol. 15, no. 1, pp. 787–793, 1998.
- [58] B. Bittner, H. Isel, and R. J. Mountfield, "The use of electron paramagnetic resonance spectroscopy in early preformulation experiments: The impact of different experimental formulations on the release of a lipophilic spin probe into gastric juice," *Eur. J. Pharm. Biopharm.*, vol. 51, no. 2, pp. 159–162, 2001.
- [59] C. Ladaviere, T. Delair, A. Domard, C. Pichot, and B. Mandrand, "Covalent immobilization of biological molecules to maleic anhydride and methyl vinyl ether copolymers - A physico-chemical approach," *J. Appl. Polym. Sci.*, vol. 71, no. 6, pp. 927–936, Feb. 1998.
- [60] A. Heyd, D. O. Kildsig, and G. S. Banker, "Dissolution of Macromolecules II: Dissolution of an Ethylene-Maleic Acid Copolymer," *J. Pharm. Sci.*, vol. 59, no. 7, pp. 947–949, 1970.
- [61] N. De Jaeger, H. Demeyere, R. Finsy, R. Sneyers, J. Vanderdeelen, P. van der Meeren, and M. Van Laethem, "Particle Sizing by Photon Correlation Spectroscopy Part I: Monodisperse Latices: Influence of scattering Angle and Concentration of Dispersed Material," *Part. Part. Syst. Charact.*, vol. 8, pp. 179–186, 1991.
- [62] R. Finsy and N. De Jaeger, "Particle Sizing by Photon Correlation Spectroscopy Part II: Average Values," *Part. Part. Syst. Charact.*, vol. 8, pp. 187–193, 1991.
- [63] P. Garidel and F. Kebbel, "Protein therapeutics and aggregates characterized by photon correlation spectroscopy," *Bioprocess Int.*, vol. 8, no. 3, pp. 38–46, 2010.



- [64] P. A. Hassan, S. Rana, and G. Verma, "Making sense of brownian motion: colloid characterization by dynamic light scattering.," *Langmuir*, vol. 31, no. 1, pp. 3–12, 2015.
- [65] V. Filipe, A. Hawe, and W. Jiskoot, "Critical evaluation of nanoparticle tracking analysis (NTA) by NanoSight for the measurement of nanoparticles and protein aggregates," *Pharm. Res.*, vol. 27, no. 5, pp. 796–810, 2010.
- [66] C. Gillespie, P. Halling, and D. Edwards, "Monitoring of particle growth at a low concentration of a poorly water soluble drug using the NanoSight LM20," *Colloids Surfaces A Physicochem. Eng. Asp.*, vol. 384, no. 1–3, pp. 233–239, 2011.
- [67] B. Carr and M. Wright, "Nanoparticle Tracking Analysis - A review of applications and usage 2010-2012," *NanoSight Ltd.* p. 188, 2013.
- [68] C. W. Woodruff, G. E. Peck, and G. S. Banker, "Dissolution of Alkyl Vinyl Ether-Maleic Anhydride Copolymers and Ester Derivatives," *J. Pharm. Sci.*, vol. 61, no. 12, pp. 1916–1921, 1972.
- [69] Y. Mo, G. E. Peck, A. Heyd, and G. S. Banker, "Recording pH Method of Characterizing Composition and Monitoring Dissolution Profile of an Anhydride-Acid Copolymer and Its Salt Derivatives," *J. Pharm. Sci.*, vol. 66, no. 5, pp. 713–717, 1977.
- [70] J. Kuntsche, J. C. Horst, and H. Bunjes, "Cryogenic transmission electron microscopy (cryo-TEM) for studying the morphology of colloidal drug delivery systems," *Int. J. Pharm.*, vol. 417, no. 1–2, pp. 120–137, 2011.
- [71] P. Dubin and U. P. Strauss, "Hydrophobic hypercoiling in copolymers of maleic acid and alkyl vinyl ethers," *J. Phys. Chem.*, vol. 71, no. 8, pp. 2757–2759, 1967.
- [72] P. L. Dubin and U. P. Strauss, "Hydrophobic bonding in alternating copolymers of maleic acid and alkyl vinyl ethers," *J. Phys. Chem.*, vol. 74, no. 14, pp. 2842–2847, 1970.
- [73] C. Ladaviere, T. Delair, A. Domard, C. Pichot, and B. Mandrand, "Covalent Immobilization of Bovine Serum Albumin onto (Maleic Anhydride – alt-Methyl Vinyl Ether) Copolymers," *J. Appl. Polym. Sci.*, vol. 72, pp. 1565–1572, 1999.
- [74] C. Kroll, "Analytik, Stabilität und Biotransformation von Spinsonden," Humboldt-Universität zu Berlin, 1999.
- [75] A. Rube, "Development and physico-chemical characterization of nanocapsules," Martin-Luther Universität Halle-Wittenberg, 2006.
- [76] D. J. Lurie and K. Mäder, "Monitoring drug delivery processes by EPR and related techniques - principles and applications," *Adv. Drug Deliv. Rev.*, vol. 57, no. 8, pp. 1171–1190, 2005.
- [77] S. Kempe, H. Metz, and K. Mäder, "Application of Electron Paramagnetic Resonance (EPR) spectroscopy and imaging in drug delivery research - Chances and challenges," *Eur. J. Pharm. Biopharm.*, vol. 74, no. 1, pp. 55–66, 2010.

- [78] T. Higuchi, T. Miki, A. C. Shah, and A. K. Herd, "Facilitated Reversible Formation of Amides from Carboxylic Acids in Aqueous solutions. intermediate Production of Acid Anhydride," *J. Am. Chem. Soc.*, vol. 85, pp. 3655–3660, 1963.
- [79] J. P. Wang, X. P. Zhao, and D. W. Wang, "Preparation of nanocapsules containing the two-phase core materials.," *J. Microencapsul.*, vol. 24, no. 8, pp. 757–766, 2007.
- [80] K. Jores, W. Mehnert, M. Drechsler, H. Bunjes, C. Johann, and K. Mäder, "Investigations on the structure of solid lipid nanoparticles (SLN) and oil-loaded solid lipid nanoparticles by photon correlation spectroscopy, field-flow fractionation and transmission electron microscopy," *J. Control. Release*, vol. 95, no. 2, pp. 217–227, 2004.
- [81] J. Kuntsche, K. Westesen, M. Drechsler, M. H. J. Koch, and H. Bunjes, "Supercooled smectic nanoparticles: a potential novel carrier system for poorly water soluble drugs," *Pharm. Res.*, vol. 21, no. 10, pp. 1834–1843, 2004.
- [82] A. Béduneau, P. Saulnier, N. Anton, F. Hindré, C. Passirani, H. Rajerison, N. Noiret, and J. P. Benoit, "Pegylated nanocapsules produced by an organic solvent-free method: Evaluation of their stealth properties," *Pharm. Res.*, vol. 23, no. 9, pp. 2190–2199, 2006.
- [83] V. A. Golubev, E. G. Rozantsev, and M. B. Neiman, "Some reactions of free iminoxyl radicals with the participation of the unpaired electron," *Bull. Acad. Sci. USSR Div. Chem. Sci.*, vol. 14, no. 11, pp. 1898–1904, 1965.
- [84] V. A. Golubev, V. D. Sen', I. V. Kulyk, and A. L. Aleksandrov, "Mechanism of the oxygen disproportionation of ditert-alkylнитеoxyl radicals," *Bull. Acad. Sci. USSR Div. Chem. Sci.*, vol. 24, no. 10, pp. 2119–2126, 1975.
- [85] V. D. Sen and V. A. Golubev, "Kinetics and mechanism for acid-catalyzed disproportionation of 2,2,6,6-tetramethylpiperidine-1-oxyl," *J. Phys. Org. Chem.*, vol. 22, no. 2, pp. 138–143, 2008.
- [86] R. Rowe, P. Sheskey, and M. E. Quinn, *Handbook of pharmaceutical excipients*, Sixth edit. Washinton, DC: Pharmaceutical Press, 2009.
- [87] K. W. Y. Lee, C. J. H. Porter, and B. J. Boyd, "Gastric pre-processing is an important determinant of the ability of medium-chain lipid solution formulations to enhance oral bioavailability in rats," *J. Pharm. Sci.*, vol. 102, no. 11, pp. 3957–3965, 2013.

## **9. Acknowledgements**

I would like to thank the Prof. Dr. Karsten Mäder for the opportunity to join his research group and develop this impressive work. I thank him for the scientific guidance, the words of encouragement and the kind treatment.

I would like to thank Dr. Hendrik Metz for his valuable support regarding DLS, EPR, and BTNMR/MRI measurements. Besides, I want to thank him for long and fruitful discussions about science and about the life.

I thank Dr. Annette Meister and Dr. Gerd Hause for performing the transmission electron microscopy. Heike Rudolf for the ATR-FTIR spectroscopy analysis and Manuela Woigk for the HPLC analysis. I also thank Kerstin Schwarz for the thermogravimetric analysis and Ute Menzel for the laboratory assistance. I also thank Christin Zlomke and Tom Wersig for their help and constructive discussions as well as all colleagues for their support.

Special thanks to Claudia Bertram not only for the invaluable assistance in organizational matters but mainly for her kindly presence at different times.

I would like to thank my parents and brothers for the examples of love, perseverance, and dedication. I also thank my husband for his support to start this life project and for his kindness and always supportive presence at all times.

## **10. Curriculum Vitae**

### ***Personal information***

Name	Ligia Elena de Souza
Address	Laurentiusstraße, 5 06108 – Halle (Saale), Germany
Date of birth	27 September 1976
Place of birth	Belo Horizonte, Brazil

### ***Academic education***

2014 – 2017	Student in the group of Prof. Dr. habil. Karsten Mäder, Institute of Pharmacy, Martin Luther University Halle-Wittenberg.
2011 – 2013	Master degree in Biological Sciences – Physiology, Laboratory of Biophysics of Nanostructured Systems at the Biological Sciences Institute, Federal University of Minas Gerais, UFMG, Belo Horizonte, Brazil.
2003 – 2004	Specialization – Studies in Health Management, Pontifical Catholic University of Minas Gerais, PUC – Minas, Belo Horizonte/MG, Brazil.
1997 – 2001	Bachelor in Pharmacy – Federal University of Minas Gerais, UFMG, Belo Horizonte/MG, Brazil.
1992 – 1994	Secondary school – Federal Center of Technological Education of Minas Gerais, CEFET-MG, Belo Horizonte/MG, Brazil.

### ***Work experience***

01/2011 – 08/2011	Volunteer trainee – Laboratory of Biophysics of Nanostructured Systems at the Biological Sciences Institute Federal University of Minas Gerais, UFMG, Belo Horizonte/MG, Brazil.
03/2007 – 03/2010	Supply Chain Manager – Hospital Nossa Senhora das Graças, Sete Lagoas/MG – Brazil.
11/2005 – 01/2007	Supervisor of Pharmacy – Hospital Mater Dei S.A., Belo Horizonte/MG, Brazil.
05/2005 – 11/2005	Supervisor of Pharmacy – Hospital São Francisco de Assis, Belo Horizonte/MG, Brazil.
01/2004 – 01/2005	Supervisor of Pharmacy – Hospital Vera Cruz S.A., Belo Horizonte/MG, Brazil.

- 09/2002 – 12/2003 Supervisor of Pharmacy – Hospital Santa Casa de Belo Horizonte, Belo Horizonte/MG, Brazil.
- 10/2001 – 09/2002 Pharmacist – Hospital Espírita André Luiz, Belo Horizonte/MG, Brazil
- 1999 – 2001 Chemistry Teacher for Secondary School – State Secretary of Education of Minas Gerais, Belo Horizonte/MG, Brazil

### **Publication**

- E. G. Azevedo, R. R. Ribeiro, S. M. da Silva, C. S. Ferreira, L. E. de Souza, R. A. Oliveira e Castro, C. Demicheli, S. A. Rezende, and F. Frézard, "Mixed formulation of conventional and pegylated liposomes as a novel drug delivery strategy for improved treatment of visceral leishmaniasis," *Expert Opin. Drug Deliv.*, vol. 11, pp. 1–10, 2014

### **Conferences**

- 09/2015 4<sup>th</sup> International Symposium on Phospholipids in Pharmaceutical Research. Heidelberg, Germany.
- 04/2014 9<sup>th</sup> World Meeting on Pharmaceutics, Biopharmaceutics and Pharmaceutical Technology. Lisbon, Portugal. Poster presentation: "Improved pharmacokinetic of a mixture of conventional and pegylated liposomes for treatment of visceral leishmaniasis."
- 11/2013 Symposium on Nanotechnology and its Applications in Health – 10 Years of the NANOBIOIMIG NETWORK. Belo Horizonte, Brazil. Oral presentation: "Pharmacokinetic gains with conventional and stealth liposomes. "
- 05/2013 5<sup>th</sup> World Congress on Leishmaniasis – Worldleish 5. Porto de Galinhas, Brazil.
- 04/2011 8<sup>th</sup> International Symposium on Vasoactive Peptides. Ouro Preto, Brazil.

## **11. Erklärung**

Hiermit erkläre ich an Eides statt, dass ich die vorliegende Dissertationsschrift selbständig und ohne fremde Hilfe verfasst habe, keine anderen als die von mir angegebenen Quellen und Hilfsmittel benutzt habe und die den benutzten Werken wörtlich oder inhaltlich entnommenen Stellen als solche kenntlich gemacht habe.

Darüber hinaus erkläre ich, dass ich noch keine vergeblichen Promotionsversuche unternommen habe und dass diese Dissertation weder in der gegenwärtigen noch in einer anderen Fassung bereits einer anderen Fakultät vorgelegen hat.

Halle (Saale), 12. September 2017

---

Ligia Elena de Souza